THE UNIVERSITY OF CALGARY

A Three-Dimensional Gravity Field Model of the Kananaskis Area

by

Vladimir Argeseanu

A THESIS
SUBMITTED TO THE FACULTY OF GRADUATE STUDIES
IN PARTIAL FULFILLMENT OF THE REQUIREMENTS FOR THE
DEGREE OF MASTER OF SCIENCE

DEPARTMENT OF GEOMATICS ENGINEERING

CALGARY, ALBERTA
JUNE, 1994

ISBN   0-315-99307-3

Canada

Name **VLADIMIR ARGESEANU**

Dissertation Abstracts International is arranged by broad, general subject categories. Please select the one subject which most nearly describes the content of your dissertation. Enter the corresponding four-digit code in the spaces provided.

GEODESY

SUBJECT TERM

0 3 7 0 U·M·I

SUBJECT CODE

Subject Categories

THE HUMANITIES AND SOCIAL SCIENCES

COMMUNICATIONS AND THE ARTS
Architecture	0729
Art History	0377
Cinema	0900
Dance	0378
Fine Arts	0357
Information Science	0723
Journalism	0391
Library Science	0399
Mass Communications	0708
Music	0413
Speech Communication	0459
Theater	0465

EDUCATION
General	0515
Administration	0514
Adult and Continuing	0516
Agricultural	0517
Art	0273
Bilingual and Multicultural	0282
Business	0688
Community College	0275
Curriculum and Instruction	0727
Early Childhood	0518
Elementary	0524
Finance	0277
Guidance and Counseling	0519
Health	0680
Higher	0745
History of	0520
Home Economics	0278
Industrial	0521
Language and Literature	0279
Mathematics	0280
Music	0522
Philosophy of	0998
Physical	0523

Psychology	0525
Reading	0535
Religious	0527
Sciences	0714
Secondary	0533
Social Sciences	0534
Sociology of	0340
Special	0529
Teacher Training	0530
Technology	0710
Tests and Measurements	0288
Vocational	0747

LANGUAGE, LITERATURE AND LINGUISTICS
Language
General	0679
Ancient	0289
Linguistics	0290
Modern	0291
Literature
General	0401
Classical	0294
Comparative	0295
Medieval	0297
Modern	0298
African	0316
American	0591
Asian	0305
Canadian (English)	0352
Canadian (French)	0355
English	0593
Germanic	0311
Latin American	0312
Middle Eastern	0315
Romance	0313
Slavic and East European	0314

PHILOSOPHY, RELIGION AND THEOLOGY
Philosophy	0422
Religion
General	0318
Biblical Studies	0321
Clergy	0319
History of	0320
Philosophy of	0322
Theology	0469

SOCIAL SCIENCES
American Studies	0323
Anthropology
Archaeology	0324
Cultural	0326
Physical	0327
Business Administration
General	0310
Accounting	0272
Banking	0770
Management	0454
Marketing	0338
Canadian Studies	0385
Economics
General	0501
Agricultural	0503
Commerce-Business	0505
Finance	0508
History	0509
Labor	0510
Theory	0511
Folklore	0358
Geography	0366
Gerontology	0351
History
General	0578

Ancient	0579
Medieval	0581
Modern	0582
Black	0328
African	0331
Asia, Australia and Oceania	0332
Canadian	0334
European	0335
Latin American	0336
Middle Eastern	0333
United States	0337
History of Science	0585
Law	0398
Political Science
General	0615
International Law and Relations	0616
Public Administration	0617
Recreation	0814
Social Work	0452
Sociology
General	0626
Criminology and Penology	0627
Demography	0938
Ethnic and Racial Studies	0631
Individual and Family Studies	0628
Industrial and Labor Relations	0629
Public and Social Welfare	0630
Social Structure and Development	0700
Theory and Methods	0344
Transportation	0709
Urban and Regional Planning	0999
Women's Studies	0453

THE SCIENCES AND ENGINEERING

BIOLOGICAL SCIENCES
Agriculture
General	0473
Agronomy	0285
Animal Culture and Nutrition	0475
Animal Pathology	0476
Food Science and Technology	0359
Forestry and Wildlife	0478
Plant Culture	0479
Plant Pathology	0480
Plant Physiology	0817
Range Management	0777
Wood Technology	0746
Biology
General	0306
Anatomy	0287
Biostatistics	0308
Botany	0309
Cell	0379
Ecology	0329
Entomology	0353
Genetics	0369
Limnology	0793
Microbiology	0410
Molecular	0307
Neuroscience	0317
Oceanography	0416
Physiology	0433
Radiation	0821
Veterinary Science	0778
Zoology	0472
Biophysics
General	0786
Medical	0760

EARTH SCIENCES
Biogeochemistry	0425
Geochemistry	0996

Geodesy	0370
Geology	0372
Geophysics	0373
Hydrology	0388
Mineralogy	0411
Paleobotany	0345
Paleoecology	0426
Paleontology	0418
Paleozoology	0985
Palynology	0427
Physical Geography	0368
Physical Oceanography	0415

HEALTH AND ENVIRONMENTAL SCIENCES
Environmental Sciences	0768
Health Sciences
General	0566
Audiology	0300
Chemotherapy	0992
Dentistry	0567
Education	0350
Hospital Management	0769
Human Development	0758
Immunology	0982
Medicine and Surgery	0564
Mental Health	0347
Nursing	0569
Nutrition	0570
Obstetrics and Gynecology	0380
Occupational Health and Therapy	0354
Ophthalmology	0381
Pathology	0571
Pharmacology	0419
Pharmacy	0572
Physical Therapy	0382
Public Health	0573
Radiology	0574
Recreation	0575

Speech Pathology	0460
Toxicology	0383
Home Economics	0386

PHYSICAL SCIENCES
Pure Sciences
Chemistry
General	0485
Agricultural	0749
Analytical	0486
Biochemistry	0487
Inorganic	0488
Nuclear	0738
Organic	0490
Pharmaceutical	0491
Physical	0494
Polymer	0495
Radiation	0754
Mathematics	0405
Physics
General	0605
Acoustics	0986
Astronomy and Astrophysics	0606
Atmospheric Science	0608
Atomic	0748
Electronics and Electricity	0607
Elementary Particles and High Energy	0798
Fluid and Plasma	0759
Molecular	0609
Nuclear	0610
Optics	0752
Radiation	0756
Solid State	0611
Statistics	0463
Applied Sciences
Applied Mechanics	0346
Computer Science	0984

Engineering
General	0537
Aerospace	0538
Agricultural	0539
Automotive	0540
Biomedical	0541
Chemical	0542
Civil	0543
Electronics and Electrical	0544
Heat and Thermodynamics	0348
Hydraulic	0545
Industrial	0546
Marine	0547
Materials Science	0794
Mechanical	0548
Metallurgy	0743
Mining	0551
Nuclear	0552
Packaging	0549
Petroleum	0765
Sanitary and Municipal	0554
System Science	0790
Geotechnology	0428
Operations Research	0796
Plastics Technology	0795
Textile Technology	0994

PSYCHOLOGY
General	0621
Behavioral	0384
Clinical	0622
Developmental	0620
Experimental	0623
Industrial	0624
Personality	0625
Physiological	0989
Psychobiology	0349
Psychometrics	0632
Social	0451

Nom _____

Dissertation Abstracts International est organisé en catégories de sujets. Veuillez s.v.p. choisir le sujet qui décrit le mieux votre thèse et inscrivez le code numérique approprié dans l'espace réservé ci-dessous.

□□□□ **U·M·I**

SUJET   CODE DE SUJET

Catégories par sujets

HUMANITÉS ET SCIENCES SOCIALES

COMMUNICATIONS ET LES ARTS
Architecture 0729
Beaux-arts 0357
Bibliothéconomie 0399
Cinéma .:.............................. 0900
Communication verbale 0459
Communications 0708
Danse 0378
Histoire de l'art 0377
Journalisme 0391
Musique 0413
Sciences de l'information 0723
Théâtre 0465

ÉDUCATION
Généralités 515
Administration 0514
Art 0273
Collèges communautaires 0275
Commerce 0688
Économie domestique 0278
Éducation permanente 0516
Éducation préscolaire 0518
Éducation sanitaire 0680
Enseignement agricole 0517
Enseignement bilingue et
   multiculturel 0282
Enseignement industriel 0521
Enseignement primaire. 0524
Enseignement professionnel 0747
Enseignement religieux 0527
Enseignement secondaire 0533
Enseignement spécial 0529
Enseignement supérieur 0745
Évaluation 0288
Finances 0277
Formation des enseignants 0530
Histoire de l'éducation 0520
Langues et littérature 0279

Lecture 0535
Mathématiques 0280
Musique 0522
Orientation et consultation 0519
Philosophie de l'éducation 0998
Physique 0523
Programmes d'études et
   enseignement 0727
Psychologie 0525
Sciences 0714
Sciences sociales 0534
Sociologie de l'éducation 0340
Technologie 0710

LANGUE, LITTÉRATURE ET LINGUISTIQUE
Langues
   Généralités 0679
   Anciennes 0289
   Linguistique 0290
   Modernes 0291
Littérature
   Généralités 0401
   Anciennes 0294
   Comparée 0295
   Mediévale 0297
   Moderne 0298
   Africaine 0316
   Américaine 0591
   Anglaise 0593
   Asiatique 0305
   Canadienne (Anglaise) 0352
   Canadienne (Française) 0355
   Germanique 0311
   Latino-américaine 0312
   Moyen-orientale 0315
   Romane 0313
   Slave et est-européenne 0314

PHILOSOPHIE, RELIGION ET THÉOLOGIE
Philosophie 0422
Religion
   Généralités 0318
   Clergé 0319
   Études bibliques 0321
   Histoire des religions 0320
   Philosophie de la religion 0322
Théologie 0469

SCIENCES SOCIALES
Anthropologie
   Archéologie 0324
   Culturelle 0326
   Physique 0327
Droit 0398
Économie
   Généralités 0501
   Commerce-Affaires 0505
   Économie agricole 0503
   Économie du travail 0510
   Finances 0508
   Histoire 0509
   Théorie 0511
Études américaines 0323
Études canadiennes 0385
Études féministes 0453
Folklore 0358
Géographie 0366
Gérontologie 0351
Gestion des affaires
   Généralités 0310
   Administration 0454
   Banques 0770
   Comptabilité 0272
   Marketing 0338
Histoire
   Histoire générale 0578

Ancienne 0579
Médiévale 0581
Moderne 0582
Histoire des noirs 0328
Africaine 0331
Canadienne 0334
États-Unis 0337
Européenne 0335
Moyen-orientale 0333
Latino-américaine 0336
Asie, Australie et Océanie 0332
Histoire des sciences 0585
Loisirs 0814
Planification urbaine et
   régionale 0999
Science politique
   Généralités 0615
   Administration publique 0617
   Droit et relations
      internationales 0616
Sociologie
   Généralités 0626
   Aide et bien-être social 0630
   Criminologie et
      établissements
      pénitentiaires 0627
   Démographie 0938
   Études de l' individu et
      de la famille 0628
   Études des relations
      interethniques et
      des relations raciales 0631
   Structure et développement
      social 0700
   Théorie et méthodes. 0344
   Travail et relations
      industrielles 0629
Transports 0709
Travail social 0452

SCIENCES ET INGÉNIERIE

SCIENCES BIOLOGIQUES
Agriculture
   Généralités 0473
   Agronomie. 0285
   Alimentation et technologie
      alimentaire 0359
   Culture 0479
   Élevage et alimentation 0475
   Exploitation des péturages 0777
   Pathologie animale 0476
   Pathologie végétale 0480
   Physiologie végétale 0817
   Sylviculture et faune 0478
   Technologie du bois 0746
Biologie
   Généralités 0306
   Anatomie 0287
   Biologie (Statistiques) 0308
   Biologie moléculaire 0307
   Botanique 0309
   Cellule 0379
   Écologie 0329
   Entomologie 0353
   Génétique 0369
   Limnologie 0793
   Microbiologie 0410
   Neurologie 0317
   Océanographie 0416
   Physiologie 0433
   Radiation 0821
   Science vétérinaire 0778
   Zoologie 0472
Biophysique
   Généralités 0786
   Medicale 0760

SCIENCES DE LA TERRE
Biogéochimie 0425
Géochimie 0996
Géodésie 0370
Géographie physique 0368

Géologie 0372
Géophysique 0373
Hydrologie 0388
Minéralogie 0411
Océanographie physique 0415
Paléobotanique 0345
Paléoécologie 0426
Paléontologie 0418
Paléozoologie 0985
Palynologie 0427

SCIENCES DE LA SANTÉ ET DE L'ENVIRONNEMENT
Économie domestique 0386
Sciences de l'environnement 0768
Sciences de la santé
   Généralités 0566
   Administration des hipitaux .. 0769
   Alimentation et nutrition 0570
   Audiologie 0300
   Chimiothérapie 0992
   Dentisterie 0567
   Développement humain 0758
   Enseignement 0350
   Immunologie 0982
   Loisirs 0575
   Médecine du travail et
      thérapie 0354
   Médecine et chirurgie 0564
   Obstétrique et gynécologie ... 0380
   Ophtalmologie 0381
   Orthophonie 0460
   Pathologie 0571
   Pharmacie 0572
   Pharmacologie 0419
   Physiothérapie 0382
   Radiologie 0574
   Santé mentale 0347
   Santé publique 0573
   Soins infirmiers 0569
   Toxicologie 0383

SCIENCES PHYSIQUES
Sciences Pures
Chimie
   Généralités 0485
   Biochimie 487
   Chimie agricole 0749
   Chimie analytique 0486
   Chimie minérale 0488
   Chimie nucléaire 0738
   Chimie organique 0490
   Chimie pharmaceutique 0491
   Physique 0494
   PolymÇres 0495
   Radiation 0754
Mathématiques 0405
Physique
   Généralités 0605
   Acoustique 0986
   Astronomie et
      astrophysique 0606
   Electronique et électricité 0607
   Fluides et plasma 0759
   Météorologie 0608
   Optique 0752
   Particules (Physique
      nucléaire) 0798
   Physique atomique 0748
   Physique de l'état solide 0611
   Physique moléculaire 0609
   Physique nucléaire 0610
   Radiation 0756
Statistiques 0463

Sciences Appliqués Et Technologie
Informatique 0984
Ingénierie
   Généralités 0537
   Agricole 0539
   Automobile 0540

Biomédicale 0541
Chaleur et ther
   modynamique 0348
Conditionnement
   (Emballage) 0549
Génie aérospatial 0538
Génie chimique 0542
Génie civil 0543
Génie électronique et
   électrique 0544
Génie industriel 0546
Génie mécanique 0548
Génie nucléaire 0552
Ingénierie des systàmes 0790
Mécanique navale 0547
Métallurgie 0743
Science des matériaux 0794
Technique du pétrole 0765
Technique minière 0551
Techniques sanitaires et
   municipales 0554
Technologie hydraulique 0545
Mécanique appliquée 0346
Géotechnologie 0428
Matières plastiques
   (Technologie) 0795
Recherche opérationnelle 0796
Textiles et tissus (Technologie) ... 0794

PSYCHOLOGIE
Généralités 0621
Personnalité 0625
Psychobiologie 0349
Psychologie clinique 0622
Psychologie du comportement ... 0384
Psychologie du développement .. 0620
Psychologie expérimentale 0623
Psychologie industrielle 0624
Psychologie physiologique 0989
Psychologie sociale 0451
Psychométrie 0632

✲

THE UNIVERSITY OF CALGARY
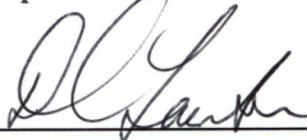
FACULTY OF GRADUATE STUDIES

The undersigned certify that they have read, and recommend to the Faculty of Graduate Studies for acceptance, a thesis entitled "A Three-Dimensional Gravity Field Model of the Kananaskis Area" submitted by Vladimir Argeseanu in partial fulfillment of the requirements for the degree of Master of Science.

Supervisor, Dr. M. G. Sideris
Department of Geomatics Engineering

Dr. M. A. Chapman
Department of Geomatics Engineering

Dr. D. C. Lawton
Department of Geology and Geophysics

Dr. K. P. Schwarz
Department of Geomatics Engineering

Date: June 30, 1994

ii

ABSTRACT

The research objective is the development, in the Kananaskis area situated in the Canadian Rocky Mountains, of a homogenous and accurate gravity field model on the surface of the Earth and at elevation above it, as a reference for testing of a gravity-based airborne system. Random point gravity data collected from existing sources and by measurement, processed in a consistent manner and taking into account digital elevation models, are used to predict grids of surface free-air, Bouguer, and isostatic gravity anomalies. The prediction methods are least squares collocation and weighted means. Covariance analysis of the predicted gravity anomalies indicates that the gravity field can be recovered at approximately 1 mGal level if the data spacing is less than 3 km. This precision is achieved within an area bounded by latitudes 50°40' and 51°05' and by longitudes 244°38' and 245°08'. Spatial gravity anomaly fields, at altitude above the topography, are computed from two-layer point mass models and by using the Poisson integral with reduced surface gravity anomaly data. The results are very sensitive, especially at low altitudes, to the method by which the surface data are reduced to a reference surface.

ACKNOWLEDGEMENTS

TABLE OF CONTENTS

LIST OF TABLES

LIST OF FIGURES

NOTATION

A	design matrix, covariance function parameter, area, scale factor
a	regression coefficient, equatorial radius
B	covariance function parameter
b	covariance function parameter, regression coefficient
C.U.	gravity meter counter unit
C_{ll}	covariance matrix of observations
C_{nn}	covariance matrix of noise
C_{ss}	covariance matrix of signals
C_{sl}	cross-covariance matrix of signals and observations
C_0	variance of gravity anomalies
$C(s)$	covariance function
$C(\psi)$	covariance function
$C(i, j)$	covariance function
c_{ij}	coefficient of polynomial surface
c_n	anomaly degree variance
$\bar{C}_{nm}^*$, $\bar{S}_{nm}$	fully normalized potential coefficients
D	covariance function parameter, depth of point mass layer
D'	covariance function parameter
d	distance, mean data spacing
$D(t)$	drift parameter
D_M	distance Earth-Moon
D_S	distance Earth-Sun
dv	volume element
dx	North-South planar grid spacing
dy	East-West planar grid spacing
$E\{\cdot\}$	expectation

$E_{\hat{s}\hat{s}}$	error matrix of estimated signals
F	attraction force
$F(z)$	transformation function for C.U. into gravity units
$F_0(z)$	approximation of transformation function for C.U. into gravity units
$f(x, y)$	function
$F\{\Delta g(k, l)\}$	Fourier transform applied to gravity anomalies
$F\{m(i, j)\}$	Fourier transform applied to point masses
G	Newton's gravitational constant
g	gravity
G_0	variance of horizontal gradients
h	height
H	orthometric height
H^*	normal height
h_0	upward continuation distance above reference
h^s	height of reference topographic surface
k	elasticity proportionality constant
$L(T)$	functional of the disturbing potential
l	spring balance length, distance from computation point to data point, vector of observations
l_0	spring balance initial length, distance from computation point to data point
M	mass of the Earth, mass anomaly variance, number of data points in the x direction
M_M	mass of the Moon
M_S	mass of the Sun
m	particle of mass, point mass, order of expansion
$M(\cdot)$	averaging operator
$m^2_{\Delta g_{h_0}}$	upward continuation gravity anomaly mean square error
n	noise, degree of expansion
N	number of data points in an area, number of data points in the y direction
N_0	level of gravity meter
$P_n(\cos\psi)$	Legendre's polynomials

q	circular frequency
R	mean radius of the Earth's sphere
R_B	radius of the Bjerhammar sphere
r	position vector, radial distance
$S_{mm}(u, v)$	power spectral density of the mass distribution
$S_{\Delta g \Delta g}(u, v)$	power spectral density of the gravity anomalies
s	signal, distance, square of ratio of the Earth's and Bjerhammar radii
$\hat{s}$	estimated signal
t	time, thickness of compensating root, statistic
t_0	reference time
s_0	distance
T	anomalous potential, normal thickness of Earth's crust
V	normal gravitational potential
u, v	spatial frequencies in cycles per distance unit in the x, y directions
v	correction to the observation
X	vector of parameters
$\hat{X}$	vector of parameters
$X_{1/2}$	correlation distance
x, y, z	cartesian coordinates
z	gravity meter reading in C.U.
z_m	mean of elevations of the computation and data points
α	angle of gravity meter with the vertical
α_M	geocentric angle to the Moon
α_S	geocentric angle to the Sun
β, β_1	constants related to the reference ellipsoid gravity characteristics
γ	normal gravity
γ_e	normal gravity on the ellipsoid at the equator
γ_0	normal gravity on the ellipsoid
δ	root mean square discrepancy statistic
δg_{atm}	atmospheric gravity correction
$\delta g_{free-air}$	gravity free-air reduction
$\delta g_{isostatic}$	attraction of compensating masses

δg_{plate}	attraction of Bouguer plate
δg_{tc}	terrain correction
δg_{tidal}	tidal acceleration effect
$\delta g_{topography}$	topographic reduction
Δg	gravity anomaly
$\overline{\Delta g}$	average gravity anomaly
$\Delta g_{Bouguer}$	Bouguer gravity anomaly
$\Delta g_{free-air}$	free-air gravity anomaly
$\Delta g_{isostatic}$	isostatic gravity anomaly
Δg_s	surface gravity anomaly
Δg^d	deterministic (i.e., trend) gravity anomaly
Δg^r	residual gravity anomaly
Δg^S	gravity anomaly from spherical harmonic coefficients
Δg^t	gravity anomaly due to the topography
Δg^*	root mean square variation in the gravity anomaly data
$\Delta \rho$	density contrast
ε_{h_0}	upward continuation gravity anomaly error
$\overline{\varepsilon}$	average effect of gravity anomalies coming from the area beyond distance s_0
κ	curvature of covariance function at distance $s = 0$
λ	longitude
μ	power of prediction for weighted means
σ	area
σ_d	standard deviation of discrepancy
σ_e	standard deviation of range of gravity anomalies
σ_h	standard deviation of the height
σ_r	standard deviation of representation
$\sigma_{\delta g_{free-air}}$	standard deviation of free-air reduction
$\sigma_{\delta g_{plate}}$	standard deviation of Bouguer plate reduction
$\sigma_{\Delta g}$	standard deviation of gravity anomaly
$\sigma_{\Delta g_{Bouguer}}$	standard deviation of Bouguer gravity anomaly
$\sigma_{\Delta g_{free-air}}$	standard deviation of free-air gravity anomaly

ρ	density of mass ρ_0 normal density
Φ	centrifugal potential
ϕ	latitude
χ	curvature parameter of the covariance function
ω	angular velocity of the Earth
Ω	volume of source body

CHAPTER 1

INTRODUCTION

1.1 Background

The study of the Earth's gravity field is of interest for geodetic and geophysical applications. In geodesy, gravity data is used to address the principal task of geodesy, i.e., the determination of the surface of the Earth and its exterior gravity field. In geophysics, gravity data on the Earth's surface is an important source of information to determine the mass distribution of the interior of the Earth.

Classical methods of sensing the change in shape of the equipotential surfaces of the gravity field use static gravimeters and/or astronomical determination of the deflections of the vertical for the acquisition of gravimetric data at discrete points. Although the attainable accuracies are high, such methods are time consuming, expensive and difficult to carry out in areas not easily accessible.

The capacity to measure gravity from an aircraft (i.e., airborne gravimetry) can provide uniform, dense and high resolution coverage for local gravity field applications regardless of access and nature of an area, with cost efficiency. The integration, in an airborne platform, of the navigation information (i.e., spatial location, velocity, acceleration) coming from Inertial Navigation Systems (INS) and receivers of the Global Positioning System (GPS), has been an area of interest for geodesy and geophysics in recent times. LaCoste et al. (1982), Hammer (1983), Brozena and Peters (1988), Brozena et al. (1989), Colombo (1990), Knickmeyer (1990), Brozena (1991), and Schwarz et al. (1991) have discussed, applied and analyzed the measurement of gravity from aircraft for the purpose of charting the gravity field.

The Department of Geomatics Engineering at The University of Calgary and Canagrav Research Ltd. are pursuing research and development for a gravity vector system as part of a gravity based airborne system for oil and mineral exploration. The gravity vector system should have the capability of achieving a resolution of better than 1 mGal for wavelengths ranging between 3 to 10 km. The proposed system will combine the output of GPS receivers and INS to achieve the objective (i.e., determine the magnitude and direction of the anomalous gravity vector at the necessary level of accuracy and resolution).

The gravity vector system must be tested under typical operational conditions encountered in exploration. For this task, detailed three-dimensional gravity field models are required for designated test areas. This requires for dense gravity data coverage and detailed elevation models of the topography. Exploratory studies give an indication that the Kananaskis area in the Canadian Rocky Mountains meets the requirements (i.e., large variations of the anomalous gravity field) needed for testing the gravity vector system in a mountainous area (Forsberg, 1986; Schwarz et al., 1990).

For the purpose stated above, existing gravity data provided by the Department of Energy, Mines and Resources (now Department of Natural Resources) are combined with data from gravity surveys performed with spring gravimeters for or by The University of Calgary in an area bounded by latitudes 50°15' to 51°30' and longitudes 244°15' to 245°30'. Within the core region of this area lies part of the Kananaskis area. It is endeavored to have a uniform point distribution representative in horizontal position and elevation. The point gravity data are subsequently converted to gravity anomalies and archived in a data base comprising all the available gravimetric information (i.e., identification source number, spatial location, observed gravity, reductions, gravity anomalies, precisions). In order to produce a consistent data set, an attempt is made to apply standard procedures and recommendations throughout the collection, processing and combination of the available gravity data as presented in the scientific literature regarding gravimetric surveys and their products. References dealing with these matters include Morelli (1976), Uotila (1978), McConnell (1982), Dobrin and Savit (1988), Torge (1989), and LaFehr (1991).

The wide variety of applications in geodesy and geophysics involving gravity data require, in general, the operation of prediction. Of special interest is the prediction from point gravity anomalies data of values on a regular pattern (i.e., gridding). Methods used for this purpose include least squares surface fitting, simple and least squares plane fitting,

minimum curvature surface, solids of revolution, least squares collocation, series approximations, splines, and inverse distance weighting. Developments regarding the prediction of gravity anomaly data at other random points and/or grids are found in Briggs (1974), Kassim (1980), Sünkel (1981b), Merry (1983), Tscherning and Forsberg (1983), and Morrison and Douglas (1984). In this investigation, two methods were chosen for gridding the point gravity data in the Kananaskis area, namely inverse distance weighting and least squares collocation. The performances (i.e., accuracy of prediction, precision estimation, computation requirements) of the prediction methods are evaluated.

The analysis of the information coming from different parts of the spectrum of the gravity anomaly field is important for geodetic and geophysical applications. Schwarz (1985) and Vassiliou and Schwarz (1987) used a spectral analysis approach regarding the investigation of the resolution of the gravity anomaly field for different data distributions. Tscherning (1975, 1985) investigated the density of the gravity data distribution using covariance functions in order to obtain the required precisions in subsequent gravity anomaly field estimations.

The gravity anomalies on the Earth's surface can be regarded as the effects of buried source bodies of different size, shape and density. The complex source bodies can be approximated by a series of bodies of regular shape (e.g. points, spheres, cylinders, prisms) and of assumed density. Analytical methods for the three-dimensional modelling of the gravity anomaly field have been developed in applied geophysics (e.g. Talwani and Ewing, 1960; Cordell and Henderson, 1968; Barnett, 1976; Götze and Lahmeyer, 1988; Bhaskara Rao et al.,1990).

From the different mass models considered as gravity anomaly sources, the point mass model has the simplest form. It is both fast (i.e., real-time computations) and flexible (i.e., local applications). After a point mass model is derived from existing surface gravity anomaly data, the estimation of the gravity anomaly field in the three-dimensional space can be easily performed. This aspect is of interest in the present research (i.e., modelling the gravity anomaly field at a constant elevation above a reference surface). Details regarding point mass modelling of the gravity anomaly field can be found in Sünkel (1981c, 1983), Forsberg (1984b), and Vassiliou (1986).

The spatial modelling of the gravity anomaly field can also be carried out by upward continuation of the surface gravity anomaly data. One method for upward continuation modelling is the continuous approach. For this case, the surface gravity anomalies are assumed first to be known at every point on the Earth's surface and secondly are referred to a level surface. The external gravity anomaly field can be generated by spherical or planar approximations using an upward continuation integral. Heiskanen and Moritz (1967) point out that the upward continuation operation is basically a local problem and, thus, the contribution coming from distant areas is small. Investigations regarding the upward continuation method are reported in Moritz (1962), Hirvonen and Moritz (1963), Rapp (1966), and Cruz and Laskowski (1984).

Another method for upward continuation modelling is the discrete approach. Here, the surface gravity anomalies are known only at discrete points on the Earth's surface and least squares collocation can be utilized. The requirement for data on a level surface is now bypassed. However, extensive computational requirements (i.e., large matrix inversion) may be perceived as a drawback. The application of the discrete approach is described in Rapp (1978), Moritz (1980), Sünkel (1981a), and Cruz (1985).

Other concerns regarding the modelling of gravimetric data include the evaluation of the different frequency parts of the gravity anomaly field and the use of computationally efficient algorithms. Tscherning et al. (1983) investigate the role of spherical harmonic coefficients of the geopotential to represent the long wavelength component of the gravity anomaly field. Models of the geopotential to high degree and order (e.g. Rapp et al., 1991), are used for the representation of the contribution coming from distant regions. This allows for reduced requirements regarding the size of collection areas for data in local gravity field applications and for planar approximation in the calculations.

Topographic heights can be effectively used in local gravity field approximation to model the short wavelength component of the gravity anomaly field. They also offer the advantage of being more readily available than gravity data. The use of topographic heights as a tool in modelling the gravity field is presented in Forsberg and Tscherning (1981b) and Forsberg (1984a). The residual gravity field resulting from the subtraction of the long and short wavelength components is smoother and better suited for modelling by the various algorithms.

Sideris (1984) and Schwarz et al. (1990), among others, have shown that the application of spectral methods based on the Fast Fourier Transform (FFT) algorithms for the solution of problems concerning local gravity field approximation are as accurate as classical methods, but are more efficient.

1.2 Thesis Outline

The objective of the research carried out in this thesis is to produce a consistent, detailed and accurate three-dimensional gravity field model for a mountainous area with rough topography and, consequently, with large variations of the gravity field by combining terrestrial gravity data with elevation data. The Kananaskis area in the Canadian Rocky Mountains was chosen for this task. The terrestrial gravity anomaly data is estimated in space (i.e., at different flight elevations over the investigation area) using complementary models (i.e., point mass and upward continuation integration) as a reference for testing the airborne sensed gravity field. The research is documented in five chapters.

Chapter 2 addresses, firstly, the aspects regarding local terrestrial gravimetric surveys and the calculation of gravity anomalies. Secondly, it is concerned with the collection of the already available terrestrial gravity data and digital elevation models and the densification gravity survey carried out as part of this research. A consistent data base of point gravity data covering the investigation area is compiled and analyzed.

Chapter 3 deals with the usage of the gravity data contained in the data base to produce a regular pattern (i.e., gridding) of surface free-air gravity anomalies. The main method of prediction is least squares collocation with a local covariance function for the data. Different trend removal procedures are employed. For comparison, the interpolation method based on inverse distance weighting is also used. The statistical behavior of the estimated grids of free-air, Bouguer and isostatic gravity anomalies for the test area is analyzed using their covariance functions. The anomaly degree variances provide information on the resolution of the gravity data in the area.

Chapter 4 investigates the spatial modelling of the gravity field by point masses. A two-layer (deep and shallow) point mass model is generated from the surface gravity anomalies. The point mass model is then used to calculate the spatial gravity anomaly field. The computations are carried out in the frequency domain.

Chapter 5 studies the spatial modelling of the surface gravity anomalies by using the upward continuation integration (i.e., Poisson integral) in planar approximation. Specific handling of the different wavelengths components of the gravity field lead to direct and indirect treatment approaches. Investigations regarding the sensitivity of the models, the error aspects and comparisons of results originating from the different methods are incorporated.

Chapter 6 gives conclusions and recommendations following the research.

CHAPTER 2

GRAVIMETRIC SURVEYS

2.1 General

Gravimetry (Latin: gravis = heavy; Greek: μετρω = to measure) means the measurement of the magnitude (i.e., intensity) of the gravity acceleration vector g on or near the surface of the earth. In the following, we will restrict ourselves to terrestrial gravimetry.

The foundation of gravimetry (or gravity surveying) is Newton's law of gravitation ("Philosophiae Naturalis Principia Mathematica", 1685-1687), which formulates the force of attraction F between two particles of masses m_1 and m_2 with very small dimensions with respect to the distance l between them. The scalar equivalent of the force F is expressed by

$$F = \frac{Gm_1m_2}{l^2} \tag{2.1}$$

where G is Newton's gravitational constant.

Furthermore, the attraction of a spherical, non-rotating, homogeneous Earth of mass M and radius R on a small mass m on its surface can be considered. Substituting in equation (2.1), the force of attraction (or gravitational attraction) becomes

$$F = \frac{GM}{R^2}m = mg \tag{2.2}$$

As force is associated to mass by an acceleration, the term

$$g = \frac{GM}{R^2} \tag{2.3}$$

performs that role and represents the magnitude of the gravitational acceleration. For this idealized situation, the gravity would be constant all over the Earth's surface.

If the Earth's rotation is also considered, the result of gravitation (i.e., gravitational acceleration) and centrifugal acceleration (due to the Earth's rotation) is the vector of gravity acceleration (i.e., has both direction and magnitude). The magnitude of the gravity vector is the gravity g. For computational considerations, it is more convenient to define the attraction in terms of the work done to move a unit mass within the gravity field (i.e., potential). The gravitational potential and the centrifugal potential are respectively

$$V = \frac{GM}{r} \tag{2.4}$$

and

$$\Phi = \frac{1}{2}\omega^2(x^2 + y^2) \tag{2.5}$$

where V and Φ are both scalar (i.e., have only magnitude), r is the distance from the Earth's centre of mass to the unit mass, and x and y are Cartesian coordinates of the unit of mass. The sum of the gravitational potential and the centrifugal potential is the gravity potential of the Earth. The first derivative of the gravity potential in any direction provides the gravity component in that direction.

Due to the Earth's ellipsoidal shape, rotation, irregular surface features and internal mass distribution, and the effect of extraterrestrial masses, the gravity varies over the Earth's surface. For an Earth fixed mass point P, gravity can be expressed as a function

$$g_P = g[G, \omega^2; \underline{r}, \rho(\underline{r}'); t] \tag{2.6}$$

where the universal gravitational constant G (6.673×10^{-11} m³kg⁻¹s⁻²) and the square of the Earth's rotation angular velocity ω ($7.292\ 115 \times 10^{-5}$ rads⁻¹) are scaling factors taken as constant parameters. Gravity changes with the point position vector $\underline{r}$ and is also related to the density function $\rho(\underline{r}')$ of the Earth's masses with the position vector $\underline{r}'$ of the mass element dm (= ρdv, with ρ the density and dv the volume element). The term t in equation (2.6) indicates the temporal variation of gravity.

In the Système International d'Unités (SI), the unit of gravity is ms⁻². A mean value (i.e., global average) of g on the Earth's surface is 9.80 ms⁻². For deviations of the gravity values from a model, the unit 1 μms⁻² = 10^{-6} ms⁻² (also denoted as the "gravity unit", g. u.) is also utilized. In this thesis, an additional unit named after Galilei (1 Gal = 1 cms⁻²), 1 mGal = 10^{-5} ms⁻², will be used. Though this is not an SI unit, it is still widely used in geodesy and geophysics.

The gravity measured on the surface of the Earth, being a function of position (i.e., vector $\underline{r}'$), contains information about the measurement location (geodetic application). In addition, the dependence of gravity on the density function $\rho(\underline{r}')$ of the Earth's mass elements provides information about the mass distribution in the interior of the Earth (geophysical application).

The main objectives of gravimetry in geodesy are the determination of the Earth's surface and gravity potential, the reduction of geodetic observables with orientation in the gravity field, and the investigation of vertical crustal movements. The main objective of gravimetry in geophysics is to resolve the density distribution within the Earth (i.e., terrestrial mass distribution).

A global reference system of well established gravity stations of high accuracy (i.e., a gravimetric datum), providing absolute gravity level and scale, is required to achieve a certain level of homogeneity of gravity measurements for geodetic and geophysical purposes. The International Gravity Standardization Net 1971 (I.G.S.N.71) was introduced by a resolution of the International Union of Geodesy and Geophysics (I.U.G.G.), (Morelli et al., 1974). It comprises 1854 gravity stations distributed (not uniformly) over the Earth and the mean accuracy of the network is ± 0.1 mGal. This gravimetric datum replaces the Potsdam Gravity System established in 1909.

As gravity is an acceleration, its measurement comprises length and time determination. Even with such seemingly basic measurements, the precision and accuracy demands in geodesy and geophysics are hard to meet. Absolute gravity measurements require both complex instrumentation and long duration of observation. However, the determination of the relative change of gravity between sites is comparatively easy and is the conventional approach in gravimetric surveys. Absolute gravity values at different locations can be determined by relative gravity measurements at the latter and at I.G.S.N.71 stations.

A comprehensive reference regarding the science of measuring gravitational acceleration (i.e., gravimetry) is Torge (1989).

2.2   Relative Measurement of Gravity

2.2.1 Gravity Instrumentation

The relative measurement of gravity by sensing devices is limited to the observation of one of the two primary acceleration elements (i.e., length and time). By sensing these quantities over two observation points, the gravity difference between them can be determined.

Instruments capable of readily measuring relative gravity variations are known as (relative) gravity meters or gravimeters. These instruments consist essentially of a constant mass fixed at the end of a spring. A change in gravity causes a variation in the weight of the mass and this leads to a modification of the length of the spring. Conversely, a restoring force (realized by the elastic/balance spring) returns the mass to equilibrium and allows the determination of the change in gravity. According to Torge (1989), a mass m suspended by a vertical (direction z) spring balance of initial length l_0 that changes to a length l because of a change in the gravity g, has the equilibrium condition equation for the gravity force mg and the spring force $k(l-l_0)$

$$mg - k(l - l_0) = 0 \qquad\qquad (2.7)$$

where k is a proportionality constant according to Hooke's law of elasticity (formulated in 1678, and relating change in force with change in length). Gravimeters developed based on this linear system are known as stable or static gravimeters.

The gravity values over the Earth's surface vary in a relatively narrow interval of approximately 5500 mGal and 0.1 mGal represents about 1×10^{-7} of the gravity at any point on the Earth. In order to detect small changes in gravity between points, the sensitivity requirements for gravimeters are high. The dual role of the spring as support for the mass m and as a measuring device for the length $(l - l_0)$ impeded the sensitivity of early gravimeters.
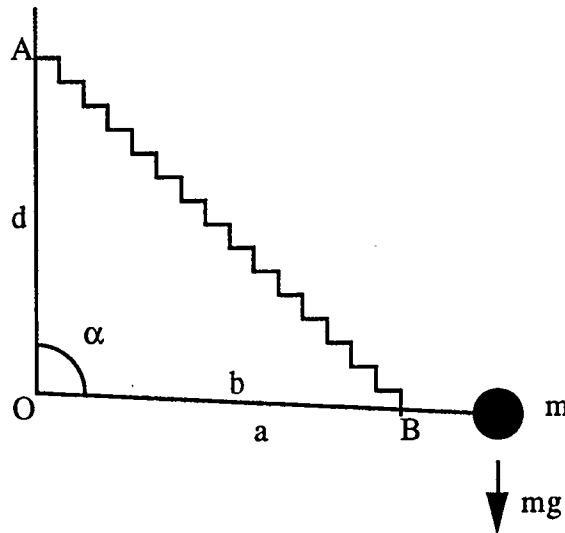
Figure 2.1 Principle of the gravimeter with horizontal lever and oblique restoring spring
(a = Om, b = OB, d = OA)

This problem is overcome in current gravimeters by using a supplementary (amplifying) force acting in the same sense as the extension/contraction of the spring. The result is an increase of the displacement of the spring due to a change in gravity. Such a system consists of a lever (or beam) and a restoring force (realized by the spring balance) that returns the beam to the horizontal (or null) position. The equilibrium condition equation for this rotating system is (Torge, 1984)

$$mga - kbd\sin\alpha = 0 \qquad (2.8)$$

if $l_0 = 0$ (zero-length spring) is considered; α is the angle of the beam with the vertical, and a, b, and d are distances within the component segments of the system (see Figure 2.1). This causes the restoring force to be proportional to the physical length l of the spring rather than its incremental length $(l - l_0)$. The result is a more sensitive response to changes in gravity and a wider measuring range. Gravimeters based on this non-linear system are known as unstable or astatic.

A null instrument indicates changes in gravity by an arbitrary scale. In order to convert the scale (or counter) units (C.U.) into gravity units, a calibration function is necessary. By design, a linear correspondence is sought between the reading in counter units and gravity [i.e., $F(z) = g$, where z is the reading (in C.U.)]. However, non-linear and periodic errors are still present in the transformation function. The manufacturer establishes a calibration function in the laboratory (by simulating gravity changes) and/or in the field environment (by using points with known gravity or gravity differences). This function could be the sum of an approximation by a low degree polynomial (for the linear and non-linear parts) and by a Fourier series (for the periodic part). Because the calibration function changes with time, repeated checks by the user over a reasonable part of the instrument measuring range is warranted. A basic formulation of the calibration function $F(z)$ is given by Torge (1989) as

$$F(z) = N_0 + F_0(z) + \Delta F(z) \tag{2.9}$$

where N_0 is the instrument level, $F_0(z)$ is an approximation of the calibration function, and $\Delta F(z)$ is a correction to the approximation. By differencing the readings over two points, the term N_0 is eliminated.

Two of the most widely used gravimeters are the LaCoste-Romberg and Worden instruments. The LaCoste-Romberg system (Krieg, 1981) is an astatized metal spring instrument and was the first to introduce the zero-length spring. The model G has a precision of ± 0.004 mGal and an approximate measurement range of 7000 mGal. The Worden system (Woollard, 1950) is an astatized quartz spring instrument. Its principle is similar to the LaCoste-Romberg system. However, in this case the lever beam is supported by two springs. One is used as a measuring device and the other can alter the level of the reading range of the instrument. The Master model of the Worden system has

a precision of ±0.01 mGal and a measuring range of approximately 200 mGal, and by resetting the instrument the range can be extended to approximately 6000 mGal. The sensitivity to temperature, pressure, and magnetic field changes is reduced by particular manufacturing design features of the two gravimeter systems.

Information regarding existing gravimeter systems can be found, among others, in Parasnis (1979), Torge (1989) and Telford et al. (1990).

2.2.2 Instrumental Error Sources and Accuracies

Several interferences can adversely affect the measurement system of spring gravimeters. Though their effect is diminished by special provisions in the instrument design, residual effects with random and/or systematic attributes still remain. The errors can be categorized according to their source as instrument related and external.

The instrument errors are due to the gravimeter characteristics and comprise reading errors, leveling errors, elastic hysteresis, errors in calibration function, and unsteady voltage. The external errors come from variations in the atmospheric temperature and pressure, magnetic fields, and shocks.

A systematic error related both to instrumental and external factors is the gravimeter drift. This is a gradual variation in time of the null (i.e., zero) reading position. This error is exhibited both in stationary and field (i.e., transport) operations, and affects quartz spring gravimeters more than metal spring gravimeters.

The drift of a gravimeter can be modeled as a function of time (Drewes, 1978) with a Taylor series expansion of the reading z (in counter units) or F(z) (in gravity units) as

$$z(t) = z(t_0) + D(t) \qquad (2.10)$$

where $z(t)$ is the reading at a particular time t, $z(t_0)$ is the reading at a reference time t_0, and $D(t)$ is the sum of the time dependent higher order terms in the series expansion. The drift can be determined by repeated measurements (i.e., station reoccupation) according to an appropriate measuring schedule.

The accuracy of relative gravity observables can be estimated a priori from an error budget of the different error sources, and a posteriori from a least-squares adjustment. Torge (1984) estimated standard deviations from the error budget of LaCoste-Romberg gravimeters. Gravity differences of less than 100 mGal observed once with average measuring conditions can be determined with a model G gravimeter with a standard deviation of ±0.017 mGal considering only random error components and with a standard deviation of ±0.027 mGal if systematic components are included. Accuracies achievable for other gravimeter systems can be found, for example, in Torge (1989).

2.2.3 Gravity Corrections and Reductions

Gravity measurements should undergo certain corrections and reductions before their use in computations. Two of these corrections (i.e., conversion from counter units to acceleration and drift correction) have been introduced in Section 2.2.2. Other reductions can minimize the temporal gravity changes and refer the data to a particular point.

Temporal gravity changes are due mainly to earth tides, polar motion, variations of atmospheric pressure, and ground water level and soil moisture. The latter three have very small influence and should be considered only for very high accuracy requirements. The former which is due to the variation in gravitational attraction of the Moon and the Sun, can have a maximum amplitude of up to 0.3 mGal in a period of approximately 12 hours. The theoretical tidal gravity variations can be calculated by different approaches depending on the accuracy requirements. The computation from the expansion of the tidal potential after Cartwright-Tayler-Edden (Cartwright and Tayler, 1971; Cartwright and Edden, 1973) is indicated by the I.A.G. Recommendation No. 11, 1971. According to Nettleton (1976), a simpler formula for the tidal acceleration effects, δg_{tidal}, is

$$\delta g_{tidal} = \frac{3GRM_M}{2D_M^3}(\cos 2\alpha_M + \frac{1}{3}) + \frac{3GRM_S}{2D_S^3}(\cos 2\alpha_S + \frac{1}{3}) \qquad (2.11)$$

where M is the mass, D is the distance from the Earth, α is the geocentric angle, and the subscripts M and S refer respectively to the values for the Moon and Sun.

Corrections to the measurements in the horizontal and vertical directions ascribe the data to a reference point. The height reductions are made usually with the normal gravity

gradient (i.e., 0.3086 mGal/m). Using the same instrument height can alleviate the necessity for this correction when the relative gravity change is determined between sites.

2.3 Gravity Anomalies

2.3.1 General

The intensity of gravity over the surface of the Earth depends mainly on latitude, elevation, topography of surrounding terrain, and density variations in the subsurface including the surrounding terrain. In order to make the gravity measurements more amenable for calculations (especially in geodesy) and for interpretations (especially in geophysics), certain reductions should be carried out. These reductions produce the most important disturbing quantity related to the gravity field, namely the gravity anomaly. The gravity anomaly Δg_P is the difference between the observed gravity g_P at point P on a geopotential surface and the gravity caused by a particular model for the gravity on a spheropotential surface

$$\Delta g_P = g_P - \gamma_Q \tag{2.12}$$

where γ_Q is the normal gravity at point Q which is the projection of point P onto the spheropotential surface.

Gravity varies with latitude due to the Earth's ellipsoidal shape and its rotation; it increases from equator to the poles. Heiskanen and Moritz (1967) express the dependency of the normal gravity γ_0 [or $\gamma(\phi)$] to latitude ϕ on a reference ellipsoid with the standard equation

$$\gamma_0 = \gamma_e(1 + \beta \sin^2 \phi - \beta_1 \sin^2 2\phi) \tag{2.13}$$

where γ_e is normal equatorial gravity and β, β_1 are constants related to the characteristics of the reference ellipsoid. By differentiation of equation (2.13), the latitude correction for the gravity on an ellipsoid (or meridian gravity gradient) is in spherical approximation

$$\delta g_{latitude} = \frac{\partial \gamma(\phi)}{\partial(R\phi)} = \frac{1}{R} \frac{\partial \gamma(\phi)}{\partial \phi} \doteq 0.8 \sin 2\phi \ mGal/km \tag{2.14}$$

and it must be added to γ from the equator to the poles. Considering the parameters given by Moritz (1984) for the Geodetic Reference System 1980 (GRS80), the meridian gravity gradient is $0.813\sin2\phi$ mGal/km.

Examining equation (2.3), gravity varies inversely with the square of the radial distance. If no gravitational effect of masses between points at different ellipsoidal heights h is taken into account (i.e., free-air), the average rate of change in gravity (or vertical gravity gradient) can be obtained by differentiating equation (2.3) (i.e., spherical approximation) in a normal gravity field

$$\delta g_{\text{free-air}} = \frac{\partial g}{\partial h} = \frac{\partial g}{\partial R} = -\frac{2GM}{R^3} \doteq -\frac{2\gamma}{R} \doteq -0.3 \text{ mGal/m} \tag{2.15}$$

The minus sign indicates that gravity decreases with increasing elevation. The application of this reduction to gravity measurements accounts only for the difference in elevation between points (i.e., free-air reduction). The vertical derivative of a series expansion of the normal gravity to the order of flattening of the ellipsoid yields at latitude 45° a normal vertical gravity gradient of 0.3086 mGal/m.

In view of the dependency on latitude and height of the gravity, normal gravity can be expressed in the vicinity of the Earth by the series expansion (Heiskanen and Moritz, 1967)

$$\gamma(\phi,h) = \gamma_0 + [\frac{\partial\gamma(\phi)}{\partial h}]_0 h + \frac{1}{2}[\frac{\partial^2\gamma(\phi)}{\partial h^2}]_0 h^2 +... \tag{2.16}$$

Torge (1989) expresses the normal gravity for the GRS80 reference ellipsoid as

$$\gamma(\phi,h) = \gamma_0 - 0.30877(1 - 0.00142\sin^2\phi)h + 0.75 \times 10^{-7}h^2 \text{ mGal} \tag{2.17}$$

where the ellipsoidal height h is in m.

The normal gravity calculated with the equation and parameters of the GRS80 contains the gravitation of the atmospheric mass. If this equation is used for the computation of

gravity anomalies, an atmospheric gravity correction δg_{atm} has to be added to the observed gravity. Torge (1989) gives the following equation for its calculation

$$\delta g_{atm} = 0.874 - 0.99 \times 10^{-4} h + 0.356 \times 10^{-8} h^{-8} \text{ mGal} \qquad (2.18)$$

where the height h is in m. On the ellipsoid, its value amounts to 0.87 mGal and it decreases with increasing height. Values for the atmospheric gravity correction are tabulated in Moritz (1984).

2.3.2 Free-air, Bouguer and Isostatic Gravity Anomalies

According to the type of reduction, i.e., removal of attraction effect of the visible mass anomalies and of the compensating masses, there are several types of gravity anomalies. A free-air reduction of gravity measured on the surface of the Earth is obtained by applying the vertical component of the gravity gradient combined with the height of the point above the geoid, and furthermore by subtracting the normal gravity calculated on the reference ellipsoid. The equation for the resulting free-air anomaly $\Delta g_{\text{free-air}}$ is

$$\Delta g_{\text{free-air}} = g - \frac{\partial g}{\partial H} H - \gamma_0 = g + \delta g_{\text{free-air}} - \gamma_0 \qquad (2.19)$$

where $\partial g / \partial H$ is the vertical component of the gravity gradient. Usually $\partial \gamma / \partial h$ is substituted for $\partial g / \partial H$, and by subtracting from the surface gravity the normal gravity evaluated with equation (2.16) or (2.17) the resulting anomaly is the surface free-air anomaly. The presence of the point height in the reduction indicates a strong correlation between the free-air gravity anomaly and the height.

The combination of the free-air reduction with a further removal of the gravitational attraction of the topographic masses from the surface point down to a reference (usually the geoid) is called complete Bouguer reduction. The resulting value is the Bouguer gravity anomaly

$$\Delta g_{\text{Bouguer}} = g + \delta g_{\text{free-air}} - \delta g_{\text{topography}} - \gamma_0 = \Delta g_{\text{free-air}} - \delta g_{\text{topography}} \qquad (2.20)$$

where $\delta g_{\text{topography}}$ is the topographic reduction.

The Bouguer gravity anomaly can be obtained in a first approximation by taking into account only the gravitation of a horizontal plate with infinite radius and thickness equal to the height of the computation point. With a standard density ρ = 2.67 g/cm^3, the attraction of the Bouguer plate is

$$\delta g_{plate} = 2\pi G \rho h = 0.1119 h \text{ mGal} \tag{2.21}$$

where G is the gravitational constant and the height h is in m. To account for variations of the topography from the idealized Bouguer plate, a terrain correction can be included for improved accuracy of the topographic reduction. The terrain correction is always positive and can be evaluated by integrating bodies of constant density deviating from the Bouguer plate (Hammer, 1939). Moritz (1968) gives a linear approximation equation for the terrain correction as

$$\delta g_{tc} \doteq \frac{1}{2} G \rho \iint_{\sigma} \frac{(h - h_P)^2}{l_0^3} dx dy \tag{2.22}$$

where the integration is carried out in a limited area σ, h_P and h are the heights of the computation point and the data points, respectively, and $l_0 = [(x_P - x)^2 + (y_P - y)^2]^{1/2}$ is the distance from the computation point to the height data. The evaluation of the terrain correction can be performed by efficient spectral domain techniques (Sideris, 1984; Forsberg, 1985). By utilizing additional slope information, the accuracy of the terrain correction calculation (Blais and Ferland, 1984) can be improved significantly in areas of rugged topography. Other work regarding the computation of terrain corrections can be found for example in Sideris (1990), Li (1993), Sideris and Li (1993), and Li and Sideris (1994).

The application of the terrain correction to the Bouguer anomaly obtained by considering only the attraction of the Bouguer plate, produces the refined Bouguer gravity anomaly. Usually in practice, the Bouguer reduction is calculated by applying first the Bouguer plate reduction and then the terrain correction. However, the calculation of the two can be combined by computing by integration the total effect of the topographic masses as

$$\delta g_{topography} = \delta g_{plate} - \delta g_{tc} \qquad (2.23)$$

This can be done efficiently by three-dimensional Fast Fourier Transform (Peng, 1994; Peng et al., 1994).

The following remarks can be made about the Bouguer gravity anomalies: are dependent on the density value used in computing them; do not depend locally on the topography, but over a region they present strong correlations with the topographic features; in mountainous areas they have large negative values. An explanation of the latter is that the visible topography is compensated to account for a possible mass deficiency under mountains according to an isostatic model. Heiskanen and Vening Meinesz (1958) and Heiskanen and Moritz (1967) present some of the most common systems for the isostatic reduction (i.e., Pratt-Hayford, Airy-Heiskanen, Vening Meinesz). The consideration of the attraction of the compensating masses $\delta g_{isostatic}$ in gravimetric reductions leads to the isostatic gravity anomalies

$$\Delta g_{isostatic} = g + \delta g_{free-air} - \delta g_{topography} + \delta g_{isostatic} - \gamma_0 \qquad (2.24)$$

These anomalies are small, smooth and randomly positive and negative. The former two characteristics make the isostatic anomalies better suited for predictions than the other anomalies.

Comprehensive material on gravimetric reductions can be found in Heiskanen and Vening Meinesz (1958) and Heiskanen and Moritz (1967).

2.4 Regional/Local Gravimetric Surveys

2.4.1 Gravity Survey Considerations and Calculations

Geodetic and geophysical applications require collection of gravity data by gravimetric surveys. Subsequently, the observed point gravity data are reduced to gravity anomalies. Usually a homogenous representation is required for the gravity field, and prediction of estimates from the discrete data becomes necessary. To assist in the adequate representation of the gravity field in an area, a gravity survey should consider the

following aspects for the selection of the observation points: size of the area to be surveyed; magnitude and variation of the gravity field; representative spatial distribution of measurements; accuracy of gravity measurements and of their spatial location; access capabilities; time requirements.

Regional and local gravity surveys are carried out with spring gravimeters. The gravity measurements are performed in a controlled manner (i.e., repeated measurements, loops) and tied to a control gravity network. The misclosures can then be proportionally distributed as a function of time. For a better modelling of the gravity field observations, a least-squares adjustment has to be considered. The parametric functional model can use as an observable either the calibrated counter reading l_i at each station i, or the calibrated counter reading difference $\Delta l_{i,j}$ between each pair of stations i and j. The former and the latter models (Torge, 1989) are given by the equations

$$l_i + v_i = g_i - N_0 - \Delta F(z_i) + D(t_i) \qquad (2.25)$$

$$\Delta l_{i,j} + v_{i,j} = g_j - g_i - [\Delta F(z_j) - \Delta F(z_i)] + [D(t_j) - D(t_i)] \qquad (2.26)$$

where v is the correction to the observation, g is the gravity value, N_0 is the gravimeter level unknown, $\Delta F(z)$ is the calibration correction, and D(t) is the drift parameter. The precision estimates for measurements and parameters are evaluated as part of a least-squares adjustment.

The spatial location of the gravity stations must be established for identification and computation of gravity reductions. The methods for horizontal and vertical location should be in accordance with the precision requirements for the gravimetric products. Available information from existing control points, topographic maps, and aerial photographs can be used for spatial location of the gravity points. However, if such information is not available, terrestrial and/or space methods of spatial location have to be utilized.

An examination of the equations in Section 2.3.2 and Section 2.3.3 can give an indication about the influence of precision of the horizontal and vertical positions for certain gravimetric computations. The calculation of the normal gravity on the reference ellipsoid varies with the latitude coordinate. According to equation (2.14), the normal gravity value

can be calculated at an accuracy level of ±0.05 mGal, if the latitude is determined with a precision of approximately ±2" (i.e., ±60 m). This corresponds to ±1.3 mm precision for scaling from a 1:50 000 map. However, the requirements for the precision of heights in gravimetric reductions are more stringent. Height differentiation of the free-air reduction equation (2.19) and of the Bouguer reduction (only the plate reduction) equation (2.20), leads respectively to the equations

$$\sigma_{\delta g_{free-air}} = 0.3086\sigma_h \qquad (2.27)$$

$$\sigma_{\delta g_{plate}} = 0.1967\sigma_h \qquad (2.28)$$

where σ_h is the precision of the height measurement, $\sigma_{\delta g_{free-air}}$ is the precision of the free-air reduction, $\sigma_{\delta g_{plate}}$ is the precision of the Bouguer plate reduction, the coefficient 0.3086 represents the normal free-air gradient, and the coefficient 0.1967 is the difference between the free-air gradient and the Bouguer plate gradient (i.e., 0.1119 for standard density $\rho = 2.67$ g/cm^3). If the precision for the free-air and Bouguer plate reductions are given in mGal, the resulting height precision is in m. According to the former and the latter equations, a precision of ±1 mGal for the free-air and the Bouguer plate reductions will be obtained if height precisions of ±3.2 m and ±5.1 m, respectively, are available.

Aspects on gravity surveys (including field procedure, data reduction and adjustment, precision) are treated, among others, in Nilsen (1976), Drewes (1978), Torge (1984), and Torge (1989).

2.4.2 Gravimetric Products and Archival of Data

The main gravimetric products are point gravity data and point gravity anomalies. These quantities can be considered as immediate gravimetric products. The archival of these data for further usage is of utmost importance. The information considered useful is dictated by the type of gravity survey. Regional and local surveys are less demanding regarding the information for each gravity point. However, the following items are necessary: station number, geographical or plane coordinates, height, gravity, gravity anomaly, associated precisions. This information can be supplemented with photographs, sketches, and topographic map extracts.

However, for many applications in geodesy and geophysics there is a requirement to derive other products originating from the primary gravimetric data. These are mean gravity anomalies, maps of isoanomalies, and gravity anomalies on regular grids.

The large amount of gravity data acquired from gravimetric surveys is usually compiled into data bases. The data coming from different sources must undergo quality checks, transformations to a unified reference system, and application of standard reductions for conversion to gravity anomalies.

Torge (1989) reviews extensively this topic. Buck and Tanner (1972), Tscherning (1981), and McConnell (1982) are references for the related aspects of gravity data bases.

2.5   Gravity and Elevation Data in the Kananaskis Area

2.5.1 Existing Gravimetric and Elevation Data

The Kananaskis area is a provincial recreation area situated in the Canadian Rocky Mountains approximately 100 km west of Calgary, Alberta. Due to its high gravity field variability, the area is considered suitable for testing the airborne gravity-based system over an area with rugged topography. For this purpose, an accurate (i.e., at the level of 1mGal or better) and high resolution (i.e., gravity points with spacing of 2 km to 4 km) gravity field model is required for the area bounded by latitudes 50°30' to 51°15' and longitudes 244°30' to 245°15'. Within this core area of 83.4 km by 52.6 km (i.e., 4388.7 km²) is the location for the test. Figure 2.2 shows the topographic model for the core area at a resolution of 1' x 1' (i.e., 1.9 km x 1.2 km) derived from the 1 km x 1 km digital elevation model. The topographic model and the interpolation software was provided by the Department of Energy, Mines and Resources Canada

Because the computations required for the gravity field model on the Earth's surface and at elevations above it involve predictions (i.e., interpolation and/or extrapolation) and summations (i.e., integration), a larger area is considered for the gravity data collection. This extended area is located between the latitudes 50°15' and 51°30' and longitudes 244°15' and 245°30' and the dimensions of the rectangle are 139.0 km and 87.7 km, respectively, (i.e., 12190.7 km²). Statistics regarding the 1' x 1' topographic model for the extended and the core areas are given in Table 2.1.
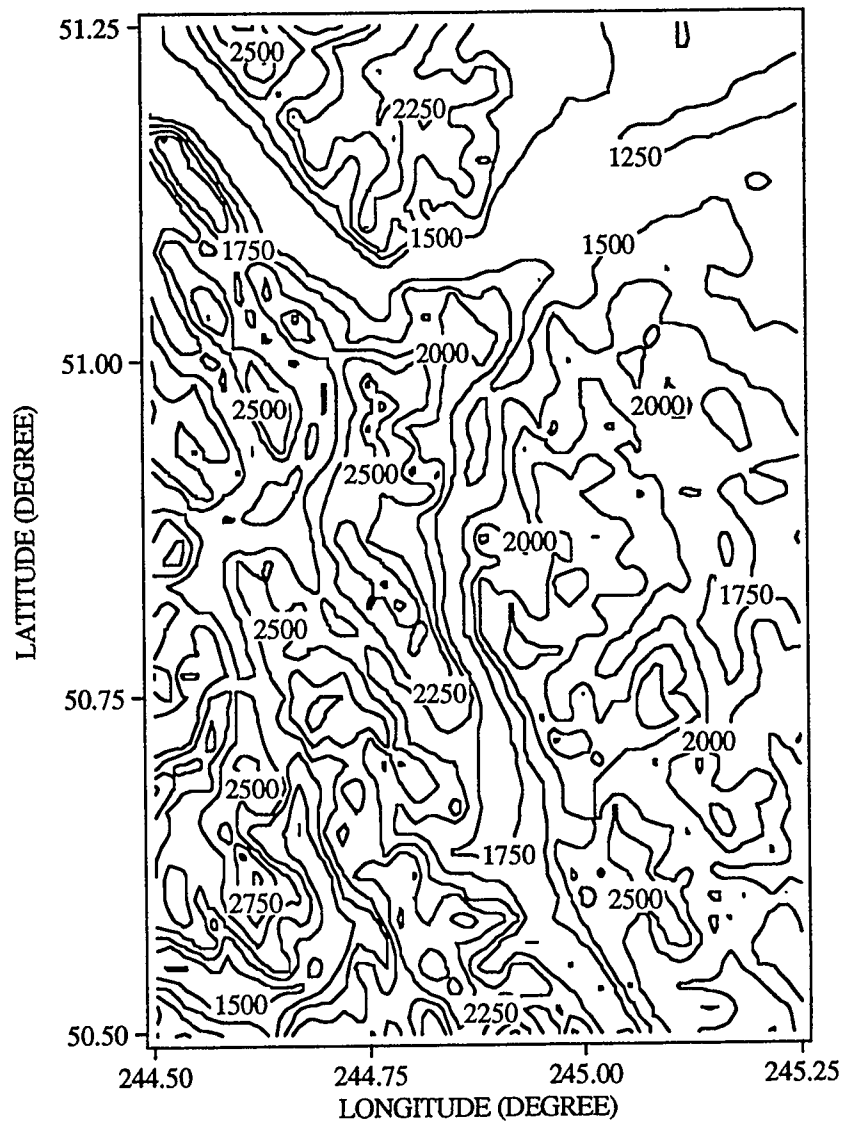
Figure 2.2 Topographic model of the Kananaskis core area (Contour interval: 250 m)

Table 2.1 Statistics of the topographic model of the Kananaskis area (Unit: m)

Area	Minimum	Maximum	Mean	Std. Deviation
Extended	908.4	3231.1	1842.8	402.3
Core	1183.0	2985.3	1962.4	373.9

A major part of the gravimetric data in the Kananaskis area comes from the data base of the Department of Energy, Mines and Resources Canada. As of November 1991, there

are 150 gravity points in the North America Gravity data base covering the Kananaskis area. From these data, 64 gravity points are situated in the core area [see Figure 2.3 (a)]. These data provide a relatively uniform coverage with an approximate data spacing of 8 km to 10 km. The information given for each data point includes: latitude (degree), longitude (degree), height (m), Faye anomaly (mGal) corrected for the atmospheric attraction, standard deviation (mGal), and terrain correction (mGal). The Faye anomaly is a free-air gravity anomaly corrected by a terrain correction (Heiskanen and Vening Meinesz, 1958; Torge, 1989). The gravity anomalies were calculated using the parameters of the Geodetic Reference System 1980 (Moritz, 1984) for the normal gravity formula and for the atmospheric gravity correction as a function of elevation.

These gravity data have been supplemented by gravity surveys carried out in the 1980's. In 1980, nine gravity base stations were established in the core area by the Department of Energy, Mines and Resources Canada [see Figure 2.3 (b)]. These stations are part of the Canadian National Gravity Net and, thus, refer to the I.G.S.N.71 (Morelli, 1974). The locations of two of these stations coincides with those of two geodetic control stations. For each station the following information is given: name, location description, latitude (degree), longitude (degree), height (m), accuracy factors for spatial location, gravity (mGal), identifier number.

In 1981, the existing gravity data were densified on behalf of The University of Calgary by the Department of Energy, Mines and Resources Canada. During this survey, 63 gravity stations were established within the core area at geodetic control points of a network set up by The University of Calgary [see Figure 2.3 (c)]. The information available for each gravity station comprises: identifier number, latitude (degree, minute), longitude (degree, minute), height (m), gravity (mGal), free-air gravity anomaly (mGal), Bouguer gravity anomaly (mGal), and accuracy factors. The gravity data refer to the I.G.S.N.71 (Morelli, 1974), the gravity anomalies were calculated with the theoretical gravity formula of the Geodetic Reference System 1967 (I.A.G., 1971), the correction for the atmospheric attraction was not applied, and the Bouguer gravity anomalies were computed using a density of 2.67 g/cm^3.
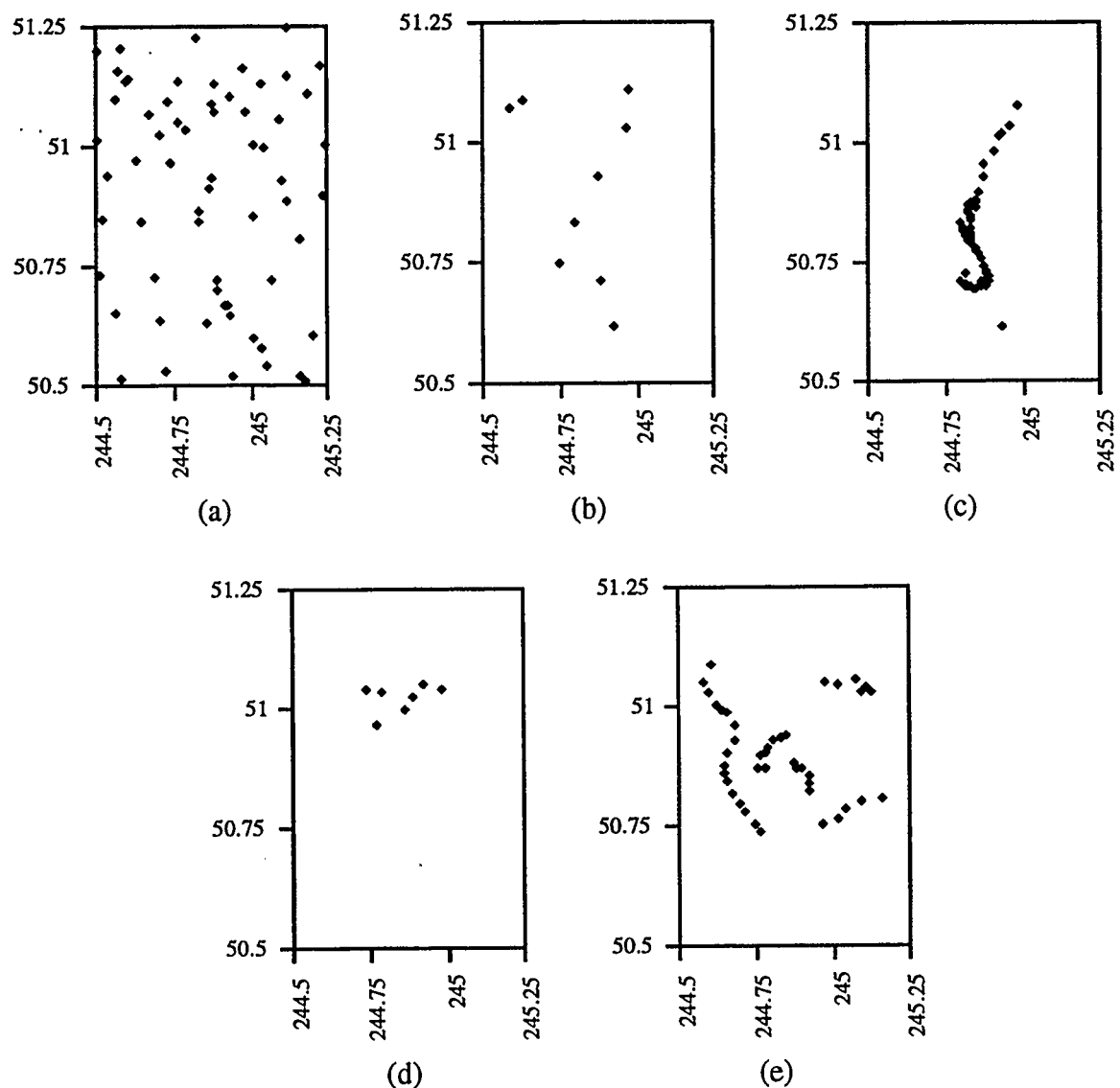
Figure 2.3 Layout of gravity points in the Kananaskis core area from (a) North America Gravity data base and the gravity surveys of (b) 1980, (c) 1981, (d), (e) 1985 (Unit of latitude 50.5 - 51.25 and longitude 244.5 - 245.25: degree)

In 1985, two densification gravity surveys were performed by The University of Calgary in the core area. The first gravity survey (Forsberg, 1986) was comprised of seven gravity points from which five stations were situated on mountain tops [see Figure 2.3 (d)]. The information for each station includes: identifier number, name, latitude (degree), longitude (degree), height (m), gravity (mGal), free-air gravity anomaly, and Bouguer gravity anomaly (mGal). The position of the stations were determined from 1:50 000

maps, the heights were measured by barometric levelling, and the gravity anomalies were calculated under the same considerations as those used for the gravity survey of 1981.

The second gravity survey carried out in 1985 (Milne, 1986) added 43 gravity stations and was aiming at a more uniform coverage within the core area [see Figure 2.3 (e)]. The documentation regarding the gravity stations provides: station number, gravity (mGal), latitude (degree, minute, second), longitude (degree, minute, second), height (m) with their associated standard deviations, and station description. The positions were determined by scaling from 1:50 000 maps and by photogrammetry, and the heights were measured by barometric levelling and by photogrammetry.

Considering the topographic characteristics of the area (i.e., rugged topography), the use of digital elevation models play an important role in improving the gravity field modelling by taking into account the gravimetric terrain effects. The Department of Energy, Mines and Resources Canada has provided a digital elevation model of 1 km x 1 km covering most of western Canada. However, in mountainous areas the influence of the topographic masses in the proximity of gravity stations can have a significant influence and a more detailed grid of elevations is necessary for adequate modelling. In view of this requirement, The University of Calgary has acquired during 1993 from Alberta Forestry, Lands and Wildlife a digital elevation model of 0.1 km x 0.1 km. The latter elevation grid covers approximately 68% of the extended area and almost 90% of the core area (see Figure 2.4). The parts of the area not covered by the detailed digital elevation model are located on the west and south-west sides. Also, investigations of the model revealed some inconstancies were present in relation to existing topographic maps on its west and south-west sides.

2.5.2 The 1992 Gravity Densification Survey

In order to improve the existing gravity coverage in the Kananaskis area, a densification gravity survey was carried out in 1992 by the Department of Geomatics Engineering of The University of Calgary. A Worden Master gravimeter (number 781) of Texas Instruments, Inc., Houston, was provided by the Department of Geology and Geophysics of The University of Calgary for this purpose. The instrument features a thermostat, a small dial constant of 0.1025 mGal/dial division, a direct measurement range of 2200

divisions (i.e., 225.6 mGal), a reading precision of 0.01 mGal, and a resetting device that allows the instrument range to be extended to more than 600 mGal.
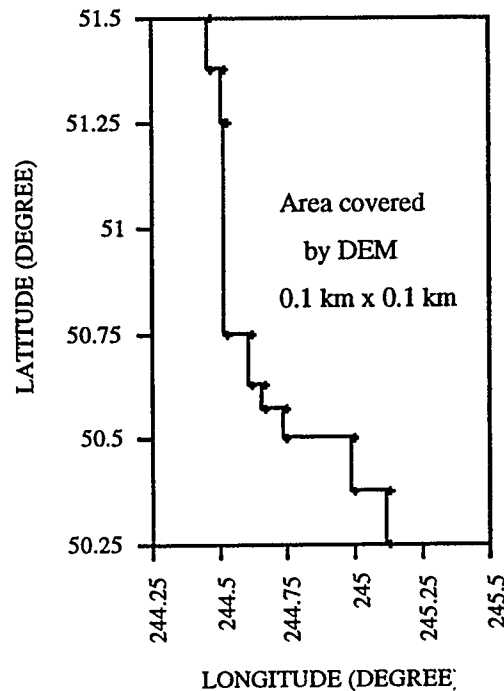
Figure 2.4 Coverage of the Kananaskis extended area by the 0.1 km x 0.1 km digital elevation model

During this campaign, 99 new gravity points were occupied with the gravimeter. Out of these, 93 points are situated in the core area [see Figure 2.5 (a)]. The access to the points was mainly by road vehicle and on foot. A total of 12 gravity points were accessed by helicopter. Five of the base stations established by the Department of Energy, Mines and Resources Canada in 1980 were used for control in the gravity densification survey. After preliminary calibration (i.e., conversion of scale units into gravity units) and reductions (i.e., gravimetric tidal reduction; vertical reduction to ground marker), a least-squares adjustment was carried out. The estimates in the adjustment are the gravity values at the observation points together with drift (one for each day of observation) and instrument scale/calibration correction (one for the whole campaign) parameters. Statistics regarding the estimated gravity values are given in Table 2.2. The gravimetric tidal reduction corrections were in a range between -0.10 mGal to 0.14 mGal. If the latter corrections would have been neglected, an evaluation of the instrument drift would not have been

possible. The estimated drift varied within a range of -0.06 mGal/hour to 0.05 mGal/hour. Because the level of the instrument had to be altered on a few occasions during the campaign, to allow measurements at different height ranges, it is not possible to comment on the overall drift pattern during the survey. The correction to the scale parameter of the gravimeter lowers the scale value by 0.2%. The conclusion that the scale parameter has changed with time cannot be made from this survey. There was no information available on the standard deviations associated with the gravity stations and of the exact position of the actual gravity point. Least-squares adjustment tests were carried out with the standard deviations assigned to the gravity control stations ranging from 0.00 mGal to 0.15 mGal. No significant differences were produced in the estimated parameters. Eventually, the gravity control stations were kept fixed in the adjustment.
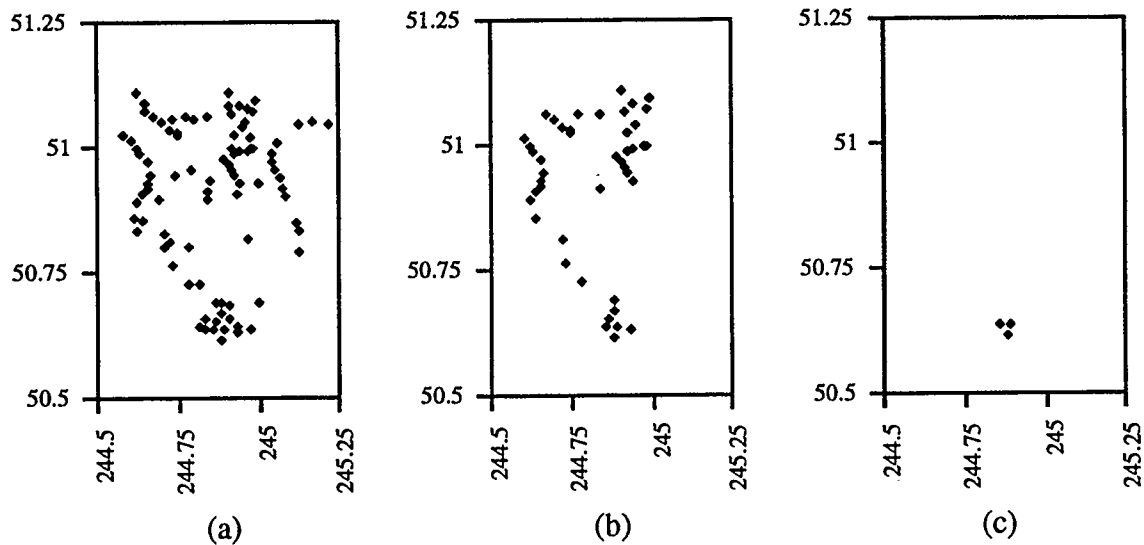
Figure 2.5 Layout of gravity points in the Kananaskis core area of the gravity survey of 1992 with heights determined by (a) barometric levelling, (b) photogrammetry, (c) GPS
(Unit of latitude 50.5 - 51.25 and longitude 244.5 - 245.25: degree)

Table 2.2 Statistics of the 1992 gravity densification survey for gravity and its standard deviation (Unit: mGal)

Data	Minimum	Maximum	Mean	Std. Deviation
Gravity	980379.4	980786.7	980657.4	93.2
Std. Dev. Gravity	0.04	0.12	0.07	0.02

For subsequent identification, gravimetric reductions, and utilization of the gravity data the spatial locations of the gravity points were determined. The horizontal positions (i.e., latitude and longitude) were scaled from 1:50 000 maps with an accuracy at the level of 0.4 mm; this accuracy corresponds to approximately 20 m on the ground, and considering the latitude component it will cause an error of less than 0.02 mGal in the calculation of normal gravity. The following maps produced by the Department of Energy, Mines and Resources Canada were used: 82/J/10, 82/J/11, 82/J/14/, 82/J/15, 82/O/2 and 82/O/3. To provide homogenous and increased accuracy for heights, 3 of the gravity control stations were connected by spirit levelling to existing levelling bench marks in the area; one of the other gravity control stations used is a geodetic control point. The heights for all gravity points were determined by barometric levelling. Additionally, 44 heights were determined by photogrammetry and 3 heights by GPS [see Figure 2.5 (b) and (c), respectively]. The final height estimates were the result of a parametric least-squares adjustment comprising the barometric derived height differences, the photogrammetric, and GPS derived heights.

Table 2.3 Statistics of the 1992 gravity densification survey for height and its standard deviation (Unit: m)

Data	Minimum	Maximum	Mean	Std. Deviation
Height	1244.6	2993.0	1708.4	397.0
Std. Dev. Height	0.4	8.5	3.5	1.6

Table 2.4 Statistics of the 1992 gravity densification survey for standard deviation of free-air and Bouguer gravity anomaly (Unit: mGal)

Std. Deviation	Minimum	Maximum	Mean	Std. Deviation
Free-air Anom.	0.1	2.6	1.1	0.5
Bouguer Anom.	0.1	1.7	0.7	0.3

Besides the statistics regarding the gravity data of the 1992 gravity densification survey in the Kananaskis area, the heights and their effect in the calculation of gravity anomalies were also investigated for the assessment of the survey. Table 2.3 gives the statistics of

the height data and their standard deviations, and Table 2.4 presents the standard deviations of gravity anomalies calculated from the estimated gravity and height data.

From Table 2.2 and Table 2.3, it can be seen that the gravity field and the topography, respectively, have large variations in this area. Table 2.4 indicates that gravity anomalies can be calculated with a precision at the level of 1 mGal. The main limiting factor in their precision comes from the standard deviation of the height component.

2.5.3 Reduction to Gravity Anomalies

It is intended to join together the different data sets and perform gravity reductions of the same standard. For each gravity point in the extended area, terrain corrected free-air, complete Bouguer, and isostatic gravity anomalies are calculated. Examining the information available for the gravity data (i.e., 371 points in the extended area, from which 279 points lie in the core area), two sub-sets of data were considered for the gravimetric reduction. One sub-set comprises a total of 221 gravity points originating from the gravity surveys of 1980, 1981, 1985, and 1992. The other sub-set contains the gravity data (i.e., 150 points) of the North America Gravity data base. The formulae used for these reductions are those from Section 2.3.2. The methodology employed for the calculation of the gravity anomalies of the first sub-set follows.

The reference normal gravity field considered is that implied by GRS80. Due to the rugged topography, the use of a simplified free-air reduction (i.e., only subtraction of the normal gravity evaluated at the height of the point on the Earth's surface) can introduce systematic effects. To reduce these adverse effects, additional precautions are taken; namely taking into account the atmospheric gravity correction, considering the dependence of the vertical gravity gradient on the geodetic latitude, and the inclusion of the second order term of the vertical gravity gradient. In the Kananaskis area, the former correction varies between 0.6 mGal and 0.8 mGal, and the influence of the latter free-air vertical gravity gradient inclusions range between 0.1 mGal and 0.6 mGal. Equations (2.17) and (2.18) were used for the calculation of the normal gravity and the atmospheric gravity correction at the gravity points, respectively. The surface free-air gravity anomalies were calculated with equation (2.12). Due to the rugged topography, the free-air gravity anomalies are corrected by gravimetric terrain corrections and the resulting anomalies are the Faye anomalies (Heiskanen and Vening Meinesz, 1958; Torge, 1989).

The terrain corrections were calculated by prism integration for each gravity station. The digital elevation models available are used in the following manner: 0.1 km x 0.1 km grid up to a radius of 2 km around the gravity station; 1 km x 1 km grid between radii of 2 km to 20 km; 5 km x 5 km grid (derived from the 1 km x 1 km grid) between radii of 20 km to 170 km. The external radius for each grid (i.e., 2 km, 20 km, 170 km) corresponds approximately to the external radii for the Hayford zones F, K, O (i.e., 2.3 km, 18.8 km, 166.7 km, respectively). The 1 km x 1 km elevation grid extends between latitudes 50°05' and 51°40' (i.e., 176.1 km) and between longitudes 244° and 245°45' (i.e., 122.8 km). The 5 km x 5 km elevation grid extends between latitudes 48°45' and 53° (i.e., 472.6 km) and between longitudes 241°45' and 248° (i.e., 438.5 km).

The terrain corrections are computed with the operational computer program documented in Forsberg (1984a). The linear approximation formula given by equation (2.22) is evaluated with the condensed approximation formula (Forsberg and Tscherning, 1981b)

$$\delta g = G\rho(z_2 - z_1) \int_{x_1}^{x_2} \int_{y_1}^{y_2} \frac{z_m}{(x^2 + y^2 + z_m^2)^{3/2}} dxdy \qquad (2.29)$$

where $z_m = (z_1 + z_2)/2$, z_1 is the elevation of the computation point and z_2 is the elevation of the data point. The latter two elevations refer to the bottom and top of the prism, respectively. To account for the curvature of the Earth, a shift of the prism from the tangential plane at the computation point is calculated as $\Delta z = l^2/2R$; l is the distance from the computation point and R is the mean radius of the Earth. For each computation point, the digital elevation models were changed to match its height.

The Bouguer reduction is accomplished by removing the attraction of a plate of constant height equal with that of the computation point and assuming the constant mass density ρ = 2.67 g/cm^3. The attraction of the Bouguer plate is calculated with equation (2.21). This reduction is applied here to the terrain corrected free-air gravity anomalies to produce the refined (i.e., terrain corrected) Bouguer gravity anomalies.

The removal of the attraction of the compensating masses for the topography in the isostatic reduction uses the Airy-Heiskanen model with the following parameters: mass density ρ = 2.67 g/cm^3 for the attraction of the topography (same as for the Bouguer

reduction); normal thickness of the Earth's crust T = 30 km; and density contrast across the base of the crust $\Delta\rho$ = 0.6 g/cm^3. The condition of floating equilibrium for the Airy-Heiskanen model is

$$t = \frac{\rho_0}{\Delta\rho} h = 4.45h \qquad (2.30)$$

where h is the topography height and t is the corresponding root. The crustal thickness under the mountains is T + h + t.

The integrations for the estimation of the topographic attraction and for its isostatic compensation were performed in the same manner as for the terrain correction calculations using the computer program from Forsberg (1984a).

The information contained in the second sub-set was given in Section 2.5.1. It was decided to leave the free-air gravity anomalies and their terrain corrections as they are in the data base. The refined Bouguer anomalies and the isostatic anomalies were calculated as for the gravity points comprised in the first sub-set. The following reasons were taken into account in this decision: gravity values are not given at the points; the normal gravity is calculated according to GRS80 and the atmospheric correction is considered; approximately 25% of the points lie outside the area covered by the 0.1 km x 0.1 km grid; for 5% of the points there are apparent errors in the given point heights and/or the digital elevation model and/or topographic maps 1:50 000; a cursory investigation of the gravity anomalies shows that they do not present significant differences from those contained in the first sub-set of gravity points.

At this stage, the two sub-sets were analyzed from the point of view of the correlation between the gravity anomalies and the elevations. An equation of the form y = a + bx (i.e., linear regression), where y and x stand for the gravity anomaly and for the elevation, respectively, is used for this task. The strong positive correlation of the free-air gravity anomalies with the heights is evident. This is due to the effect caused by the topographic masses in the short wavelength range. The Bouguer anomalies obtained by removing the influence of the topographic masses, show a negative correlation with the heights. The results (i.e., coefficient a in mGal, coefficient b, and correlation coefficient) for the gravity anomalies in the Kananaskis extended area are given in Table 2.5 and Figure 2.6.

The coefficient b represents the Bouguer plate gradient and, considering equation (2.21) and the values given for b in Table 2.5 for the free-air and/or Bouguer gravity anomalies, the indication is that the density is equal to 2.64 g/cm^3.

Table 2.5 Regression coefficients (a and b) and correlation coefficient for gravity anomalies and elevations (Unit a: mGal)

Gravity Anom.	Coeff. a	Coeff. b	Correl. Coeff.
Free-air	-149.8	0.1107	0.988
Bouguer	-149.8	-0.0012	-0.068
Isostatic	-7.4	0.0043	0.202

From the analysis of the gravity anomalies originating from the two sub-sets of gravimetric data, a number of gross errors and misleading information are identified. Some of the most important problems found will follow. Comparison with existing topographic 1:50 000 maps show that five gravity points of the North America Gravity data base have heights with errors varying between 120 m to 600 m. From the station description and gravity measurements, one of the base (i.e., control) gravity stations established by the Department of Energy, Mines and Resources Canada has the horizontal position in error by approximately 1.2 km in latitude and 4.1 km in longitude. In the gravity survey of 1981, two of the gravity points actually correspond to two of the base stations. However, the gravity values differ at the level of 0.5 mGal. Two pairs of other stations of the same survey overlap, but the gravity values are basically the same. One gravity station of the first gravity survey of 1985 corresponds to a gravity point from the North America Gravity data base. Although their heights are within 0.2 m, their gravity values differ at the level of 4 mGal. The second gravity survey of 1985 has one station with the gravity in error by 30 mGal, two gravity points with wrong horizontal positions, and five stations have heights with errors at the level of 10 m to 20 m. The latter survey has a common station with the North America Gravity data base. However, the gravity values differ at the level of 4 mGal; the heights differ by approximately 7 m. Figure 2.7 shows the locations were problems in the data were identified.
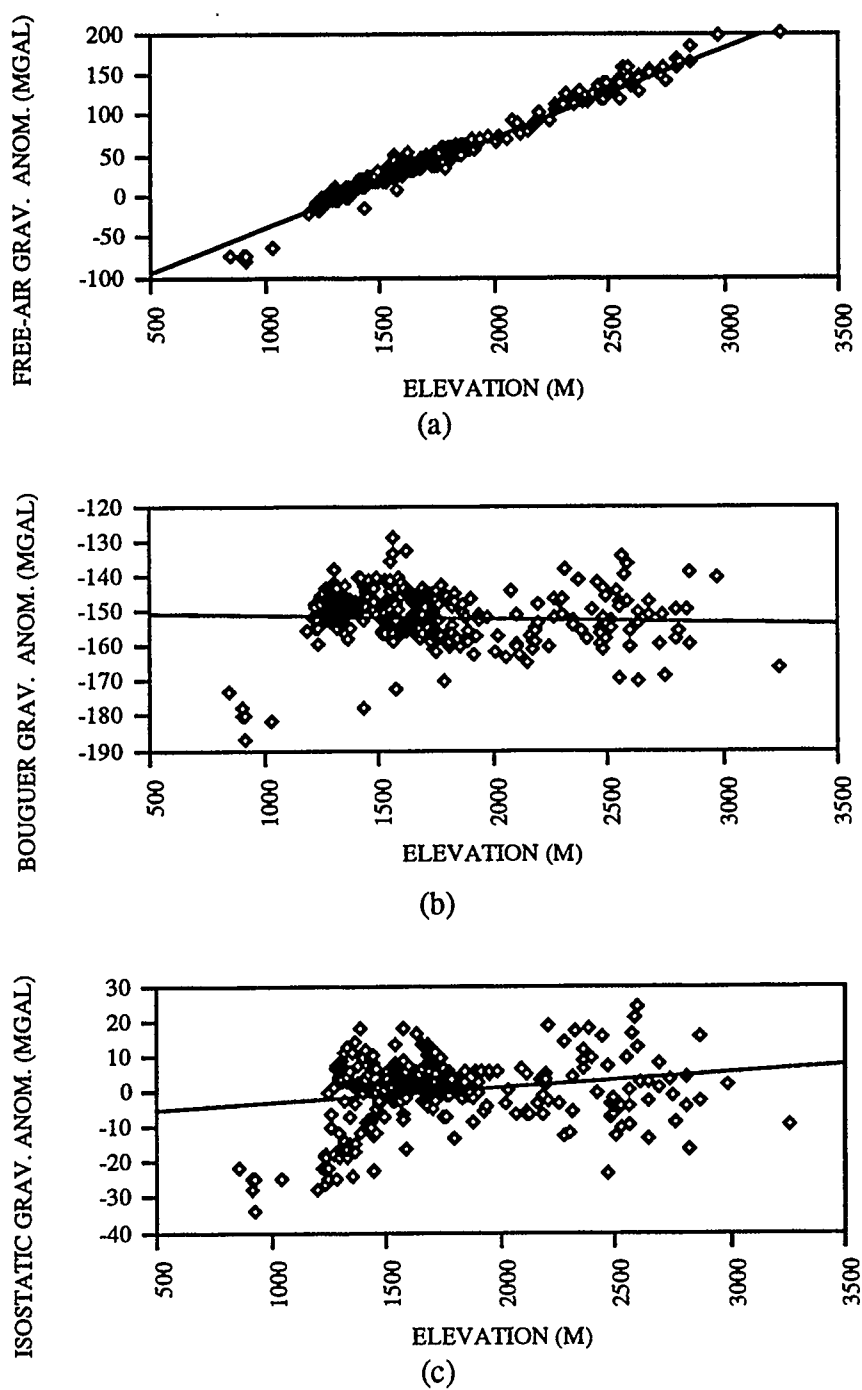
Figure 2.6 Correlation of gravity anomalies (terrain corrected) with elevation: (a) free-air, (b) Bouguer, (c) isostatic
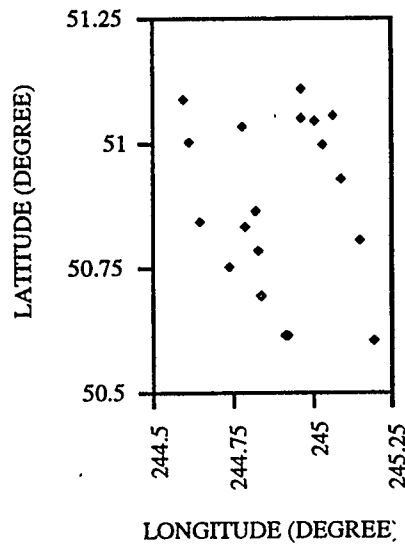
Figure 2.7 Layout of gravity stations in the Kananaskis area with errors and/or inconsistencies in the data

To avoid the adverse effect of using erroneous data in the gravimetric calculations, the identified errors were corrected and flagged. The corrections were performed on the basis of all gravimetric information available for this investigation so that all data could be used in subsequent calculations.

2.5.4 Gravimetric Data Base

The gravity information acquired for the 371 gravity points in the Kananaskis extended area is stored into a data base for subsequent use and gravimetric related calculations. Table 2.6 presents for the Kananaskis area, the source organization [i.e., Department of Energy, Mines and Resources Canada (EMR), and The University of Calgary (UOC)] and the year when the gravity data became available at The University of Calgary.

The information contained in the data base for the gravity points is the following: source, identification number, latitude, longitude, height, gravity, free-air anomaly, Bouguer anomaly, isostatic anomaly, terrain correction, standard deviations respectively for longitude/latitude, height, gravity, free-air anomaly, Bouguer anomaly. Only in the case of data originating from the North America Gravity data base, are values for the gravity and the associated standard deviation not given.

Table 2.6 Source and year of availability at The University of Calgary of point gravity data in the Kananaskis area

Organization	Year	Core Area	Extended Area
EMR	1980	9	9
EMR	1981	63	63
UOC	1985	50	50
EMR	1992	64	150
UOC	1992	93	99

Tables 2.7 and 2.8 give for the data base of the Kananaskis extended area statistics of the point data and their standard deviations, respectively.

Table 2.7 Statistics of heights, terrain corrections and gravity anomalies at the gravity points of the data base for the Kananaskis extended area (Units: height, m; terrain correction and gravity anomaly, mGal)

Data	Minimum	Maximum	Mean	Std. Deviation
Height	869.3	3266.5	1722.9	409.2
Terrain Corr.	0.0	74.4	9.4	8.8
Free-air Anom.	-82.4	198.9	40.8	45.9
Bouguer Anom.	-187.3	-129.2	-151.9	7.2
Isostatic Anom.	-33.8	23.5	0.0	8.8

Table 2.8 Statistics of the standard deviations for spatial location and for gravity data at the gravity points of the data base for the Kananaskis extended area (Units: spatial position, m; gravimetric data, mGal)

Data	Minimum	Maximum	Mean	Std. Deviation
Lat./Long.	0.5	20.0	10.5	7.0
Height	0.0	12.0	2.9	2.0
Gravity	0.02	0.25	0.09	0.03
Free-air Anom.	0.05	3.70	0.97	0.50
Bouguer Anom.	0.05	2.36	0.65	0.29
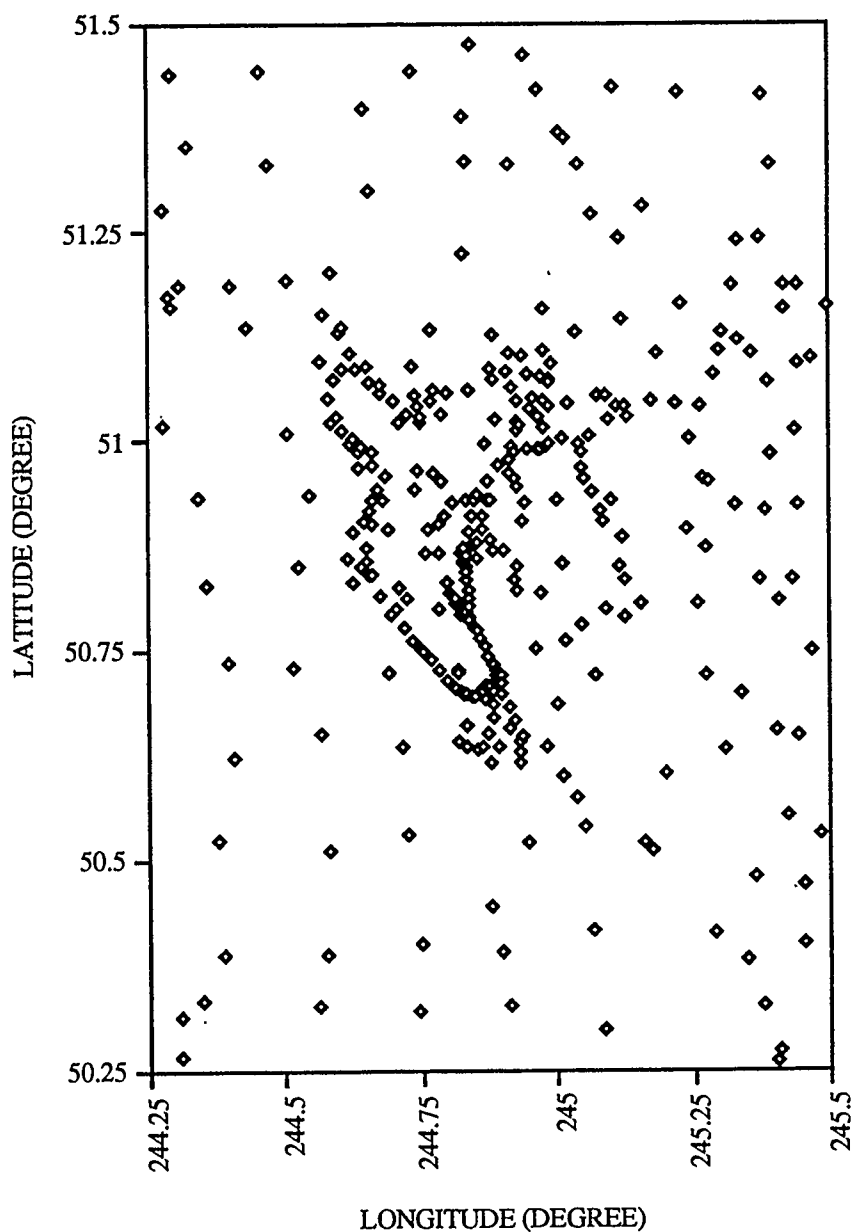
Figure 2.8 Point gravity data in the Kananaskis extended area

The standard deviations given in Table 2.8 originate from the information included in the documentation of the different sources of gravity data (see Section 2.5.1). For the gravity densification survey carried out in 1992, the standard deviations were estimated as part of a least-squares adjustment and/or by error propagation.

An illustration of the density (i.e., spacing) and coverage of the area by gravity points is shown in Figure 2.8; the high concentration of gravity points inside the core area is evident. Figure 2.8 also indicates that additional gravity measurements in the south-west and south-east parts of the core area can provide a better data density and coverage for the Kananaskis core area. Subsequently, the attempt will be made to use all the quantities contained in the data base to produce a more homogeneous representation of the gravity field for the Kananaskis area.

CHAPTER 3

PREDICTION OF GRAVITY ANOMALIES AND STUDY OF THEIR STATISTICAL BEHAVIOUR

3.1 General Methodology and Data Requirements

Terrestrial gravity data are acquired at specific observation points, usually not regularly distributed. A wide variety of applications in geodesy and geophysics, both with scientific and economic significance, require gravity anomaly data to be arranged more homogeneously over the area of investigation. For evaluation, interpretation, methodology, and computational efficiency purposes, a regular data distribution (i.e., grid) is particularly useful. This requires the prediction of gravity anomaly data. The prediction methods are based on the premise that the data is single-valued at any point, that the field is continuous over the area, and that there is a positive auto-correlation of the data over some distance.

Heiskanen and Moritz (1967) review general aspects regarding the prediction of gravity anomalies. To predict gravity anomalies, information about the gravity anomaly function is necessary. The primary source of information are the observed gravity anomaly values. Additional knowledge regarding the form of the gravity anomaly function is also required. Dense and homogeneous data distribution by gravity anomalies allows for a simpler type of prediction, namely a linear prediction. This is dependent only on the relative position of the prediction points and the observation points. An easy solution is to assign to the prediction point the closest available observed gravity anomaly value. Another simple approach is to predict the required gravity anomaly as a function of the distance to the data points, i.e. weighted mean. A further improvement to the prediction model is to use least-squares adjustment to determine the coefficients of a (low-order) polynomial surface that fits the existing data.

If additional information provided by the auto-correlation relationship (i.e., covariance function) between gravity anomalies is included in the mathematical model, better estimates for the prediction values are expected. This is a statistical approach to the prediction of gravity anomalies (Rapp, 1964); the gravity anomalies are considered now as statistically dependent signals. The inclusion of this aspect in the least-squares adjustment model leads to the least-squares collocation technique (Moritz, 1980), where besides parameters, signal quantities are also estimated at locations other than the observation points.

Regardless of the method used to predict gravity anomalies on the Earth's surface, the quality of prediction will depend on the data density, the variance of gravity anomalies and their correlation characteristics. The best results will be obtained when the data used has small variance and a strong correlation. Adequate terrain reductions (Forsberg, 1984a) will improve the smoothness characteristics of the data, making it more suitable for prediction.

The topographic reduction (i.e., complete Bouguer reduction) computationally removes the visible topography. This reduction produces a smooth gravity anomaly field, but there is a large negative bias in mountainous areas. The former means a strong correlation and indicates that the field is suitable for prediction.

If the topography compensation at depth is also considered in the reduction scheme (i.e., topographic-isostatic reduction), the large biases are removed in the remaining gravity anomaly field, and besides smoothness, the data presents a low variance too. The isostatic reduction should be global. A terrain reduction that approximates the isostatic reduction characteristics is the residual terrain model (RTM) reduction advocated by Forsberg and Tscherning (1981b) and Forsberg (1984a). For this reduction, only the short wavelength component of the topography is considered in relation to a smooth mean height surface over the limited area. The deviations of the topography from this smooth surface are computationally taken into account by a remove-restore technique. This reduction may be regarded as the difference between two Bouguer reductions where the visible topography is removed and the smoothed topography is added.

If free-air gravity anomalies have to be predicted, the direct use of free-air anomalies at the observation points in the prediction process will not produce good results. This is due to the large variance and weak auto-correlation characteristics associated with the data. For these reasons, the free-air gravity anomalies are predicted by using an intermediate

prediction with Bouguer, isostatic, or residual terrain model gravity anomalies. However, if the correlation of the free-air gravity anomaly with its elevation is considered in the prediction algorithms, improved estimations are possible.

Especially in mountainous areas, the free-air gravity anomalies should be terrain corrected. The resulting anomalies (i.e. Faye anomalies) are then reduced by using a linear correlation model with two parameters (i.e., $\Delta g = a + bh$) to account for the height correlation component. The parameters a and b are estimated by a least-squares adjustment; 'a' represents a mean value and 'b' has the role of the Bouguer gradient. The reduced free-air gravity anomalies have now the characteristics of the Bouguer gravity anomalies, but without the large bias. The estimated Bouguer gradient tends to have smaller values than the standard one (i.e., 0.1119) due to the incomplete modelling (i.e., the horizontal positions of the observation points were not taken into account). This problem can be rectified by adding new parameters (i.e., polynomial coefficients) that depend on observation coordinates. Details regarding the prediction of free-air anomalies can be found in Rapp (1964), Uotila (1967), Lachapelle and Schwarz (1980), Sünkel (1981b), Sünkel and Kraiger (1983), and Kearsley et al. (1985).

The prediction outcome will be dependent on the data density, distribution and observational errors. The reduction errors coming from the terrain correction computation, the resolution and errors associated with the digital elevation model data, and the considered assumptions (e.g. density, etc.) for the chosen model will also bear on the gravity anomaly field prediction. Sünkel (1984) investigates the errors contributing to the total prediction error of gravity anomalies.

Methods of prediction were developed and extensively applied in geodesy and geophysics, aiming to produce a homogeneous and adequate representation for the gravity anomaly data. In geodesy, statistical methods are widely employed. In geophysics, Briggs (1974) introduced the minimum curvature algorithm for gridding, which is widely used due to its smoothness properties. The method produces a surface having continuous second derivatives and minimal total squared curvature. Because of possible large oscillations and inflections of the computed surfaces, Smith and Wessel (1990) have improved the method by adding tension parameters to the algorithm of the minimum curvature method.

The frequency domain approach to optimal gravity anomaly data gridding has gained importance (Vermeer, 1992) because of its computational efficiency aspect.

The current work attempts the prediction of gravity anomalies in an area of rugged topography. The methods used are least-squares collocation and weighted means with gravity anomalies as input.

3.2 Two Prediction Methods for Gravity Anomalies

3.2.1 Least-Squares Collocation

The method of collocation is extensively used in geodesy for solving boundary value problems [i.e., the determination of the Earth physical surface from values of the disturbing potential T and of its functionals L(T) given on it]. In statistical collocation, the anomalous gravity field is considered a stochastic process and, thus, the solution represents a statistical approximation of the field. Least-squares collocation is defined as that collocation method which minimizes the variance of the estimated quantities. In this case, functionals of the disturbing potential (e.g. gravity anomalies, deflections of the vertical, geoid-ellipsoid separations, etc.) and unknown parameters (e.g. spatial coordinates, trend, etc.) are used.

In least-squares collocation, the observational equations are represented by the mathematical model

$$l = AX + s + n \tag{3.1}$$

where l is the vector of observations, A is a matrix (i.e., sensitivity/design matrix) expressing the effect of the vector of parameters X on the vector of observations l, s is the vector comprising signals (at the observational and respectively prediction points) expressed by the functionals applied to the anomalous potential T, and n is the vector of observational errors (i.e., noise). The signal denotes the errorless part of the observation and represents the effect of the anomalous gravity field.

In the least-squares collocation model, the expectations for the signal and the noise are zero (i.e., centered quantities)

$$E\{s\} = 0, E\{n\} = 0 \tag{3.2}$$

The covariance (i.e., second product moment of two quantities about their mean) matrices for the random quantities of signal and noise in the equation (3.2) are

$$C_{ss} = E\{ss^T\} \tag{3.3}$$

$$C_{nn} = E\{nn^T\} \tag{3.4}$$

, respectively.

In the equations (3.2), (3.3) and (3.4), the expectation $E\{\cdot\}$ is the mean in the sense of both statistical and global average (Moritz, 1980). Because the signal s and the noise n are uncorrelated, the covariance matrix of the observations l is

$$C_{ll} = C_{ss} + C_{nn} \tag{3.5}$$

The formal solution for the mathematical model expressed by the equation (3.1) is obtained by using the finite minimum norm principle

$$s^T C_{ss}^{-1} s + n^T C_{nn}^{-1} n = \text{minimum} \tag{3.6}$$

Equations for the least-squares collocation vectors of estimates for the parameters and for the signals, together with their associated error covariance matrices, can be found in Moritz (1980). Considering the determination of the parameters X as the adjustment, the removal of noise n as the filtering, and the computation of the signal s at points other than the observation points as the prediction, the model expressed by equation (3.1) combines adjustment, filtering and prediction. The least-squares collocation solutions have the following characteristics: the result is independent of the number of signal quantities to be estimated; the observed and estimated quantities can be heterogeneous; the method is invariant with respect to linear transformations of data and results; the solution is optimal on the basis of the data and covariance functions used.

If a non-parametric model (i.e., no systematic part, X = 0) is considered, equation (3.1) becomes

$$l = s + n \qquad (3.7)$$

and the solutions for the estimated signals and for their error matrix, respectively, are simplified by setting matrix $A = 0$.

The method of least-squares collocation is extensively used for the prediction of gravity field related quantities (i.e. functionals of the disturbing potential) such as gravity anomalies, geoidal heights, deflections of the vertical, etc. Considering the case of prediction of gravity anomalies from gravity anomalies (i.e., homogeneous data), the vector of observations l is comprised of residual gravity anomaly values

$$\Delta g_i^r = \Delta g_i - \Delta g_i^d \qquad (3.8)$$

where Δg_i is the observation at point i, Δg_i^d is the calculated/deterministic (i.e., trend) part, and Δg_i^r is the resulting residual gravity anomaly. For example, the trend can be represented by the linear correlation parameters between free-air anomalies and their topographic heights and/or a low-order polynomial surface, function of position. The trend parameters have to be determined prior to the usage of the least-squares collocation model given by equation (3.7). The formal solution of the gravity anomaly signal vector and corresponding error covariance matrix is given by

$$\hat{s} = C_{sl} C_{ll}^{-1} l \qquad (3.9)$$

$$E_{\hat{s}\hat{s}} = C_{ss} - C_{sl} C_{ll}^{-1} C_{ls} \qquad (3.10)$$

The estimated gravity anomaly at a point P, $\Delta \hat{g}_P$, is then obtained as

$$\Delta \hat{g}_P = \hat{s}_P + \Delta g_P^d \qquad (3.11)$$

where $\hat{s}_P$ is the signal part of the gravity anomaly and Δg_P^d represents the deterministic component.

If large amounts of data are considered in the prediction least-squares collocation algorithm, there will be a substantial computational effort due to the inversion of large and full

covariance matrices. A practical approach is to use smaller areas for data collection, having thus a manageable number of observations. The size of the collection area can be determined in relation to the local characteristics of the anomalous gravity field portrayed by the covariance function of the gravity anomalies.

The formulation and the solution to gravity field related problems by least-squares collocation is directly related to covariance functions of signals at the observation and at the prediction points. Aspects of their fundamental role, empirical evaluation, essential characteristics, and analytical approximation will be addressed in a subsequent section.

An introduction, a review, and a detailed presentation of the theory and applications of least-squares collocation, respectively, are found in Moritz (1972, 1978, 1980).

3.2.2 Weighted Means

A simple deterministic method for prediction of gravity anomalies is the based on the inverse distance weighted means. In this approach, the gravity anomaly at a prediction point is the weighted mean of observations located at arbitrary points. The weights are allocated inversely proportional to the distance between prediction point to observation points.

Morrison and Douglas (1984) give the fundamental equation used for prediction with the inverse distance weighted means method. Considering a set of functions $f(x_i, y_i)$ given at i = 1, 2, ..., n points with plane coordinates (x_i, y_i), the fundamental equation for the prediction of a function $f(x, y)$ is

$$f(x,y) = \frac{\sum_{i=1}^{n} f(x_i,y_i) w(x,x_i,y,y_i)}{\sum_{i=1}^{n} w(x,x_i,y,y_i)} \qquad (3.12)$$

with

$$w(x,x_i,y,y_i) = [(x - x_i)^2 + (y - y_i)^2]^{-\mu/2} \qquad (3.13)$$

where μ is the power of prediction. A common value for the power of prediction is $\mu = 2$. Sjöberg (1975) suggested values of approximately 3 to 4 for the parameter μ. However, the choice of this parameter seems arbitrary.

Kassim (1980) has used the inverse distance weighted means approach for estimation of gravity anomalies in several areas with particular topographic characteristics (i.e., flat, gently rolling, and mountainous). No recommendations were given regarding specific power coefficients for different types of terrain.

The error associated with the prediction of the gravity anomaly at point P, Δg_P, from gravity anomalies, Δg_i, at i =1, 2, ..., n points situated at distances d_{Pi}, is a function of the standard deviations of the observations and respectively of distances. By propagation of variances, $\sigma^2_{\Delta g_i}$, associated with the gravity anomaly observations, the variance, $\sigma^2_{\Delta g_P}$, of the predicted value is

$$\sigma^2_{\Delta g_P} = (\frac{\partial \Delta g_P}{\partial \Delta g_i})^2 \sigma^2_{\Delta g_i} \qquad (3.14)$$

or by substituting the partial derivatives from equation (3.12), equation (3.14) becomes

$$\sigma^2_{\Delta g_P} = \frac{\sum_{i=1}^{n}(1/d_{Pi}^{\mu})^2 \sigma^2_{\Delta g_i}}{\sum_{i=1}^{n}(1/d_{Pi}^{\mu})^2} \qquad (3.15)$$

The investigations carried out by Sjöberg (1975), Kassim (1980), and Morrison and Douglas (1984) with the inverse distance weighted means method to predict gravity anomalies, conclude that adequate results are obtained when interpolation is performed. However, the method performs poorly when the data coverage is sparse and/or presents large variations.

3.3 Covariance Functions and Statistical Behaviour of Gravity Anomalies

The covariance functions, represented in the least-squares collocation solution by covariance matrices, play a fundamental role in the estimation process.

Under the assumption that gravity anomalies are statistical quantities with a mean value of zero, the covariance function is defined as the average product of all pairs of gravity anomalies Δg_i and Δg_j that are at a constant distance s apart. The covariance function can be written symbolically as

$$C(s) = cov(\Delta g_i \, \Delta g_j, \, s) = M(\Delta g_i \, \Delta g_j)_s \qquad (3.16)$$

where and $M(\cdot)$ is an averaging operator. If the operator M is homogeneous (i.e., independent of position) and isotropic (i.e., independent of azimuth), the covariance function $C(s)$ will be only dependent on the distance s between the points i and j. The covariance function characterizes the statistical behaviour of the gravity anomaly field (i.e., pairs of close gravity anomaly points, due to local disturbances, tend to have similar size and sign) and gives information regarding the structure of the gravity field.

The best approximation to the gravity anomaly field in an area, from a standard error of prediction point of view, is obtained when an empirical covariance function determined from the available local data is used. In this way, the structure of the gravity anomaly field will be portrayed by the local covariance function. It is required, however, to remove the long wavelength component (i.e., trend) from the local data before determining the covariance function (i.e., the calculations will be performed with residual gravity anomaly data). The removal of the long wavelength component is achieved by the subtraction of model anomalies calculated from the coefficients of a spherical harmonic series of the geopotential and/or a low degree surface polynomial, or by removal of mean of the data. When the trend is removed by the former, the local and global covariance functions are linked and treatment of heterogeneous data in the least-squares collocation model is possible. If the trend in the local data is removed by one of the latter two, the expected values for the data become zero, the frequency spectrum is now changed, and the local and global covariance functions are not related anymore. The removal of a geopotential model from the local data improves in general the characteristics of isotropy and homogeneity for non-mountainous areas. For mountainous areas the latter characteristics are usually improved if the linear height correlation is removed from the data.

The empirical covariances between gravity anomaly values Δg_i and Δg_j are expressed by

$$C(s_k) = \frac{1}{n_k} \sum_{i=1}^{n} \sum_{j=1}^{n} \Delta g_i \Delta g_j \qquad (3.17)$$

where k refers to the class of distances s_k and n_k is the number of products in each class. The empirical covariance function determined with equation (3.17) has to be approximated by an analytical model in order to use its information in the prediction process. For computational convenience, this model should have simple form (i.e., characterized only by a few parameters). Moritz (1976) has introduced for homogeneous and isotropic covariance functions a representation by three essential parameters considered adequate to portray the local behaviour of the gravity anomaly field.

Moritz (1976, 1978, 1980) give the following essential parameters: the variance C_0, the correlation length $X_{1/2}$, the curvature parameter χ and/or the gradient variance G_0. The variance C_0 is the value of the covariance function $C(s)$ for the argument s= 0

$$C_0 = C(0) \qquad (3.18)$$

The correlation length $X_{1/2}$ is the value for the argument for which $C(s)$ has decreased to half of its value at s = 0

$$C(X_{1/2}) = \frac{1}{2} C_0 \qquad (3.19)$$

The curvature parameter χ is a dimensionless quantity related to the curvature κ of the covariance curve at s = 0

$$\chi = \kappa X_{1/2}^2 / C_0 \qquad (3.20)$$

The gradient variance G_0 is the variance of the horizontal gradient of Δg and is related to the curvature parameter by

$$G_0 = \chi C_0 / X_{1/2}^2 \qquad (3.21)$$

Covariance functions that have the same essential parameters indicate a similar general behaviour of the gravity anomalies. The variance C_0 plays the role of a scale factor for the prediction errors; the correlation length $X_{1/2}$ characterizes the covariance function over distances of the order of $X_{1/2}$ itself; the curvature parameter χ is representative for very small distances. From an empirical determination point of view it is more convenient to work with the horizontal gradient variance G_0 than with the curvature parameter χ. Thus, the former is usually the third essential parameter.

Schwarz and Lachapelle (1980) and Goad et al. (1984) give details on the calculation of local empirical covariance functions. The covariances are calculated by forming products between all pairs of gravity anomalies in the area and by grouping and averaging the products according to the class interval distance. Equation (3.17) is used for this task. For the distance equal to zero, the resulting value is the variance C_0 (units are mGal^2). The variance of the horizontal gradients, G_0, is obtained from the average gradients (i.e., ratio of difference in gravity anomalies at two points and the distance separating them); units are E^2, $1E = 0.1$ mGal/km.

Moritz (1976) states that the choice of the covariance function has a limited effect in prediction computations, however the error estimates can be strongly influenced by it. Thus, the presence of the homogeneity and isotropy characteristics in the data are essential for the estimation of prediction errors. To verify the assumption of anisotropy, a comparison of the estimated $X_{1/2}$, G_0, or χ for the meridian and longitudinal empirical covariance functions or between extreme values over all the azimuths, can indicate the degree of anisotropy in the gravity anomaly data (Lachapelle et al., 1983). Forsberg (1984a) and Tscherning (1985) use as a measure of anisotropy the ratio between the maximal and the minimal correlation lengths.

Plane covariance models prove to be quite adequate for homogeneous (e.g. gravity anomalies) data prediction. Moritz (1976, 1978, 1980) gives a number of analytical expressions that can be used to approximate the local empirical covariance functions. Their expressions (they must be positive definite) are the following:

$$C(s) = C_0 e^{-A^2 s^2} \qquad (3.22)$$

$$C(s) = \frac{C_0}{(1 + B^2 s^2)^m} \tag{3.23}$$

$$C(s) = \frac{C_0 b}{[s^2 + (z_i + z_j + b)^2]^{1/2}} \tag{3.24}$$

$$C(s) = \frac{C_0 b^2 (z_i + z_j + b)}{[s^2 + (z_i + z_j + b)^2]^{3/2}} \tag{3.25}$$

$$C(s) = C_0 e^{-s/D} \tag{3.26}$$

$$C(s) = C_0 (1 + \frac{s}{D}) e^{-s/D} \tag{3.27}$$

$$C(s) = C_0 [1 + (\frac{s}{D}) + (\frac{s^2}{3D^2})] e^{-s/D} \tag{3.28}$$

Equations (3.22) to (3.29) are the Gaussian, Hirvonen (when m = 1), inverse distance, Poisson, first-order Markov, second-order Markov, and third-order Markov models, respectively. The coefficients A, B, b, D are related to the correlation length essential parameter. The equations (3.24) and (3.25) represent an extension of the plane covariance of equation (3.23) into the upper half space; z_i and z_j are elevations above the horizontal plane. Detailed explanations regarding these models (i.e., relations of constants/parameters with the essential parameters, specific characteristics, etc.) are found in Moritz (1978, 1980).

Even more simple analytical approximations to the empirical covariance functions are available (see, for example, Goad et al., 1984). Other approximation procedures regarding the covariance functions can also be found in Sünkel (1978, 1979).

The covariance function associated with the spherical harmonic expansion of degree n of the gravity anomalies may be expressed (Heiskanen and Moritz, 1967) as

$$C(\psi) = \sum_{n=2}^{\infty} c_n P_n (\cos \psi) \tag{3.29}$$

where ψ is the spherical distance corresponding to the linear distance s, c_n are positive coefficients, and $P_n(\cos\psi)$ are Legendre's polynomials. The exclusion of the degrees zero and one in equation (3.29) (i.e., summation starts from degree n = 2), indicates that the covariance function refers to a geocentric positioned ellipsoid of the same mass as the mass of the Earth. The coefficients c_n (also denoted as σ_n^2) are called anomaly degree variances. They describe the variance of the field for a particular degree of the spherical harmonic expansion.

All covariance functions and their covariance matrices must be positive definite (i.e., the spectrum of the function is non-negative). The positive definitness of the covariance functions is assured by the non-negativity of all coefficients c_n.

Equation (3.29) can be extended outside the sphere r = R (where R is the mean radius of the Earth) with the consideration that the covariance function C(i, j) in space must be harmonic (i.e., must satisfy Laplace's equation) with respect to both points i and j. A rotationally symmetric harmonic covariance function of gravity anomalies in space can be expressed in a general form as

$$C(i,j) = \sum_{n=2}^{\infty} c_n \left(\frac{R^2}{r_i r_j}\right)^{n+2} P_n(\cos\psi) \qquad (3.30)$$

A global covariance function was estimated (including closed covariance expressions for computation) by Tscherning and Rapp (1974) and it has the form

$$C(\psi) = A \sum_{n=3}^{\infty} c_n s^{n+2} P_n(\cos\psi) \qquad (3.31)$$

where A and s are parameters characterizing the model. A third parameter, B, is implicitly contained in the coefficients c_n. The model of Tscherning and Rapp (1974) is a logarithmic covariance function. Moritz (1977) and Jekeli (1978) suggest additional parameters to the above model, to take care of local characteristics of the gravity anomaly field. Critiques of these models are found in Moritz (1978, 1980) and Schwarz and Lachapelle (1980).

Empirical local covariance function data (i.e., the essential parameters calculated from a certain local field) can be fitted to the model given by equation (3.31). This implies changing the parameters (i.e., A, B, s) in equation (3.31) to match the local data (i.e., C_0, G_0, $X_{1/2}$). Because B cannot be obtained from local information, only A and s can be changed. Schwarz and Lachapelle (1980) present this problem in detail.

Torge (1989) indicates that the spectral decomposition of equation (3.30) allows the computation of anomaly degree variances from a covariance function derived from available gravity anomaly data as follows

$$\sigma_n^2 = \frac{2n+1}{2} \int_{\psi=0}^{\pi} \text{cov}(\Delta g_i \Delta g_j, \psi) P_n(\cos\psi) \sin\psi d\psi \qquad (3.32)$$

3.4 Prediction of Gravity Anomalies in the Kananaskis Area

3.4.1 Least-Squares Collocation

Empirical Covariance Functions

The fundamental role of the covariance function in the least-squares collocation solution was pointed out in Section 3.2.1. For local applications, covariance functions estimated by considering gravity anomaly values only inside a local area, will lead to an optimum solution. Usually the data distribution is not homogeneous and this could lead to an inadequate estimation with equation (3.17) of the covariance function values, according to the class interval. To estimate a representative covariance function of gravity anomalies for an area, a regular data distribution would be needed. This could be achieved by either selecting the points according to some criteria in order to have a more even data distribution, or by predicting the data on a regular grid. Then, the essential parameters characterizing the local empirical covariance function can be estimated.

Figure 2.8 shows that in the extended Kananaskis area the gravity anomaly data distribution is not uniform throughout. The mean data spacing in km can be calculated with the equation given by Forsberg and Tscherning (1981a)

$$d = (A / N)^{1/2} \tag{3.33}$$

where A is the area size in km^2 and N is the number of points. If only the data from the North America Gravity data base is taken into account, the mean data spacing in the Kananaskis core and extended area is at a level of 8 to 9 km. However, if all the data available for this investigation is considered, the mean data spacing is at a level of 4 to 6 km. The latter numbers can be misleading, since most of the additional data are concentrated within the core area. It was decided to select the point data such, that the spacing is approximately at the level of 5 to 9 km. With this arbitrary choice, 131 points were selected for the determination of empirical covariance functions for the free-air, Bouguer and isostatic anomalies (see Figure 3.1).
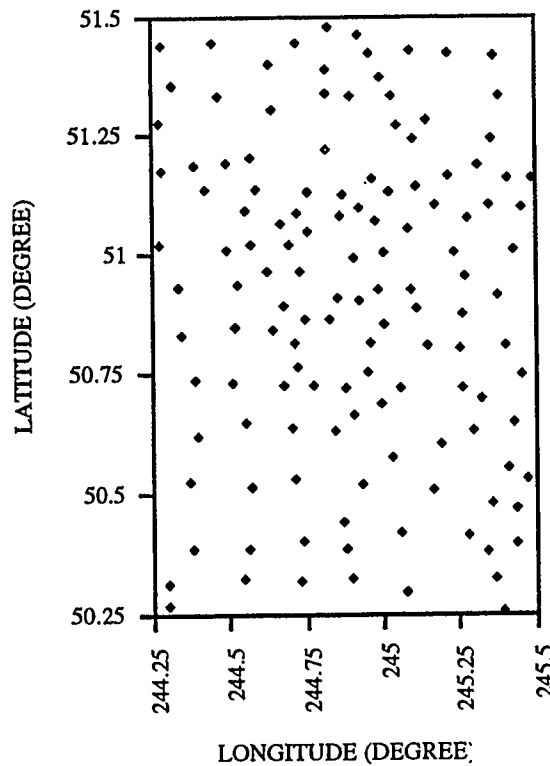
Figure 3.1 Layout of points in the Kananaskis extended area, selected for estimation of empirical covariance functions

Before the gravity anomalies are used to estimate the covariance functions, the trend from the data must be removed; thus the resulting residual data will have a mean equal to zero. In

this investigation, the trend is removed by subtracting the contribution coming from a low-order polynomial surface

$$\Delta g_n(x,y) = \sum_{i=0}^{n} \sum_{j=0}^{i} c_{ij} x^{i-j} y^j \qquad (3.34)$$

where n is the degree of the polynomial, c_{ij} are coefficients of the polynomial and (x, y) are plane Cartesian coordinates. The local Cartesian coordinates are determined from the geographic coordinates (i.e., latitude ϕ and longitude λ) of the gravity anomaly points, with the equations

$$x = R(\lambda - \lambda_0)\cos\phi$$
$$y = R(\phi - \phi_0) \qquad (3.35)$$

where (ϕ_0, λ_0) are mean geographic coordinates for the area (i.e., 50.875° and 244.875°, respectively, in the Kananaskis), and R = 6371 km is the mean radius of the Earth.

The coefficients c_{ij} are estimated from a parametric least-squares adjustment. The current investigation uses polynomial surfaces of zero (i.e., simple mean), first (i.e., simple surface) and second degree, respectively. Because of the strong correlation of the free-air gravity anomalies with their corresponding heights, prior to their reduction by the low degree polynomial surface given by equation (3.34), their linear correlation with the heights has to be removed. The equation used is

$$\Delta g_h = a + bh \qquad (3.36)$$

where the coefficient a is the mean gravity anomaly value for the area, b has the role of the Bouguer gradient, and h is the height. The coefficients a and b for the Kananaskis area were calculated in Chapter 2.

Using the selected 131 points in the extended Kananaskis area, local empirical covariance functions are estimated for the trend reduced Bouguer, isostatic and free-air gravity anomalies. A class interval of 3 arcmin was used for the calculation of the covariance values; and all points less than 6.5 km apart were used for the calculation of the variance of the horizontal gradients. The results (i.e., data statistics and covariance function essential

parameters) are presented in Tables 3.1, 3.2 and 3.3, respectively. Figure 3.2 shows the local empirical covariance functions estimated from Bouguer gravity anomalies. The covariance functions were estimated for the three different types of gravity anomalies, to assess the suitability of the data in the prediction process.

Table 3.1 Statistics of trend reduced Bouguer gravity anomalies and essential parameters of the empirical covariance functions

Trend	Minimum mGal	Maximum mGal	Std. Dev. mGal	C_0 mGal^2	$X_{1/2}$ km	G_0 E^2
Mean	-29.6	22.8	9.7	93.0	9.7	31.1
Polyn. (1st)	-16.9	12.1	6.5	42.0	8.1	23.6
Polyn. (2nd)	-20.6	12.2	5.2	27.1	6.1	17.9

Table 3.2 Statistics of trend reduced isostatic gravity anomalies and essential parameters of the empirical covariance functions

Trend	Minimum mGal	Maximum mGal	Std. Dev. mGal	C_0 mGal^2	$X_{1/2}$ km	G_0 E^2
Mean	-27.1	24.8	11.2	123.5	13.8	48.0
Polyn. (1st)	-30.5	15.3	9.5	88.7	8.8	38.3
Polyn. (2nd)	-20.7	9.7	5.2	26.5	5.5	19.6

Table 3.3 Statistics of trend reduced free-air gravity anomalies and essential parameters of the empirical covariance functions

Trend	Minimum mGal	Maximum mGal	Std. Dev. mGal	C_0 mGal^2	$X_{1/2}$ km	G_0 E^2
Mean	-30.6	22.4	9.7	92.8	9.1	30.9
Polyn. (1st)	-18.3	12.0	6.7	44.0	8.2	24.1
Polyn. (2nd)	-21.3	11.5	5.2	27.2	6.1	17.9

It would have been expected that the prediction characteristics of the isostatic gravity anomalies are better than those of the Bouguer gravity anomalies (i.e., lower variance,

longer correlation length and lower horizontal gradient variance). There is no mean bias in the isostatic gravity anomaly data (i.e., mean equal to zero) and the range of their values is the same as that of the Bouguer gravity anomalies. However, only when a second degree polynomial surface is used in their reduction, are the characteristics of the covariance function similar to those of the corresponding covariance for the Bouguer gravity anomalies. An explanation can be that the isostatic system used (i.e., Airy-Heiskanen) and/or the choice of parameters (i.e., thickness of the Earth's crust T = 30 km and density contrast $\Delta\rho = 0.6$ g/cm^3) is not appropriate for all of the area. Changes in the parameters produce only a shift of the data set (i.e., their range remains the same). Of course, gravity anomaly and digital elevation model data errors can also be a cause. Their adverse influence can create some residual effects that are eliminated only when information regarding their elevation and/or position is included in the reduction.
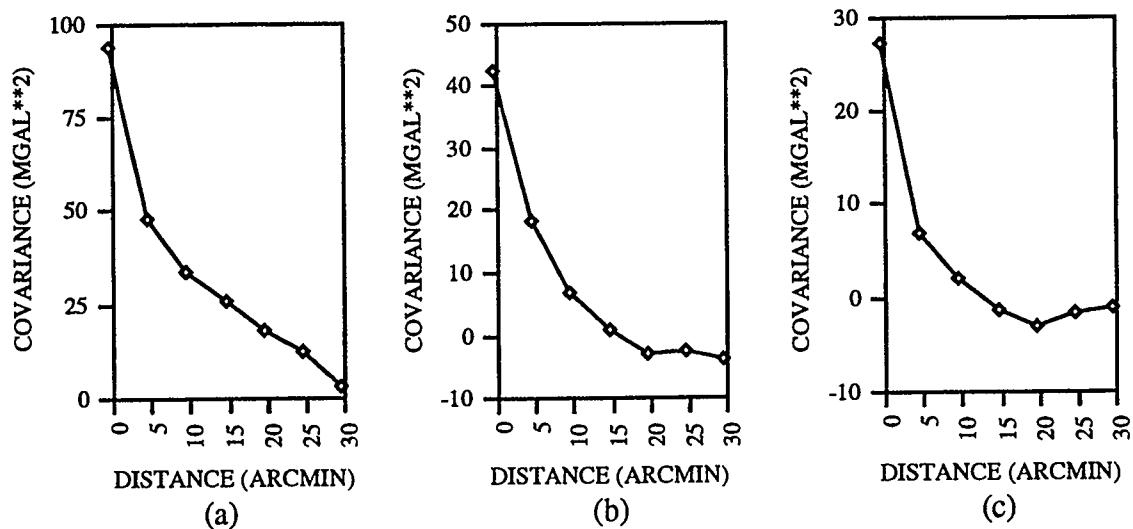
Figure 3.2 Empirical Bouguer gravity anomalies covariance functions for the Kananaskis extended area [Trend: (a) mean; (b) first degree polynomial; (c) second degree polynomial]

Terrain corrected free-air gravity anomalies with linear correlation with height subtracted and trend related on position removed produce covariance functions with the essential parameters similar to those of the corresponding Bouguer gravity anomalies. Merry (1983) used free-air gravity anomalies for prediction, reduced in this manner. Examination of the statistics of Tables 3.1 and 3.3 shows that for practical purposes the empirical covariance functions of Bouguer gravity anomalies trend reduced by a low degree polynomial surface

are the same as those of double reduced (i.e., height correlation and position trend) free-air gravity anomalies.

Analytical Covariance Functions

To use the information provided by the local empirical covariance functions in the least-squares solution, their approximation by analytical models is necessary. Because of the data distribution pattern in the Kananaskis area, it was considered that the calculation of the horizontal gradient of gravity anomalies will not be well determined. The analytical models chosen are then only fitted to C(0) and C(X$_{1/2}$) (i.e., to the gravity anomaly covariances at zero and respectively correlation length distance). Even if this arbitrary choice is not reasonable regarding the overall fit of the empirical covariance function, Moritz (1976) has shown that predicted gravity anomalies will not be affected, and only their standard error estimates will.

To give an indication on the influence in the prediction process of different analytical covariance function models, several of them are investigated. Table 3.4 shows the empirical covariance values at 5' class interval (i.e., spacing) of Bouguer gravity anomalies reduced by the mean, together with their corresponding values derived from six analytical models [see equations (3.22) to (3.28)]. With the exception of the Gaussian model, all the others lead to similar values. Using the analytical covariance models from Table 3.4, grids of 1' x 1' Bouguer gravity anomalies with corresponding estimated standard deviations were computed for the area delimited by latitudes 50°30' and 51°15' and longitudes 244°30' and 245°15' (i.e., Kananaskis core area). The statistics of the results are included in Tables 3.5 and 3.6, respectively. From the data presented, it can be seen that the predicted Bouguer gravity anomaly values are more stable than the estimates of their associated standard deviations, with change of the analytical covariance function model.

A further check on the effect of the choice of covariance function was carried out. Using the same criteria for data selection, but with a different sequence of the data, 115 points were chosen to estimate the empirical local covariance function. The essential parameters are: variance, 103.3 mGal^2; correlation length, 16.4 km; variance of horizontal gradient, 32.9 E^2. The use of the latter parameters in the prediction process, led to the same conclusions as before, i.e., the predicted gravity anomalies are, for practical purposes, the same.

Table 3.4 Bouguer gravity anomalies empirical covariance function and representation by analytical models (Units: distance, arcmin; covariance, mGal^2)

Distance	Empirical	Gaussian	Hirvonen	Inv. Dist.	Poisson	Markov (1st)	Markov (2nd)
0	93.0	93.0	93.0	93.0	93.0	93.0	93.0
5	47.1	49.2	48.5	48.0	48.7	48.0	48.5
10	33.5	7.3	19.9	26.8	16.6	24.8	15.7
15	25.5	0.3	10.0	18.3	6.6	12.8	4.3
20	18.0	0.0	5.9	13.8	3.1	6.6	1.1
25	12.5	0.0	3.9	11.1	1.7	3.4	0.3
30	2.9	0.0	2.7	9.3	1.0	1.8	0.1

Table 3.5 Statistics of Bouguer gravity anomalies on a 1' x 1' grid in the Kananaskis core area, predicted by least-squares collocation (Unit: mGal)

Analytical Model	Minimum	Maximum	Mean	Std. Dev.
Gaussian	-170.7	-136.9	-151.6	6.6
Hirvonen	-169.6	-138.2	-151.7	6.4
Inv. Dist.	-169.4	-139.8	-151.8	6.3
Poisson	-169.8	-137.6	-151.7	6.5
Markov (1st)	-168.5	-140.9	-151.8	6.1
Markov (2nd)	-169.4	-138.7	-151.7	6.4

Table 3.6 Statistics of standard deviations for Bouguer gravity anomalies on a 1' x 1' grid in the Kananaskis core area, predicted by least-squares collocation (Unit: mGal)

Analytical Model	Minimum	Maximum	Mean	Std. Dev.
Gaussian	0.2	3.2	0.9	0.6
Hirvonen	0.2	3.9	1.6	1.0
Inv. Dist.	0.3	4.2	2.0	1.1
Poisson	0.2	3.8	1.4	0.9
Markov (1st)	0.6	4.2	2.8	0.8
Markov (2nd)	0.3	3.8	1.7	0.9

Least-Squares Collocation Prediction

The 1' x 1' (i.e., 1.85 km x 1.17 km) grid of free-air gravity anomalies will be calculated via an intermediate stage of Bouguer gravity anomalies prediction. Though the calculations are done for the Kananaskis extended area, in this section, the results presented will refer only to the core area.

Three grids of Bouguer gravity anomalies are predicted using the method of least-squares collocation with the mean, first degree and second degree polynomial surface trend reduction, respectively. At first, all the gravity data points are considered. However, the number of points around each prediction point is limited to a radius of $1.5X_{1/2}$ and to 5 points per quadrant. The number of points selected for the prediction of gravity anomalies on the grid covering the Kananaskis core area is determined according to the data reduction procedure. Considering the values given for the correlation distance in Table 3.1, 342, 324 and 310 points, respectively, are used. This translates to an average of 3.2, 3 and 2.9 points per quadrant, respectively. The standard error associated with each gravity anomaly value is given as 0.65 mGal (i.e., the mean of the standard error values within the area). Arbitrarily, the second-order Markov equation was chosen to model the local empirical covariance functions. Before the data is used in the least-squares collocation solution, the trend is removed. After the estimation process, the trend is restored at the estimation points. Statistics of the predicted grids of Bouguer gravity anomalies and their corresponding standard deviations are given in Tables 3.7 and 3.8, respectively.

Subsequently, the required grids of free-air gravity anomalies and their associated standard deviations are calculated with the equations

$$\Delta g_{free-air} = \Delta g_{Bouguer} + 0.1119h \qquad (3.37)$$

and

$$\sigma_{\Delta g free-air} = [\sigma^2_{\Delta gBouguer} + (0.1119\sigma_h)^2]^{1/2} \qquad (3.38)$$

where h represents the corresponding heights from the digital elevation model of the area. The standard deviation for the heights, σ_h, is considered at the level of ± 10 m.

Table 3.7 Statistics of Bouguer gravity anomalies on a 1' x 1' grid in the Kananaskis core area predicted by least-squares collocation (Unit: mGal)

Trend	Minimum	Maximum	Mean	Std. Dev.
Mean	-169.4	-138.7	-151.7	6.4
Polyn. (1st)	-169.1	-139.4	-151.7	6.3
Polyn. (2nd)	-170.6	-140.3	-151.8	6.3

Table 3.8 Statistics of standard deviations for Bouguer gravity anomalies on a 1' x 1' grid in the Kananaskis core area predicted by least-squares collocation (Unit: mGal)

Trend	Minimum	Maximum	Mean	Std. Dev.
Mean	0.3	3.8	1.7	0.9
Polyn. (1st)	0.3	3.0	1.5	0.7
Polyn. (2nd)	0.3	2.9	1.5	0.7

The statistics of the calculated corresponding grids of free-air gravity anomalies and of their standard deviations are given in Tables 3.9 and 3.10, respectively. The resulting smaller standard deviations when the reduction of the data is carried out with a second degree polynomial surface, is due to the smaller variance that better scales the errors. As a check, the standard deviations for the free-air gravity anomaly grids were estimated from the least-squares solution of the free-air gravity anomaly data double reduced. The results are given in Table 3.11 and they are basically the same as those presented in Table 3.10. To illustrate the latter results, Figure 3.3 portrays the contoured standard deviation estimations for the grid of free-air gravity anomalies calculated by reducing the position trend by a second degree polynomial surface. Within the core area, approximately between latitudes 50°40' and 51°05' and between longitudes 244°38' and 245°08', the standard deviations are at a level of 1 to 1.5 mGal. In order to test the estimated results (i.e., gravity anomaly values and standard deviations), external checks are necessary. This matter will be discussed in Section 3.4.3.

Table 3.9 Statistics of free-air gravity anomalies on a 1' x 1' grid in the Kananaskis core area predicted by least-squares collocation (Unit: mGal)

Trend	Minimum	Maximum	Mean	Std. Dev.
Mean	-28.2	176.4	67.9	40.2
Polyn. (1st)	-28.3	176.8	67.9	40.2
Polyn. (2nd)	-28.8	175.5	67.8	40.1

Table 3.10 Statistics of standard deviations for free-air gravity anomalies (derived from Bouguer gravity anomalies) on a 1' x 1' grid in the Kananaskis core area predicted by least-squares collocation (Unit: mGal)

Trend	Minimum	Maximum	Mean	Std. Dev.
Mean	1.2	4.0	2.1	0.7
Polyn. (1st)	1.2	3.2	1.9	0.6
Polyn. (2nd)	1.2	3.1	1.9	0.5

Table 3.11 Statistics of standard deviations for free-air gravity anomalies (derived from double reduced free-air gravity anomalies) on a 1' x 1' grid in the Kananaskis core area predicted by least-squares collocation (Unit: mGal)

Trend	Minimum	Maximum	Mean	Std. Dev.
Mean	1.0	4.1	2.1	0.8
Polyn. (1st)	0.9	3.2	1.8	0.6
Polyn. (2nd)	0.9	3.1	1.9	0.6
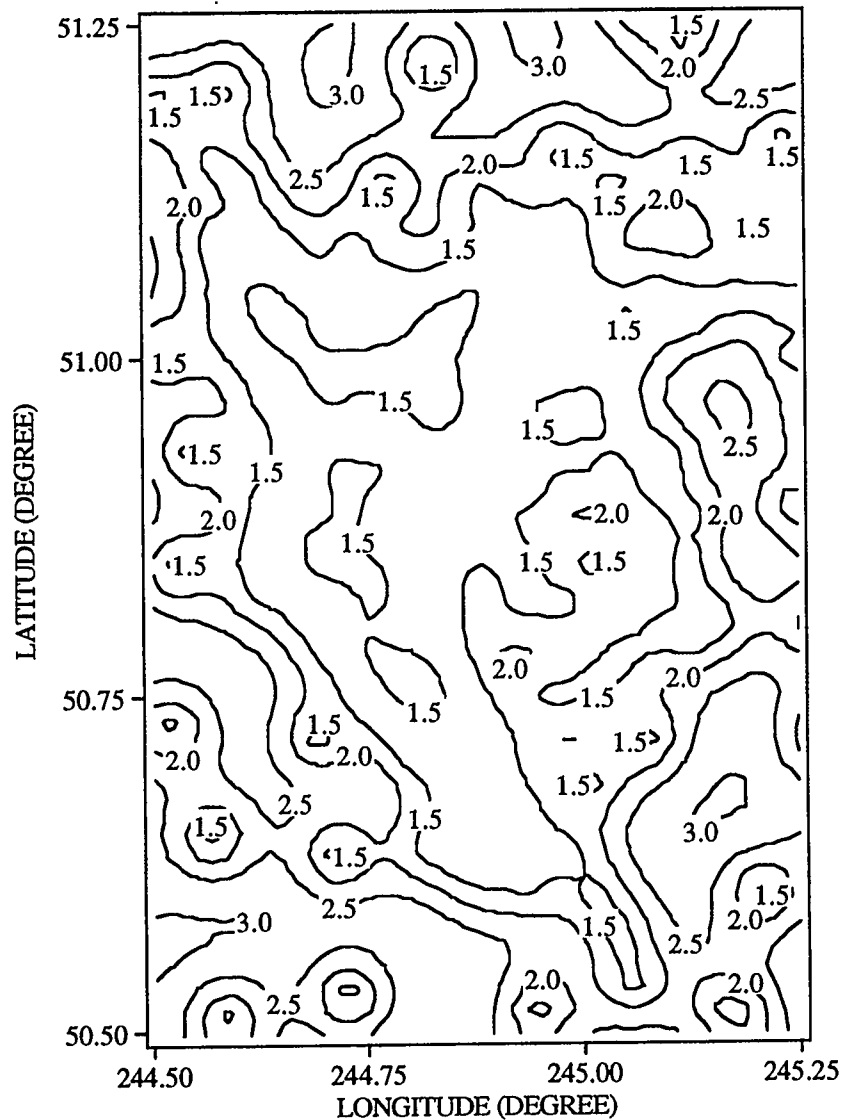
Figure 3.3 Standard deviations of free-air gravity anomalies on a 1' x 1' grid in the Kananaskis core area predicted by least-squares collocation (Contour interval: 0.5 mGal)

3.4.2 Weighted Means

To complement the investigations regarding the prediction of gravity anomalies, the weighted means method is also applied. The same kind of trend reductions will be performed on the data and the same criteria for the number of points used in the prediction process at a point will be used to allow for comparisons between the former and the latter methods.

Equation (3.13) indicates that different powers can be used in the prediction process by the weighted means method. To asses the impact of the power coefficient in the prediction of gravity anomalies, grids of 1' x 1' Bouguer gravity anomalies are predicted for the Kananaskis core area using powers from 1 to 5. The trend in the data was removed by subtracting their mean. The statistics of the results are presented in Table 3.12. With the exception of $\mu = 1$, the differences between the minimum or maximum values for the predicted grids are at the level of 1 mGal or less. Also, an inspection of the statistics shown in Table 3.7 for the predicted grids by the method of least-squares collocation indicate a good agreement between the two methods.

Table 3.12 Statistics of Bouguer gravity anomalies on a 1' x 1' grid in the Kananaskis core area predicted by weighted means (Unit: mGal)

Power Coeff.	Minimum	Maximum	Mean	Std. Dev.
1	-165.7	-143.1	-152.1	5.7
2	-168.0	-141.2	-151.9	5.8
3	-169.2	-140.8	-151.8	5.9
4	-169.4	-140.7	-151.8	6.0
5	-169.4	-140.0	-151.8	6.1

Another test carried out for the method of weighted means is the estimation of the standard deviations for a grid of free-air gravity anomalies by error propagation. First, the standard deviations for the grid of Bouguer gravity anomalies were calculated with equation (3.15). Second, equation (3.38) was used to calculate the standard deviations for a grid of free-air gravity anomalies on the grid. The statistics (i.e., minimum, maximum, mean, standard deviation) in mGal for the latter grid are 1.1, 3.4, 1.7 and 0.5, respectively. These values are at the same level with those estimated by the least-squares collocation method.

From the results available so far, it can be concluded that the weighted means method performs at the same level as the method of least-squares collocation. Additional assessment of the method is included in the next section.

3.4.3 Performance Evaluation of Methods

To obtain a better understanding of the capabilities of the two prediction methods employed in this study, and to investigate the influence of the trend reduction in the prediction process, a number of numerical tests and evaluations are carried out. All the tests use only Bouguer gravity anomalies as data.

In the first group of tests, the trend in the data is reduced by subtracting their mean. The tests are:

(i) Prediction with 131 data points (i.e., points used to estimate the empirical covariance function) at the other 240 points in the area.

(ii) Prediction with 328 data points (i.e., points of the second gravity survey of 1985 are not included) at the excluded 43 points.

(iii) Prediction with 328 data points (i.e., points of the second gravity survey of 1985 are not included) of a 1' x 1' grid and, subsequent, prediction from the grid at the excluded 43 points.

The statistics for the three tests are given in Table 3.13 for the case when the method of least-squares collocation is applied, and in Table 3.14 when the method of weighted means is used.

Table 3.13 Statistics of discrepancies in prediction of Bouguer gravity anomalies by least-squares collocation (Unit: mGal)

Prediction	Minimum	Maximum	Mean	Std. Dev.
Test (i)	-8.1	14.4	-0.5	2.8
Test (ii)	-8.0	6.6	0.0	3.4
Test (iii)	-5.4	4.6	0.0	2.2

An inspection of the measured and the predicted gravity anomalies in each test shows, that discrepancies larger than twice the root mean square, occur at 9, 1 and 3 points, respectively, for each method of prediction.

Table 3.14 Statistics of discrepancies in prediction of Bouguer gravity anomalies by weighted means (Unit: mGal)

Prediction	Minimum	Maximum	Mean	Std. Dev.
Test (i)	-9.1	14.7	-0.2	2.6
Test (ii)	-7.6	5.2	0.6	2.9
Test (iii)	-5.3	4.5	0.0	2.2

In the second group of tests, the trend in the data is removed by subtracting a low-order polynomial surface of zero (i.e., mean), first (i.e., simple surface) and second degree, respectively. All of the available 371 data points are used to predict a 1' x 1' grid of Bouguer gravity anomalies for the core area. Then the prediction from the grid to the 279 points within the core area is carried out.

The statistics for the latter tests are given in Table 3.15 for the method of least-squares collocation, and in Table 3.16 for the method of weighted means.

Table 3.15 Statistics of discrepancies in prediction of Bouguer gravity anomalies (371 points to 1' x 1' grid to 279 points) by least-squares collocation (Unit: mGal)

Trend	Minimum	Maximum	Mean	Std. Dev.
Mean	-4.6	7.1	-0.1	1.2
Polyn. (1st)	-5.0	7.3	-0.1	1.3
Polyn. (2nd)	-4.6	6.9	0.0	1.2

Table 3.16 Statistics of discrepancies in prediction of Bouguer gravity anomalies (371 points to 1' x 1' grid to 279 points) by weighted means (Unit: mGal)

Trend	Minimum	Maximum	Mean	Std. Dev.
Mean	-5.1	7.8	0.0	1.3
Polyn. (1st)	-5.1	7.8	0.0	1.3
Polyn. (2nd)	-5.1	-7.8	0.0	1.3

Upon examination, Tables 3.15 and 3.16 indicate some large discrepancies between the predicted and the measured point data, although the mean discrepancy is zero with standard deviations of 1.2 to 1.3 mGal. After eliminating two gravity points where large discrepancies were present, a 1' x 1' grid of free-air gravity anomaly errors was predicted for the Kananaskis extended area (see Figure 3.4 for the contours in the core area). The two discarded gravity points have suspected height errors and have the following approximate latitudes and longitudes, respectively: 50.65°, 244.87°; 50.94°, 244.74°.
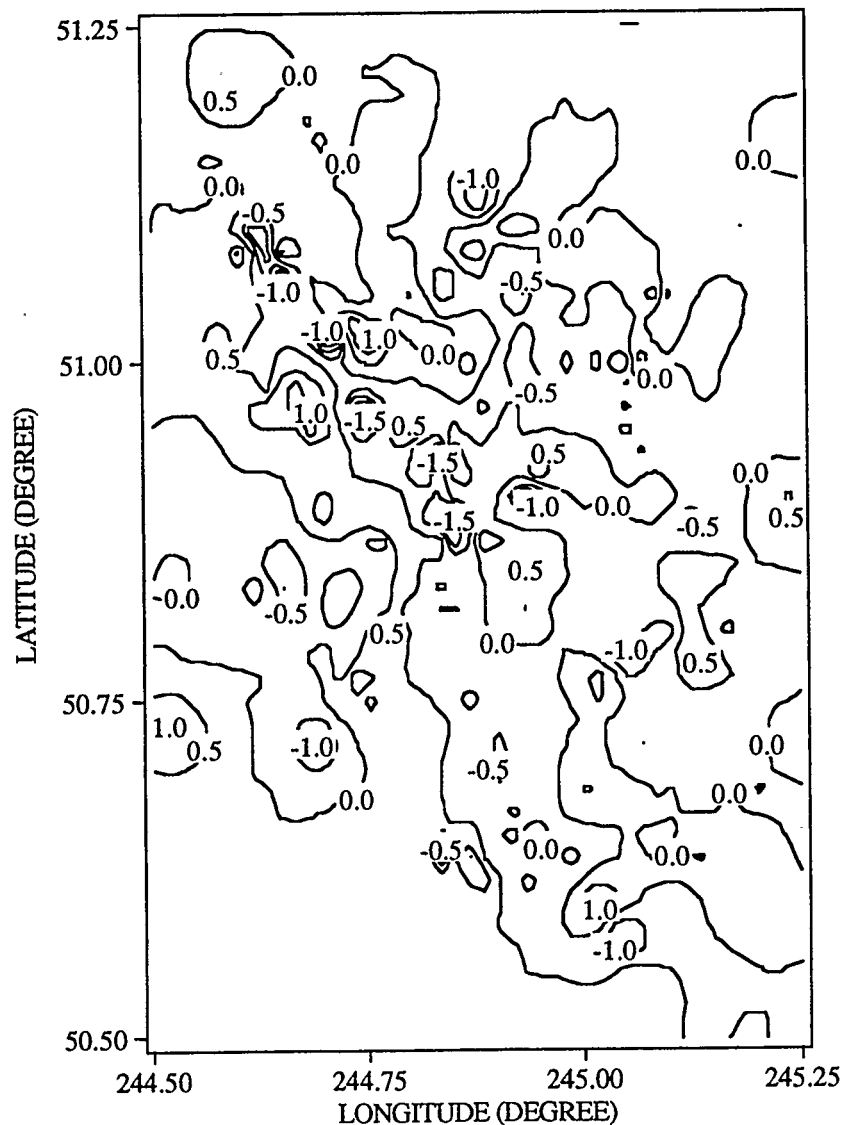

Figure 3.4 Errors of free-air gravity anomalies on a 1' x 1' grid in the Kananaskis core area predicted by least-squares collocation (Contour interval: 0.5 mGal)

The statistics (i.e., minimum, maximum, mean, standard deviation) in mGal for the errors of the free-air gravity anomalies in the Kananaskis core area are -2.3, 2.2, 0.0 and 0.3, respectively.

A very good measure of the performance of different methods of prediction of gravity anomalies, when the same data sets are used, is the root mean square discrepancy statistic

$$\delta = [\frac{1}{n}\sum_{i=1}^{n}(\Delta g_i - \Delta \hat{g}_i)^2]^{1/2} \qquad (3.39)$$

where n is the number of observations in the data set, Δg_i denotes the measured gravity anomaly value and $\Delta \hat{g}_i$ represents the correspondent prediction at point i (Merry, 1983).

The data provided by the prediction tests presented in Tables 3.15 and 3.16 indicate that root mean square discrepancies for the prediction of the Bouguer gravity anomalies by least-squares collocation and by weighted means are 1.19 and 1.28 mGal, respectively. This infers that the precision estimates for the Bouguer gravity anomalies grids, and implicitly for the free-air gravity anomalies grids, are better than the values presented in Section 3.4.2. The statistic δ indicates a slightly better performance of the least-squares collocation method over the weighted means method.

From the evaluation of all the tests, the resulting conclusion is that, for the gravity data available in the Kananaskis area, the performances of the least-squares collocation and of the weighed means methods are similar and that the accuracy of the predicted 1' x 1' grid of free-air gravity anomalies is at the approximate level of 1 mGal.

3.4.4 Statistical Behaviour of Free-air, Bouguer and Isostatic Anomalies

Statistics of Gridded Gravity Anomalies

The point gravity anomaly data in the Kananaskis area were used to produce grids of free-air, Bouguer and isostatic gravity anomalies. The Figures 3.5, 3.6 and 3.7 show the respective contour maps of the gridded 1' x 1' (i.e, 1.9 km x 1.2 km) data covering the Kananaskis core area (i.e., $50.5° \leq \phi \leq 51.25°$, $244.5° \leq \lambda \leq 245.25°$). The free-air gravity

anomaly contours in Figure 3.5 are very similar with the elevation contours in Figure 2.2. This indicates the strong correlation between the former and the latter quantities.

Because, in the following two chapters the surface terrestrial data will be used to calculate the gravity anomaly field at altitude over the Kananaskis core area, a wider coverage will be used in calculations. The statistics of the grids of gravity anomalies for the Kananaskis extended area are given in Table 3.17.

Table 3.17 Statistics of gravity anomalies on a 1' x 1' grid in the Kananaskis extended area $(50.25° \leq \phi \leq 51.5°, 244.25° \leq \lambda \leq 245.5°)$ (Unit: mGal)

Gravity Anom.	Minimum	Maximum	Mean	Std. Dev.
Free-air	-80.6	198.0	52.5	45.5
Bouguer	-186.8	-129.4	-153.7	10.4
Isostatic	-37.8	23.7	2.8	11.6

The data shows for the free-air gravity anomalies that the range (i.e., 278.5 mGal), mean and standard deviation of the field are large. The Bouguer gravity anomalies have a smaller range (i.e., 57.4 mGal) and standard deviation of the field, but there is a large negative bias in the field. The isostatic gravity anomalies have also a smaller range (i.e., 61.6 mGal) and a small standard deviation of the field and their bias is only 2.8 mGal. The latter value indicates that the area is well compensated isostatically.

As a test of the influence of the crust density in gravimetric calculations, the density $\rho = 2.64$ g/cm^3 (see Section 2.5.3) was also used. The comparison shows that the resulting grid of free-air gravity anomalies has a root mean square difference of 0.4 mGal from the grid produced from calculations that use the standard density $\rho = 2.67$ g/cm^3.

Covariance Functions of Gridded Gravity Anomalies

The covariance functions characterize the structure of the gravity anomaly field and gives information on the internal consistency of the data sets (i.e., in this case the gravity anomaly grids of the Kananaskis extended area). The gridded values are assumed stationary (i.e., independent of position). Three sets of empirical covariance functions will be estimated according to the gravity anomaly type and to the trend reduction procedure.
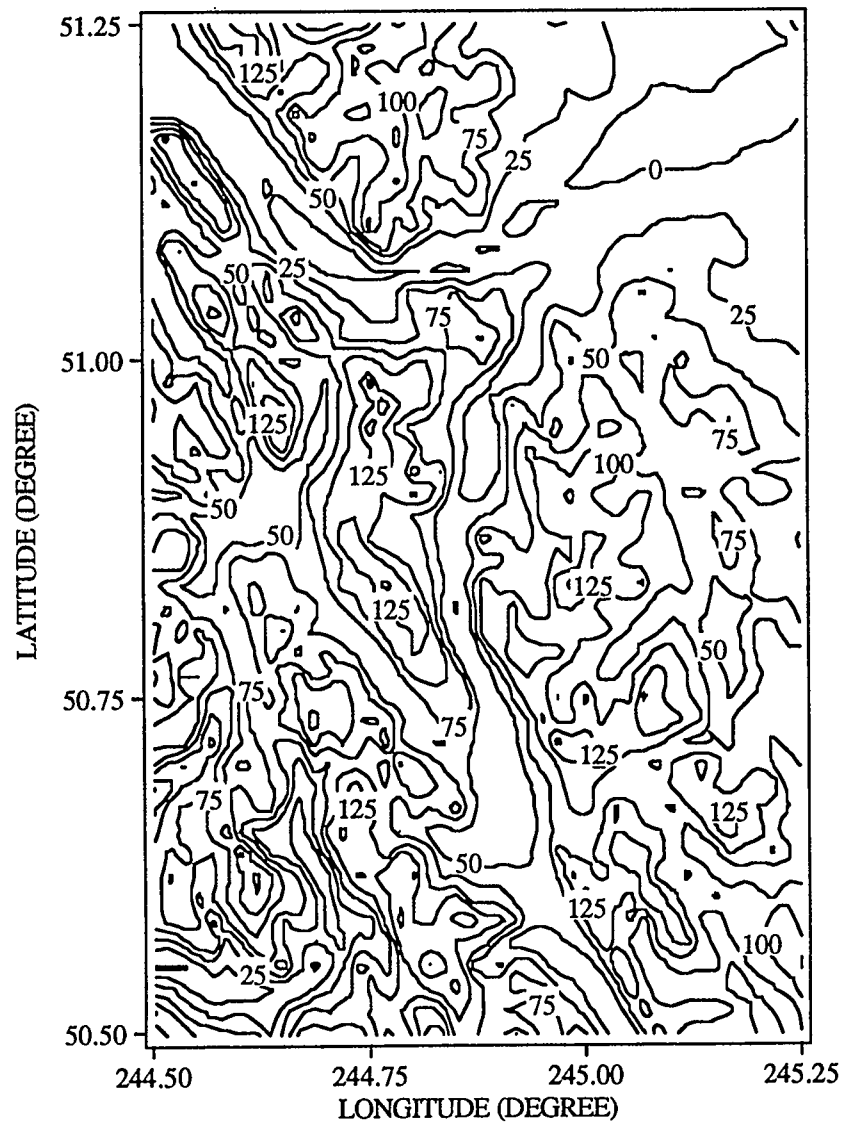
Figure 3.5 Free-air gravity anomalies on 1' x 1' grid in the Kananaskis core area

(Contour interval: 25 mGal)

For each covariance function, besides the three essential parameters (i.e., variance, correlation length, variance of horizontal gradients), the ratio $C_0/X_{1/2}$ together with an anisotropy index will be calculated. The ratio is a measure of the smoothness of the gravity anomaly field (i.e., smaller ratio indicates a smoother field). The anisotropy index proposed by Forsberg (1984a) and Tscherning (1985) as the ratio ($X_{1/2}$ maximal / $X_{1/2}$ minimal), gives information regarding the assumption that the field is isotropic (i.e., independent of direction; then the anisotropy index is equal to 1).
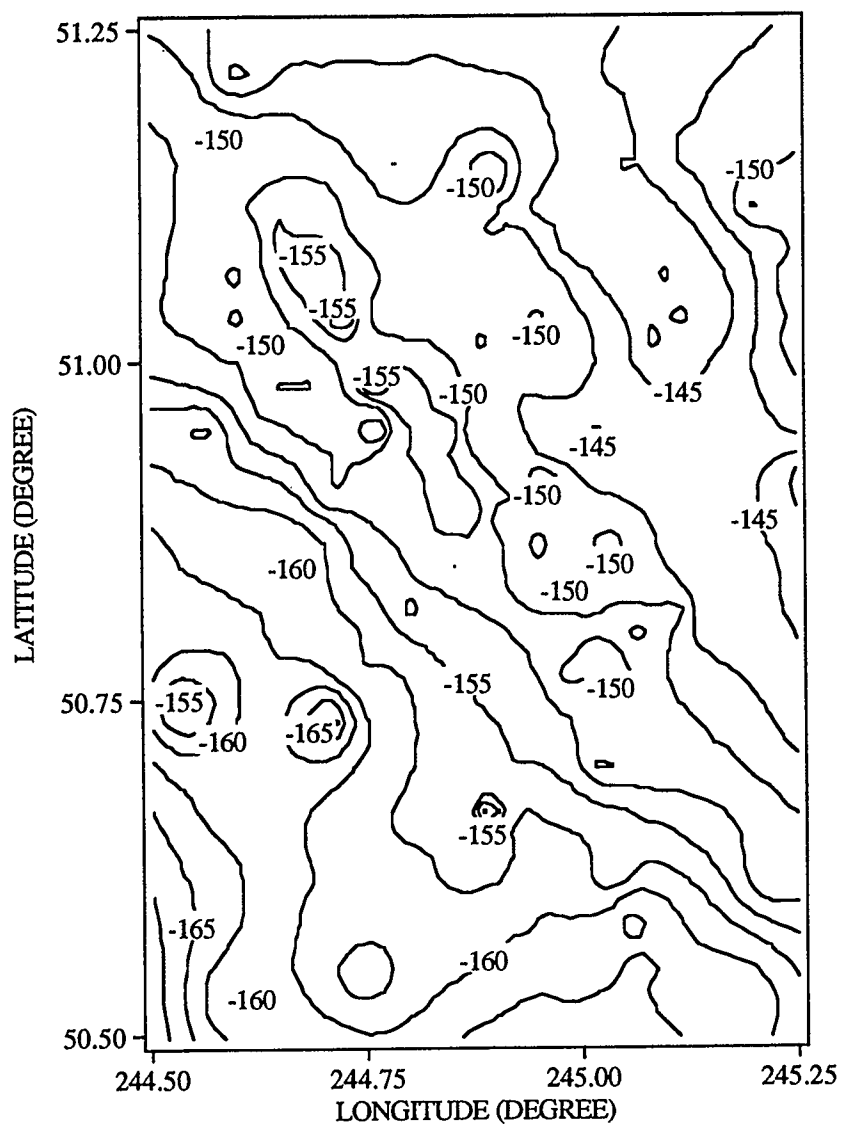
Figure 3.6 Bouguer gravity anomalies on 1' x 1' grid in the Kananaskis core area
(Contour intervals: 2.5 mGal)
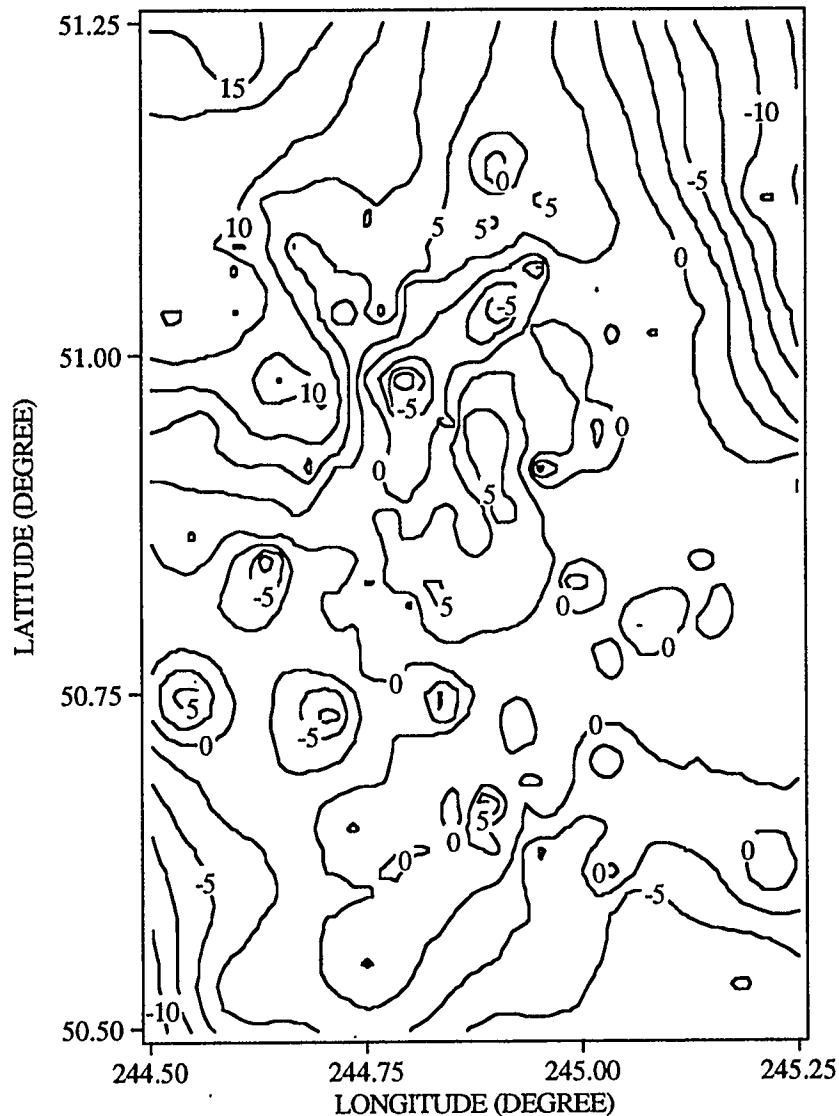
Figure 3.7 Isostatic gravity anomalies on 1' x 1' grid in the Kananaskis core area
(Contour intervals: 2.5 mGal)

Table 3.18 presents the parameters related to the free-air gravity anomaly gridded data. Three covariance functions were evaluated. The first covariance function was calculated from the free-air gravity anomalies with the trend removed by subtracting their mean. The second covariance function was calculated from a residual gravity anomaly field obtained by subtracting from the data the long and part of the medium wavelength component of the gravity anomaly field. The latter reference field, Δg_{GM}, was calculated with the spherical harmonic coefficients of the geopotential model OSU91A (Rapp et al., 1991) to degree and

order 360; this implies a resolution of the field of about 55 km. The third covariance function was calculated from a further reduced gravity anomaly field. This data set was obtained by attempting to remove from the latter residual field the short wavelength component coming from the variation of the local topography from a mean topography surface (i.e., residual terrain model, Δg_{RTM}). In this investigation, the mean height surface was calculated by averaging heights in rectangles of 30' x 30'.

Table 3.18 Covariance function parameters of free-air gravity anomalies on a 1' x 1' grid in the Kananaskis extended area

Trend	C_0 mGal^2	$X_{1/2}$ km	G_0 E^2	$C_0/X_{1/2}$ mGal^2/km	Anisotropy
Mean	2076.1	9.1	1089.1	228.6	1.8
Δg_{GM}	1211.9	4.1	782.5	295.0	1.3
$\Delta g_{GM}+\Delta g_{RTM}$	130.2	18.7	54.8	7.0	2.4

By reducing the grid of free-air gravity anomalies to the field implied by the geopotential model OSU91A and then also to the residual terrain model, the mean trend in the data reduces from 51.5 mGal to 4.8 mGal and 4.0 mGal, respectively. From Table 3.18 it can be seen that the reduction in the variance and in the variance of horizontal gradients is significant with each new reduction. Also, the latter residual field is smoother and, thus, better suited for prediction. However, the anisotropy index increases.

An attempt was made also to approximate the local empirical covariance function with a modification of the global covariance model proposed by Tscherning and Rapp (1974) [see equation (3.31)]. The coefficients were changed following the procedure given by Schwarz and Lachapelle (1980). The results are: scaling parameter $A = 1882.9$ mGal^2; and ratio parameter $s = 0.995255$. The latter value indicates a radius for the Bjerhammar sphere, $R_B = 6355.9$ km.

The other two sets of estimated covariance functions are for the grids of Bouguer and isostatic anomalies. The trend reduction was performed by subtracting a polynomial surfaces of zero (i.e., mean), first and second degree, respectively. Tables 3.19 and 3.20 give the estimated parameters. It can be seen that the grids of Bouguer and isostatic anomalies show smoother characteristics than those implied by the covariance functions

given in Section 3.4.1 for the original set of data (i.e., random point data). The trend reduction of the gravity anomalies by a second degree polynomial surface produce the same characteristics for the Bouguer and isostatic covariance functions (i.e., they nearly coincide). The same conclusions have been reached, for example, by Abd-Elmotaal (1992) in investigations in the Austrian Alps.

Table 3.19 Covariance function parameters of Bouguer gravity anomalies on a 1' x 1' grid in the Kananaskis extended area

Trend	C_0 mGal^2	$X_{1/2}$ km	G_0 E^2	$C_0/X_{1/2}$ mGal^2/km	Anisotropy
Mean	99.1	28.7	23.4	3.5	1.5
Polyn. (1)	28.8	14.7	12.3	2.0	2.3
Polyn. (2)	14.1	12.2	7.4	1.2	1.6

Table 3.20 Covariance function parameters of isostatic gravity anomalies on a 1' x 1' grid in the Kananaskis extended area

Trend	C_0 mGal^2	$X_{1/2}$ km	G_0 E^2	$C_0/X_{1/2}$ mGal^2/km	Anisotropy
Mean	118.4	23.1	36.8	5.1	1.8
Polyn. (1)	81.8	18.4	29.0	4.4	2.1
Polyn. (2)	12.7	11.6	6.9	1.1	1.3

Figure 3.8 shows for the gridded gravity anomalies in the Kananaskis extended area, the estimated covariance functions of the free-air, Bouguer and isostatic anomalies with the trend reduced by subtracting the mean. To portray the isotropic characteristics of the fields, Figure 3.9 presents two-dimensional normalized representations for the respective covariance functions of Figure 3.8.

From the analysis of the data, it can be seen that the Bouguer and the isostatic anomaly fields have good prediction characteristics. The gravity anomalies reduced by the residual terrain model were expected to have the same characteristics with those of the field of isostatic anomalies. The differences observed indicate some trends still existing in the

former gravity anomaly field. Additional position related polynomial surface trend removal makes their characteristics closer to those of the isostatic gravity anomalies.

Figure 3.8 Covariance functions for predicted 1' x 1' grids of (a) free-air, (b) Bouguer, (c) isostatic gravity anomalies in the Kananaskis extended area
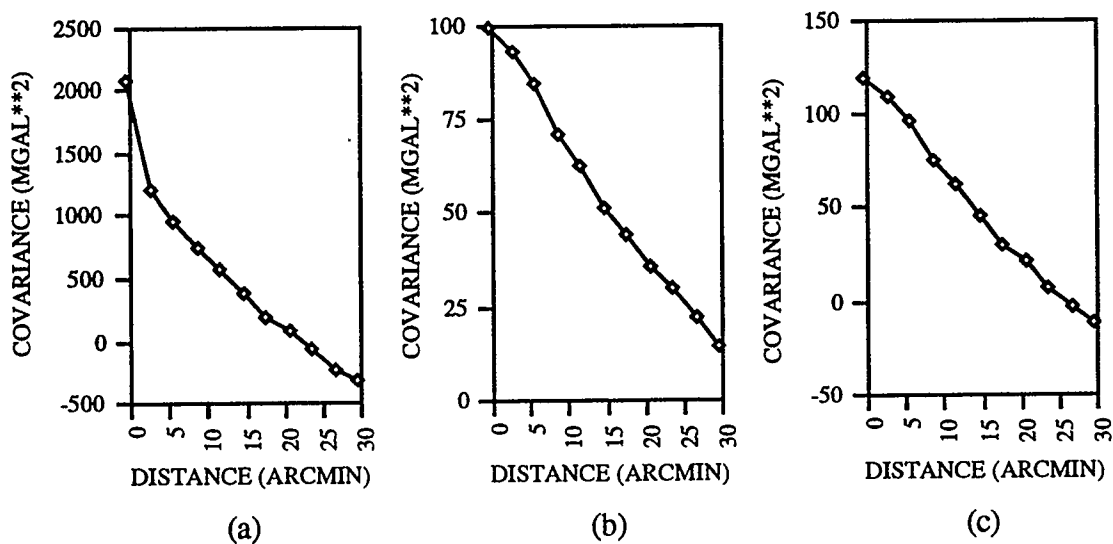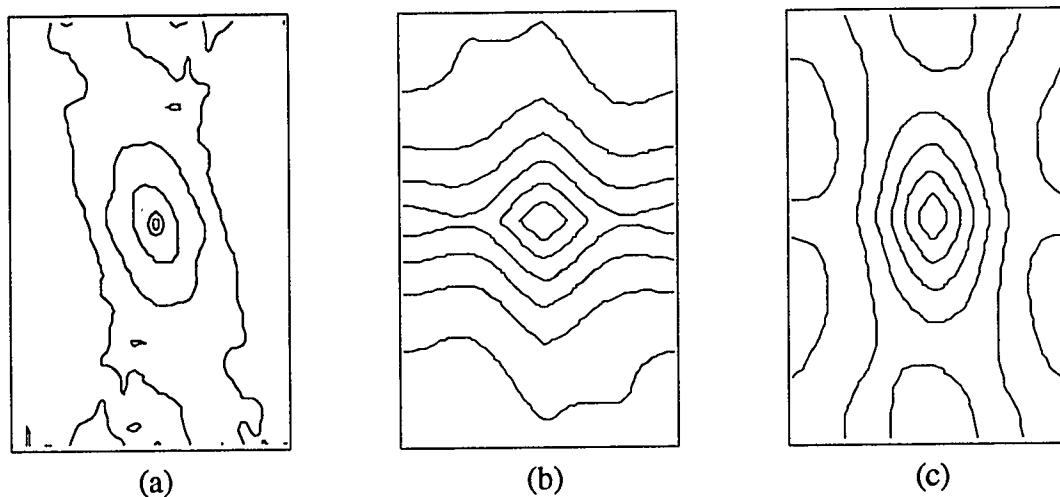

Figure 3.9 Two-dimensional normalized covariance functions for the predicted 1' x 1' grids of (a) free-air, (b) Bouguer, (c) isostatic gravity anomalies in the Kananaskis extended area

Anomaly Degree Variance of Gridded Gravity Anomalies

The spectral behaviour of the gravity anomaly field is also indicated by their anomaly degree variances (Schwarz, 1985). Assuming isotropic gravity anomaly data, the anomaly degree variances were calculated from the estimated covariance functions given above by using equation (3.32). Their analysis will give further information regarding the statistical characteristics of the medium and short wavelength part of the gravity anomaly field.

Figure 3.10 shows the anomaly degree variances for the Kananaskis extended area corresponding to the covariance functions portrayed in Figure 3.8. It can be seen that the anomaly degree variances, σ_n^2, follow a distinct pattern. Thus, they can be modelled with simple parametric equations. Two models were used. The first model is

$$\sigma_n^2 = a + b\log(n) \qquad\qquad (3.40)$$

where a is the intercept of a line segment with the anomaly degree variance axis, b is the slope of the line segment and n is the degree.

(a) (b) (c)

Figure 3.10 Anomaly degree variances for the predicted 1' x 1' grids of (a) free-air, (b) Bouguer, (c) isostatic gravity anomalies in the Kananaskis extended area
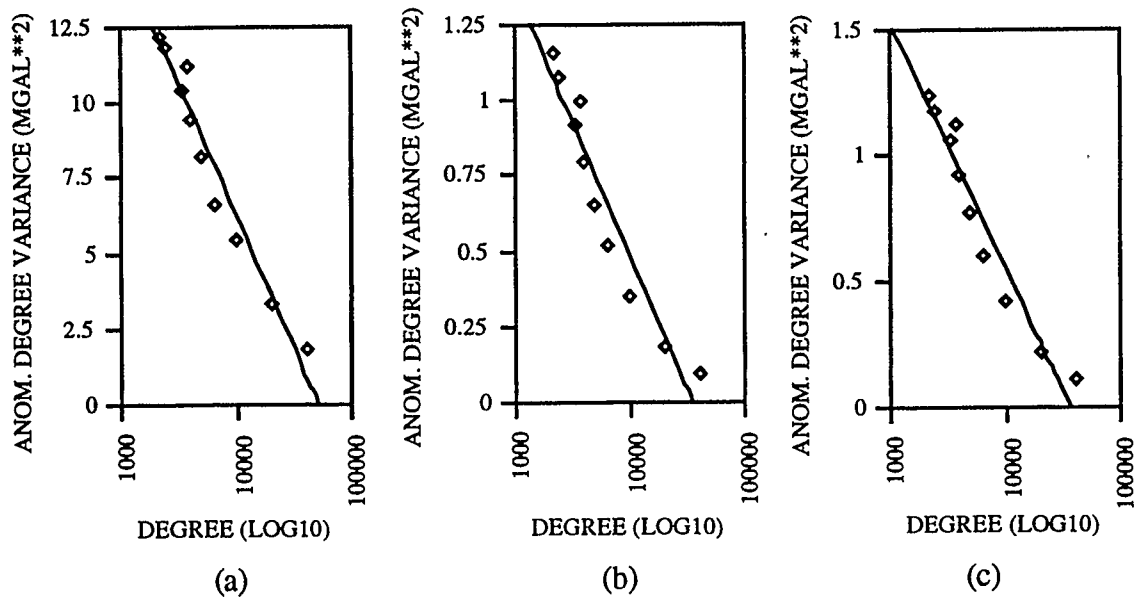
Vassiliou and Schwarz (1987) used the model according to Kaula

$$\sigma_n^2 = \frac{A}{n^{x_g}}$$ (3.41)

where A is a variable scale factor and x_g is an exponent. The scale factor depends on the power of the anomaly gravity field.

Straight line fits were performed for the two models and the estimated parameters are given in Table 3.21. The calculations were carried out for the free-air, Bouguer and isostatic gravity anomalies reduced by subtracting the mean, and also of the residual gravity field obtain by subtracting geopotential model gravity anomalies and then a further subtraction of the influence coming from the residual terrain model.

Table 3.21 Model parameters for the anomaly degree variances of gravity anomalies in the Kananaskis extended area

Gravity Anom.	a mGal^2	b	A mGal^2	x_g
Δg_{FA}	41.37	-8.74	2540.77	0.67
$\Delta g_{FA\text{-}GM}$	7.15	-1.27	33.10	0.31
$\Delta g_{FA\text{-}GM\text{-}RTM}$	4.07	-0.89	897.44	0.83
Δg_B	4.47	-0.97	1474.12	0.90
Δg_I	4.39	-0.95	1254.57	0.87

The analysis of the modelled anomaly degree variances with the parameters given in Table 3.21 indicates a 1 mGal resolution of the gravity anomaly field in the Kananaskis area if the gravity data spacing is at a level of 2.5 km to 3 km (i.e., approximately equivalent to a degree of expansion from 13000 to 16000) and if the topographic effects associated with the rugged topography are taken into account in the calculations.

CHAPTER 4

POINT MASS MODELLING OF GRAVITY ANOMALIES

4.1 Spatial Modelling of Gravity Anomalies

The anomalous gravity field originates from the variations in the density distribution within the earth. The gravitational disturbing potential T may be given as an integral over the Earth

$$T = G \int_{\Omega} \frac{\Delta \rho}{r} d\Omega \qquad (4.1)$$

where G is the gravitational constant, Ω is the volume of the source body (i.e., the Earth), r is the distance, and $\Delta \rho$ is the density anomaly or contrast (i.e., difference between the actual density and a normal density distribution). The spatial representation of the anomalous gravity field of the Earth can be carried out by mathematical models like integral formulas and series of harmonic functions.

In geophysics, the purpose of modelling gravity anomalies in an area is to acquire knowledge regarding the distribution of mass under the Earth's surface. Because there could be an infinite number of mass distributions which are accordant with the observed anomalous gravity field, use of known geophysical evidence (e.g., density contrast and its depth, etc.) is necessary to obtain relevant solutions. Techniques for calculating what should be observed according to a particular model (i.e., forward modelling) for three-dimensional bodies have been developed among others by Talwani and Ewing (1960), Barnett (1976), and Bhaskara Rao et al. (1990).

A forward modelling approach for the spatial representation of the anomalous gravity field that presents a conceptual simplicity and a direct relation to the geophysical reality is the mass model approximation by point masses. Sünkel (1981c) analyses the relation of the point mass models and the anomalous gravity field and Sünkel (1983) implements techniques to generate a point mass model from surface gravity data.

The gravitational disturbing potential T at a point P generated by a set of point masses $\{m_i\}$ is given by

$$T(P) = G\sum_{i=1}^{n} \frac{m_i}{l(P,Q_i)} \tag{4.2}$$

where G is the gravitational constant, $l(P, Q_i)$ is the spatial distance between the calculation point P and the point mass at location Q_i. The presence of the reciprocal distance in the previous equation gives a global support to the computation from point masses (i.e., all data contribute to the calculation of a single quantity). However, the long wavelength contribution coming from the remote areas can be represented by a set of spherical harmonic coefficients of the geopotential and this can assist in reducing the number of point masses used in computation. The residual data field obtained by the subtraction of the reference field allows planar approximation (i.e., flat-Earth) to be used in the formulations. Other functionals of the disturbing potential can be evaluated by applying appropriate operators to equation (4.2).

The gravity disturbance is the first-order gradient of the anomalous potential in the vertical direction and considering equation (4.2) it can be written as

$$\delta g(P) = -\frac{\partial T(P)}{\partial r} = G\sum_{i=1}^{n} \frac{r_P - r_i \cos\psi_i}{l^3(P,Q_i)} m_i \tag{4.3}$$

where r and ψ represent the radial distance and the spherical distance, respectively. The difference between the gravity disturbance and the gravity anomaly is related to the location of the point of calculation of the normal gravity. Because of the large radial distance (e.g. at least 6371 km on the reference sphere), it can be considered (Heiskanen and Moritz, 1967) that in planar approximation the gravity disturbance approximates the gravity anomaly as

$$\delta g = \Delta g + \frac{2}{r}T \doteq \Delta g \qquad\qquad (4.4)$$

According to the previous two equations, if a set of point masses (i.e., point mass model) is given, the gravity anomalies can be calculated in a simple and direct manner. In a local Cartesian coordinate system with the axes x, y, z pointing east, north and upward, respectively, the gravity anomaly generated from point masses is calculated with the equation

$$\Delta g(x,y,z) = G\sum_{i=1}^{n}\frac{(z_i - z)m_i}{[(x_i - x)^2 + (y_i - y)^2 + (z_i - z)^2]^{3/2}} \qquad\qquad (4.5)$$

where the point masses m_i , i = 1, 2, ..., n have the coordinates (x_i, y_i, z_i), respectively. The differences (z_i - z) represents the depths where the point masses are located below the reference surface.

Even with the removal of the remote zone effect calculated from spherical harmonic coefficients of the geopotential, to produce a point mass model from surface gravity data involves a large number of unknowns determined from a large number of data. Using discrete and regular (i.e., grid) data is of importance in the implementation of point mass modelling. By using data in this manner, advantage can be taken of the computation techniques used by spectral methods. Commencing with gridded gravity anomaly data in an area, a point mass model in grid form is generated at an appropriate depth. Subsequently, the set of point masses can be used for the spatial calculation of functionals of the disturbing potential (e.g. gravity anomalies at elevation above the reference surface). Even if the discrete point mass models may not be realistic, they provide a very simple and fast representation for the external gravity field.

Modelling the gravity anomalies by a point masses at the same depth (i.e., single-layer), may produce an inadequate representation. Sünkel (1981c) indicates that a better approach for this type of modelling is the use multi-layer models.

4.2 Relationship Between Covariance Functions and Mass Distributions

In Chapter 3 it was shown that the statistical behavior of the gravity anomaly field can be described by a few parameters, namely the gravity anomaly variance, C_0, the correlation length, $X_{1/2}$, and the variance of the horizontal gravity gradient, G_0. Sünkel (1981c) and Forsberg (1984b) investigate the dependency existing between the essential parameters of the empirical local covariance function and the depth D of the point mass distribution generating the covariance function. The covariance function of data at the reference surface may be regarded as gravity effects generated by a stationary white noise density layer. The covariance function can then be interpreted in terms of the statistical properties of the density anomalies generating the anomalous gravity field and thus gives information regarding the depths of density anomalies.

The variance and the correlation length of a gravity anomaly covariance function are less affected by local anomalies (i.e., topographical and density), thus they are dependent on deeper anomalies. The dependence of these two parameters on the depth of point masses generating the gravity anomalies at the reference surface has to be established.

Consider a local empirical covariance function of residual gravity anomalies. Only gravity anomaly data from the given area is used and a reference field representing the information larger than the area, expressed through a spherical harmonic expansion of the geopotential, is subtracted from the data. In this case, a planar approximation is applicable. A planar type of analytical covariance function that allows derived spatial covariances $C(s, z_i, z_j)$, is the Poisson covariance function

$$C(s) = \frac{C_0}{[1 + (s / D')^2]^{3/2}} \tag{4.6}$$

This function may be regarded as related with a white noise layer of point masses at depth $D = 1/2D'$.

The investigation of Sünkel (1981c) produced empirical approximations expressing the relationship between the gravity variance and the correlation length with the depth of the white noise layer of point masses. The variance C_0 resulting from a white noise anomalous

mass distribution diminishes with increasing depth D. For D less than 100 km, the variance is approximately proportional to D^{-2} (i.e., decreases with the square of the depth)

$$C_0 \doteq \frac{\text{const.}}{D^2} \tag{4.7}$$

The correlation length $X_{1/2}$ depends almost linearly on D with a proportionality factor of approximately 3/2

$$X_{1/2} \doteq \frac{3}{2}D \tag{4.8}$$

When multi-layer modelling is performed by a number of i layers with corresponding mass anomaly variances M_i (i.e., constants), the ratios M_i / D_i^2 must be selected appropriately for adequate results. For uncorrelated multi-layers of white noise densities, the total covariance function representing the gravity effects is the sum of the individual Poisson covariance functions corresponding to each layer. This linear combination can be written as

$$C(s) = \sum_i C_i(s) \approx \sum_i \frac{M_i}{\sum_i M_i} \frac{2D_i}{r_i^3} \tag{4.9}$$

where s the distance argument in the covariance function and r is given by·

$$r_i = [s^2 + (2D_i)^2]^{1/2} \tag{4.10}$$

The parameters D_i an M_i can be adjusted in order to realize a suitable approximation to the empirical covariance function. Forsberg (1984b) has used 3 components to approximate residual gravity models.

The gravity anomaly variances describe the power spectrum of the gravity field distributed over all frequencies. The shape of the power spectrum computed for a particular area contains information regarding the depth of the generating mass disturbances. A logarithmic plot of the power spectrum will show straight line segments portions corresponding to various depths for layers of mass anomalies. The respective depths are obtained from their slopes.

In conclusion, the investigation of the statistical behavior of the gravity anomalies in a local area will infer information regarding the parameters to be used for point mass modelling.

4.3 Spectral Solution to Point Mass Modelling

The planar approximation formulation, made possible by the use of reference gravity anomaly fields (i.e., high degree and order spherical harmonic expansion of the geopotential), and the availability of the data in gridded form allow the use of the Fourier techniques with their advantageous mathematical simplicity. The efficient Fast Fourier Transform (FFT) (Brigham, 1974) algorithm is a very powerful tool. Sideris (1984) and Schwarz et al. (1990) have reviewed the mathematics of the Fourier techniques applied to gravimetric problems in physical geodesy.

Modelling the local gravity anomaly field by point masses can use algorithms entirely based on Fast Fourier Transform methods. Forsberg (1984b) and Vassiliou (1986) have used this approach to spatially model the anomalous gravity field employing point masses on several layers at depth, representing different wavelength features. Under the premise of one-to-one correspondence between the gravity anomaly $\Delta g(x_k, y_l)$ sampled on grid on the surface of the Earth and point masses $m(x_i, y_j)$ on a layer at depth D, the relation between the former and the latter quantities is given by

$$\Delta g(x_k, y_l) = G \sum_{i=1}^{M} \sum_{j=1}^{N} m(x_i, y_j) \frac{D}{[(x_k - x_i)^2 + (y_l - y_j)^2 + D^2]^{3/2}} \qquad (4.11)$$

where G is Newton's gravitational constant, and M and N are the number of points in the x and y directions, respectively. The above equation is a convolution between a point mass at depth and a geometrical kernel. The convolution can be transformed in the frequency domain as

$$F\{\Delta g(k, l)\} = 2\pi G F\{m(i, j)\} e^{-2\pi q D} \qquad (4.12)$$

where $F\{\Delta g(k, l)\}$ and $F\{m(i, j)\}$ denote the Fourier transforms applied to the gravity anomalies and to the point masses at depth D, respectively, and q is the circular frequency. The circular frequency is equal to $(u^2 + v^2)^{1/2}$, where u and v are spatial frequencies in cycles per unit distance in the x and y directions, respectively.

Conversely from equation (4.12), the spectra of point masses can be computed with the equation

$$F\{m(i,j)\} = \frac{1}{2\pi G} F\{\Delta g(k,l)\}e^{2\pi qD} \qquad (4.13)$$

Thus the spectrum of the gridded gravity anomalies on the reference surface is modelled by the spectrum of gridded point masses at depth D. However, due to the exponential operator $e^{2\pi qD}$, some instability is associated with the downward continuation operation in equation (4.13). One approach to address this problem is to smooth the data with a low pass filter to avoid the amplification of the errors at high frequencies.

The sequence of computations is thus the following: transform gridded gravity anomalies on the reference surface from the space domain to the frequency domain; calculate the spectrum of point masses at depth D; apply the inverse Fourier transform to obtain the point masses in the spatial domain. Subsequently, the point masses can be used to calculate gravity anomalies or other functionals applied to the disturbing potential on the reference surface or at elevation above the reference surface.

Considering the convolution equation for the calculation of gravity anomalies at constant elevation h above the reference surface from point masses at depth D as

$$\Delta g(x_k,y_l) = G\sum_{i=1}^{M}\sum_{j=1}^{N} m(x_i,y_j)\frac{D+h}{[(x_k - x_i)^2 + (y_l - y_j)^2 + (D+h)^2]^{3/2}} \qquad (4.14)$$

, the correspondent equation for calculation in the spectral domain is

$$F\{\Delta g(k,l)\} = 2\pi G F\{m(i,j)\}e^{-2\pi q(D+h)} \qquad (4.15)$$

Applying the inverse Fourier transform on equation (4.15) will produce the gravity anomalies in spatial domain at elevation h above the reference surface.

The role of the covariance function to provide information regarding the depth of the layer on which the generating point masses are situated, was introduced in Section 4.2. The covariance function can also be evaluated in the spectral domain as the power spectral

density (PSD). The power spectral density of the gravity anomalies at the Earth's surface, generated by a stationary white noise distribution of point masses on a layer depth D can be written as

$$S_{\Delta g \Delta g}(u,v) = 4\pi^2 G^2 S_{mm}(u,v)e^{-4\pi qD} \qquad (4.16)$$

where $S_{mm}(u,v)$ is the power spectral density of the mass distribution. The slope of the straight line approximation to the logarithmic plot of the power spectral density is a measure of the depth of the layer of point masses.

As it was pointed out earlier, multi-layer modelling of statistically independent point masses produces better results in generating the gravity anomalies on the reference surface. Equations (4.10) to (4.16) can be transformed in synthetic equations of sums corresponding to the number of layers used for the model.

Details regarding the theory and the application of modelling the gravity anomaly field by point masses using frequency domain techniques are found in Sünkel (1981c), Sünkel (1983), Forsberg (1984b),Vassiliou (1986), and Schwarz et al. (1992).

4.4 Implementation of Point Mass Modelling in Kananaskis Area

The 1' x 1' grid of surface free-air gravity anomalies predicted in Chapter 3, extending in the area between latitudes 50°15' and 51°30' and longitudes 244°15' and 245°30', forms the basis for the spatial modelling of the local gravity anomaly field by point masses. The free-air gravity anomalies are terrain corrected (i.e., Faye anomalies). The application of terrain corrections to free-air gravity anomalies constitutes a first approximation to the problem of downward continuation of the surface values to the geoid [see Moritz (1966) and Heiskanen and Moritz (1967)].

There are 5776 surface free-air gravity anomaly points in the Kananaskis extended area, 76 points in each direction. With the mean radius of the Earth, R = 6371 km, and a mean latitude for the area, ϕ = 50.875°, the grid spacing in the North-South (i.e., dy = Rdϕ) and East-West (i.e., dx = Rcosϕdλ) directions are 1.85 km and 1.17 km, respectively. This grid spacing appears adequate to resolve the gravity anomalies at the 1 mGal level, in the Kananaskis area. However, the predicted gravity field model will have the same

smoothness as that of the actual spacing of the observation gravity points within the area. Only between latitudes 50°40' and 51°05' and longitudes 244°38' and 245°08' the mean data spacing is at a level of better than 3 km. Outside this area the gravity data is more sparse and the approximate mean data spacing is at the level of 8 km.

The first step of the modelling process, it is attempted to remove from the local gravity anomaly data the influence coming from outside the area. Gravity anomalies calculated with the spherical harmonic coefficients of the OSU91A geopotential model (Rapp et al., 1991) are subtracted from the local surface free-air gravity anomalies. This geopotential model is to degree and order 360, which indicates a resolution of about 55 km, representing the long wavelength and partially the medium wavelength features of the gravity field. The resulting residual field has a smaller variance (i.e., 1211.9 mGal^2) and a shorter correlation length (i.e., 4.1 km) than the original data, and describes the residual medium and short wavelength part of the gravity field. Planar approximation is justified now in the computations involving the residual gravity anomaly field. Additionally, the short wavelength component in the data coming from the variations of the topography in mountainous areas can be taken care of in the reduction process. This matter will be addressed in Chapter 5.

The residual gravity anomaly field will be modelled by point masses on two layers below the Earth's surface, at different depths. The point masses situated in the deep and the shallow layers cause the remaining medium wavelength and the short wavelength variations of the surface gravity anomalies, respectively. Table 4.1 gives information regarding the original data used to produce the point mass model.

Table 4.1 Statistics of gravity anomaly data used in the modelling process in the Kananaskis area (Unit: mGal)

Gravity Anom.	Minimum	Maximum	Mean	Std. Deviation
Surface Free-air	-80.6	198.0	52.5	45.5
OSU91A	-20.2	112.8	47.7	24.2
Residual	-99.7	162.0	6.4	35.1

The power spectral density corresponding to the local gravity anomalies covariance function was plotted logarithmically in Figure 4.1. By simple graphical techniques, the

variation of the gravity anomaly field can be divided into two parts represented by straight line segments. The slope of each one of them is a measure of the depth of the layer representing each source. The estimated depths for the deep and shallow layer are 8.5 km and 1.5 km, respectively.
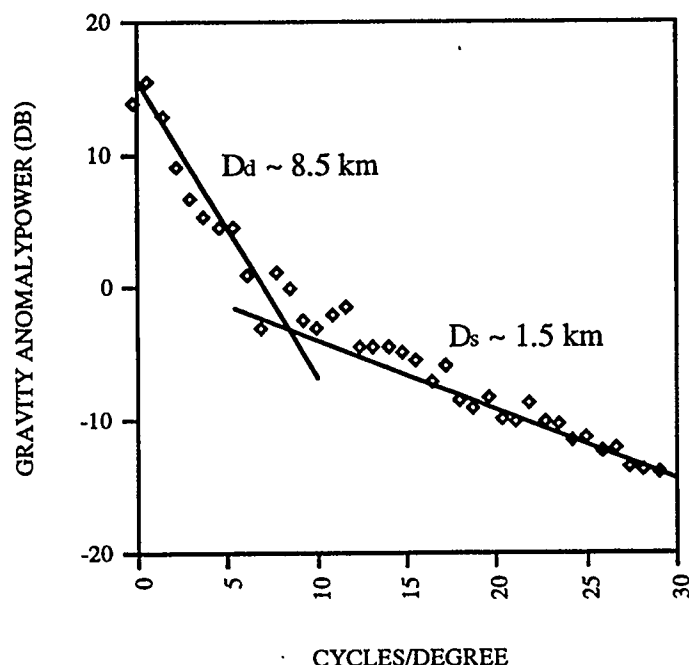

Figure 4.1 Empirical power spectral density for residual free-air gravity anomalies

However, the straight line segments are not very well defined and the depths assigned can have large uncertainties and should be regarded with caution. An attempt was made to approximate the empirical covariance function of the residual gravity anomalies by two empirical covariance functions. Arbitrarily, the covariance function portraying gravity effects resulting from point masses at a deeper layer was estimated from point gravity anomalies calculated by meaning data in 9' x 9' rectangular blocks. The data resulting from the subtraction of the mean point gravity data from the residual gravity anomaly field is used to estimate the empirical covariance function characteristic for the point masses located at a shallow depth. Each empirical covariance function component is then modelled by an analytical Poisson covariance function, and the depths are chosen based on their shape. The resulting deep and shallow layers are again at approximately 8.5 km and 1.5 km, respectively. The empirical gravity anomaly covariance functions are shown in Figure 4.2

and their characteristics (i.e., essential parameters) with the corresponding depths are given in Table 4.2.
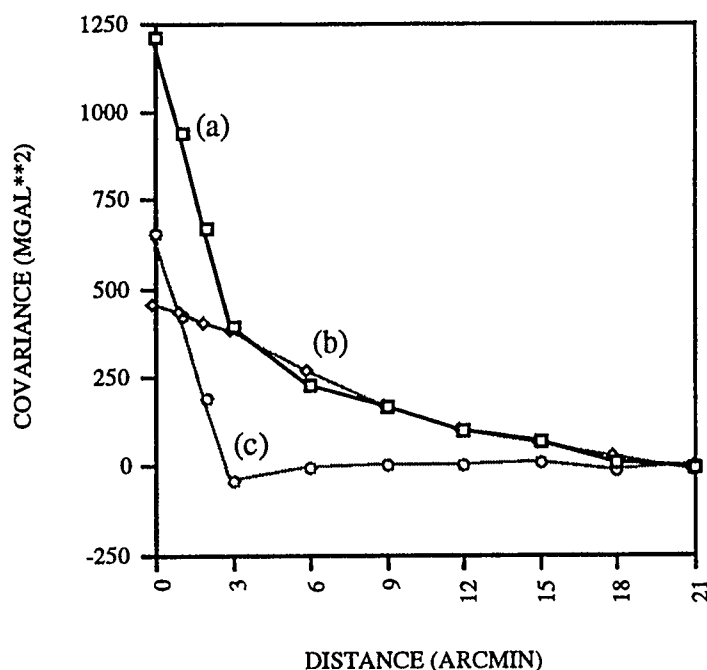
Figure 4.2 Empirical covariance functions of (a) residual surface gravity anomalies, (b) resulting from the point masses on the deep layer, (c) resulting from the point masses on the shallow layer

Table 4.2 Parameters characterizing the surface local empirical covariance function and the two components representing the effects of the deep and shallow sources

Cov. Function	C_0 mGal^2	$X_{1/2}$ km	G_0 E^2	D km
Surface	1211.9	4.1	782.5	
Deep	450.2	13.3	241.4	8.5
Shallow	654.1	2.6	460.6	1.5

The operational computer program GRADCO (Schwarz et al., 1992) is used to model the surface gravity anomaly field by point masses located on two layers, at deep and shallow depths. The high frequencies are cut off and the residual medium frequency range is

modelled on the deep layer first. Then the gravity anomaly part corresponding to the residual medium frequency range is subtracted from the surface residual gravity anomalies and the high frequencies are modelled on the shallow layer. The sum of the gravity anomalies corresponding to the estimated point masses on the two layers reproduced the original gridded gravity anomaly data exactly, even when the depths of the layers were changed at the level of 0.5 km to 1 km.

The aim was to use the two-layer point mass model to calculate the spatial free-air gravity anomaly field at altitudes above the reference surface (i.e., geoid). The area of interest for the gravity model at higher altitude is located between latitudes 50°30' and 51°15' and between longitudes 244°30' and 245°15'. Two elevations were considered for calculations, i.e., 3 km and 4 km, respectively. The spatial gravity anomaly model is the result of the sum of gravity anomalies originating at the deep and the shallow layers, respectively, and because the contribution to the gravity anomaly field coming from outside the area was removed from the original data, its influence must now be restored by adding the spherical harmonic gravity anomalies evaluated at altitude. Statistical results for the gravity anomalies modelled at altitudes of 3 km and 4 km for the Kananaskis core area are given in Table 4.3 and Table 4.4, respectively. The data include information coming from the two-layer point mass modelling, the contribution from the geopotential model, and the total resulting field at elevation. Free-air gravity anomaly field models at 3 km and 4 km are shown in Figure 4.3 and Figure 4.4, respectively.

Table 4.3 Statistics of the free-air gravity anomaly field modelled at 3 km elevation above the reference surface (Unit: mGal)

Gravity Anom.	Minimum	Maximum	Mean	Std. Deviation
Residual	-33.4	40.2	7.0	18.0
OSU91A	14.6	78.0	54.3	10.3
Total	-1.0	96.9	61.3	22.7

Figure 4.3 Spatial free-air gravity anomaly field at 3 km elevation above the reference, from two-layer point mass model (Contour interval: 5 mGal)

Table 4.4 Statistics of the free-air gravity anomaly field modelled at 4 km elevation above the reference surface (Unit: mGal)

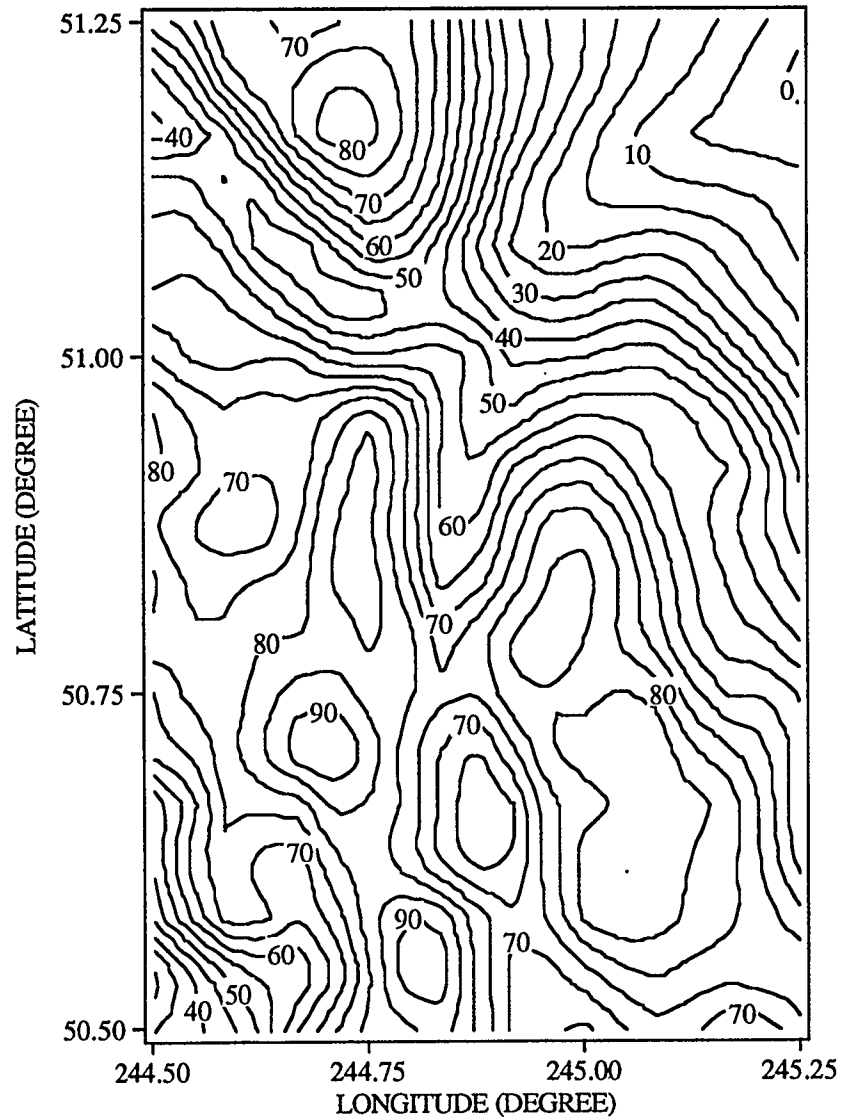| Gravity Anom.	Minimum	Maximum	Mean	Std. Deviation
Residual	-28.9	33.9	6.8	16.2
OSU91A	14.9	76.2	53.0	10.0
Total	1.1	87.8	59.9	21.0
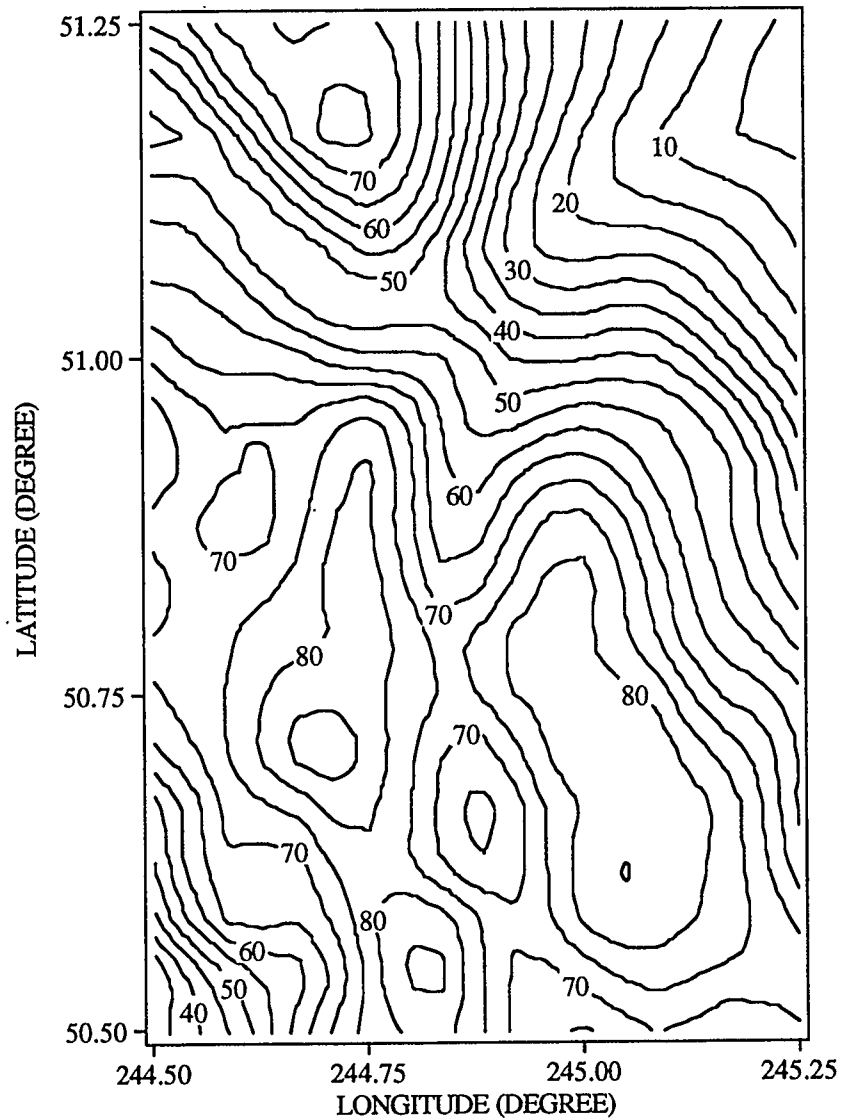
Figure 4.4 Spatial free-air gravity anomaly field at 4 km elevation above the reference, from two-layer point mass model (Contour interval: 5 mGal)

From Table 4.1, Table 4.3 and Table 4.4 it can be seen that the root mean square variation in the gravity anomaly field decreases with elevation, from 69.4 mGal on the reference surface, to 65.4 mGal and 63.4 mGal at 3 km and 4 km, respectively. This indicates an attenuation in the gravity anomaly field at the level of 3% for 1 km increase in elevation. More aspects regarding the spatial behavior of the gravity anomaly field will be discussed in Chapter 5.

CHAPTER 5

UPWARD CONTINUATION OF SURFACE GRAVITY ANOMALIES

5.1 Upward Continuation Formulation

The classical approach to the solution of the boundary value problems in physical geodesy is to produce an approximation of the disturbing potential outside the boundary surface S considering only the data on the surface. The solution is approached either by the use of a series expansion into solid harmonics or by integrals. The relation between the disturbing potential at the boundary surface and the disturbing potential in the space outside can be obtained by solving Dirichlet's problem (i.e., the first boundary value problem of potential theory). This problem can always be solved when the boundary surface is a sphere. An explicit solution of Dirichlet's problem for the exterior of the sphere is the Poisson integral. The following equations cover the main aspects from Heiskanen and Moritz (1967) regarding the formulation of the upward continuation of surface gravity anomalies using the Poisson integral.

The anomalous potential T at a point exterior to a sphere of radius R is

$$T(r,\phi,\lambda) = \sum_{n=0}^{\infty} (\frac{R}{r})^{n+1} T_n(R,\phi',\lambda') \qquad (5.1)$$

where T_n denotes the surface spherical harmonics of the disturbing potential T on the sphere and n is the degree of the harmonic, and (r, ϕ, λ) and (R, ϕ', λ') are geocentric coordinates (i.e., radius, latitude, longitude) in space and on the sphere, respectively. According to the fundamental relationship between the disturbing potential T and the

gravity anomaly Δg (i.e., $\Delta g = -\partial T / \partial r - 2T / R$), the spherical harmonic expansion of the latter can be expressed in space as

$$\Delta g(r,\phi,\lambda) = \frac{1}{r}\sum_{n=0}^{\infty}(\frac{R}{r})^{n+1}T_n(R,\phi',\lambda')$$ (5.2)

By omitting the zero and first order degree harmonics, the gravity anomaly in space is given as

$$\Delta g(r,\phi,\lambda) = \sum_{n=2}^{\infty}(\frac{R}{r})^{n+2}\Delta g_n(R,\phi',\lambda')$$ (5.3)

where Δg_n are surface spherical harmonics of the gravity anomaly field on the sphere. From equation (5.3) it can be seen that the surface harmonics of gravity anomalies attenuate as $r^{-(n+2)}$ in space. The space domain equivalent of equation (5.3) is the Poisson integral. This equation is used for the computation of gravity anomalies in space from gravity anomaly values given on the surface of a geocentric sphere, and is formulated as

$$\Delta g(r,\phi,\lambda) = \frac{R^2}{4\pi r}\iint_{\sigma}(\frac{r^2 - R^2}{l^3} - \frac{1}{r} - \frac{3R}{r^2}\cos\psi)\Delta g(R,\phi',\lambda')d\sigma$$ (5.4)

where the integration of the gravity values corresponding to surface elements $R^2 d\sigma$, is carried out over the whole surface σ of the sphere of radius R. The spatial distance l and the spherical distance ψ from the computation point to the data point are calculated with the equations

$$l = (r^2 + R^2 - 2Rr\cos\psi)^{1/2}$$ (5.5)

$$\cos\psi = \sin\phi\sin\phi' + \cos\phi\cos\phi'\cos(\lambda' - \lambda)$$ (5.6)

, respectively.

By omitting the second and the third terms in the brackets of equation (5.4), (this is related to the removal of the zero and first degree harmonics), the equation for the computation of

gravity anomalies outside a sphere from gravity anomalies given on the surface of the sphere (i.e., upward continuation of gravity anomalies) becomes

$$\Delta g(r,\phi,\lambda) = \frac{R^2(r^2 - R^2)}{4\pi r} \iint_\sigma \frac{\Delta g(R,\phi',\lambda')}{l^3} d\sigma \qquad (5.7)$$

Equation (5.7) requires the gravity anomaly data to be given on the surface of a geocentric sphere. By using gravity anomalies referred to the surface of a geocentric ellipsoid, the error introduced is of the order of the flattening (i.e., $f \doteq 0.3\%$) and can be neglected. This is a spherical approximation. Furthermore, the radial distance r can be substituted by (R + h) and a geographic latitude can be used instead of the geocentric latitude ϕ'. The height h of the computation point above the reference sphere of radius R is actually the elevation above the ellipsoid (or geoid) and represents the distance through which the data is continued upward.

In the vicinity of the calculation point, the sphere can be considered to coincide with a tangent plane. Also, the value of the integral is very small at larger distances from the computation point. Taking into account the former and the latter aspects, the upward continuation calculations can be performed using planar approximation. Considering a rectangular coordinate system (x, y, z) with the x-axis pointing east and the y-axis pointing north in the tangent plane, the planar approximation equation of the Poisson integral (Hirvonen and Moritz, 1963) is

$$\Delta g(r,\phi,\lambda) = \frac{h_0}{2\pi} \iint_A \frac{\Delta g(R,\phi',\lambda')}{l_0^3} dxdy \qquad (5.8)$$

where h_0 is the upward continuation distance above the reference surface. The integration is carried out over a fixed area A with surface elements $R^2 d\sigma \doteq dxdy$. The auxiliary equations used for the calculation of the distance l_0 is

$$l_0 = (x^2 + y^2 + h^2)^{1/2} \qquad (5.9)$$

with

$$x = R\cos\phi'\,(\lambda'-\lambda)$$
$$y = R(\phi'-\phi) \tag{5.10}$$

Equation (5.8) is the flat-Earth space domain upward continuation integral for the computation of gravity anomalies above the xy-plane from values of gravity anomalies considered to be given on the plane. From computational point of view, equation (5.8) is a convolution integral and Fourier transform techniques can be used for the calculation of the upward continued gravity anomaly field (Bhattacharyya, 1967).

Surface spherical harmonic coefficients of the geopotential on a sphere of radius a can be used to generate a gravity anomaly field on the surface of the sphere and in space. Rapp (1982) gives the expression for the computation of gravity anomalies in space from spherical harmonics as

$$\Delta g(r,\phi,\lambda) = \frac{GM}{a^2} \sum_{n=2}^{\infty} (n-1)(\frac{a}{r})^{n+2} \sum_{m=0}^{n} (\overline{C}^*_{nm} \cos m\lambda + \overline{S}_{nm} \sin m\lambda) \overline{P}_{nm}(\sin\phi) \tag{5.11}$$

where (r, ϕ, λ) are geocentric coordinates, GM is the product of the gravitational constant with the Earth's mass, a is the equatorial radius, $\overline{C}^*_{nm}$ and $\overline{S}_{nm}$ are fully normalized potential coefficients with even-degree zonal reference harmonics subtracted, n and m are the degree and order of the expansion, and $\overline{P}_{nm}$ are fully normalized Legendre functions. The summation is carried out to a finite degree $n = n_{maximum}$. The values of a and r determine if the calculations with the spherical harmonic coefficients are performed over the surface of the ellipsoid, sphere or in space.

A gravity anomaly field computed from a spherical harmonic expansion of the geopotential can be used as a reference to be subtracted from the observed gravity anomalies. This allows the integration with the residual gravity anomalies in equations (5.4) and (5.7) to be carried out only on a limited portion of the sphere. For equation (5.8), the subtraction of the reference field justifies the use of planar approximation for the residual gravity anomalies.

A review of the upward continuation formulation and computation methods can be found in Cruz and Laskovsky (1984) and Cruz (1985). The next two sections follow major aspects of their work.

5.2 Methods of Upward Continuation

5.2.1 Gravity Anomaly Data

For computations regarding the external gravity field of the Earth, the anomaly data are usually free-air gravity anomalies. The other Theoretically, the gravity anomalies refer to the geoid if the gravity gradient $\partial g / \partial h$ is used in the free-air reduction. However, when the normal free-air gradient $\partial \gamma / \partial h$ ($\doteq 0.3086$ mGal/m) is used, as is the general practice, the gravity anomalies refer to the Earth's surface rather than to the geoid. The surface free-air gravity anomaly at a point is computed as

$$\Delta g(h,\phi,\lambda) = g_P(h,\phi,\lambda) - (\frac{\partial \gamma}{\partial h})_P H - \gamma_{P'}(0,\phi,\lambda) \tag{5.12}$$

where $g_P(h,\phi,\lambda)$ is the gravity value at the surface point P with ellipsoidal height h and ellipsoidal geographic coordinates (ϕ, λ), H is the orthometric height of point P, and $\gamma_{P'}(0,\phi,\lambda)$ is the normal gravity on the ellipsoid at point P' corresponding to point P (i.e., they have the same geographic coordinates).

Using the orthometric height H instead of the normal height H* in equation (5.12) introduces a certain error in the calculation of the surface gravity anomaly. This error can be expressed as

$$\varepsilon_{\Delta g} = \Delta g_s(h,\phi,\lambda) - \Delta g(h,\phi,\lambda) = -(\frac{\partial \gamma}{\partial h})_P (H^* - H) \tag{5.13}$$

where $\Delta g_s(h, \phi, \lambda)$ is the surface gravity anomaly calculated with equation (5.12) using the normal height H*. Heiskanen and Moritz (1967) give an approximation in metres for the difference $(H^* - H)$ as

$$(H^* - H) = -\Delta g_{Bouguer}H \tag{5.14}$$

with the units of mGal and km for the Bouguer gravity anomaly and the orthometric height, respectively. With the values available from Chapter 2 and Chapter 3, an approximate mean estimate of the error $\varepsilon_{\Delta g}$ for the Kananaskis area is below 0.1 mGal.

To upward continue gravity anomaly data in space using the Poisson integral requires the data to refer to the surface of a geocentric sphere. Therefore, an analytical continuation of the surface gravity anomalies to a level surface is needed first, and then under spherical or planar approximation, produce the upward continued gravity anomaly field using the Poisson integral operator. A general approach for analytical continuation of the gravity anomalies to a level surface is to use a Taylor series to express the relationship between the surface gravity anomalies and level surface gravity anomalies. By applying corrections to the surface gravity anomalies, the solution should converge toward the level surface gravity anomalies. The equation given by Moritz (1980) expressing this operation can be written as

$$\Delta g_P^* = \Delta g_s + \frac{\partial \Delta g}{\partial h}(h_P^* - h_s) + \frac{1}{2}\frac{\partial^2 \Delta g}{\partial h^2}(h_P^* - h_s)^2 + ... \qquad (5.15)$$

where Δg_P^* is the correspondent on the level surface of the surface gravity anomaly Δg, h_P^* and h_s are their respective heights, and $\partial \Delta g / \partial h$ is the vertical gradient of gravity. If the gravity anomaly field has large variations (i.e., contains high frequencies), the difference between Δg_s and Δg_P^* can be significant. Also in areas with rugged topography, the downward continuation solution may diverge. Heiskanen and Moritz (1967) give the equation for the calculation of the vertical gradient of gravity in terms of the gravity itself as

$$\frac{\partial \Delta g}{\partial r} = \frac{R^2}{2\pi}\iint_\sigma \frac{\Delta g - \Delta g_P}{l_0^3}d\sigma - \frac{2}{R}\Delta g_P \qquad (5.16)$$

where the gravity anomaly Δg_P refers to the point at which $\partial \Delta g/\partial r$ is calculated and l_0 (=$2R\sin\psi/2$, ψ is angular distance) is the spatial distance between the point P and the running surface element $R^2 d\sigma$. The results depend strongly on the density and accuracy of the available Δg and this causes difficulties for reliable determinations. Heiskanen and Moritz (1967) and Moritz (1980) discuss the role of equation (5.16) in their analytical continuation solution to the Molodensky's problem. Additional information regarding the downward continuation of free-air anomalies can be found in Wang (1988).

In order to use the surface gravity anomalies with the Poisson integral, different methods attempt to address the data requirements.

5.2.2 Direct Method of Upward Continuation

The direct method uses the surface free-air gravity anomalies Δg_s or the terrain corrected free-air anomalies (i.e., Faye anomalies) $(\Delta g_s + \delta g_{tc})$ as direct input in the Poisson upward continuation integral to calculate the gravity anomaly field in the space outside the Earth's surface. According to the planar approximation equation (5.8) of the Poisson integral, the respective upward continued fields are

$$(\Delta g_s)_{h_0} = \frac{h_0}{2\pi} \iint_A \frac{\Delta g_s}{l_0^3} dxdy \qquad (5.17)$$

and

$$(\Delta g_s + \delta g_{tc})_{h_0} = \frac{h_0}{2\pi} \iint_A \frac{(\Delta g_s + \delta g_{tc})}{l_0^3} dxdy \qquad (5.18)$$

The value of the upward continuation distance h_0 depends on the choice of reference surface.

The requirement for the input anomalies in equations (5.17) and (5.18) is that they be close to their corresponding values on a level surface. The application of terrain corrections to the surface free-air gravity anomalies is a first order approximation to reduce the anomalies to a level surface (Moritz, 1966). If no distinction is considered between the resulting anomalies and their corresponding values on the geoid, the upward continuation distance is then the height measured from the geoid to the upward continuation level. In areas with rugged topography and for low upward continuation altitudes, this could lead to unacceptable errors. Another choice of reference level could be the average elevation over the area where the surface gravity anomalies are located. Keeping in mind that the reference surface positioned at the average elevation is not a level surface and considering the variation of the topography in the area from the average elevation, the errors introduced in calculations can still be significant.

For high accuracy requirements in areas with rugged topography, data reduction to the geoid or to other level surface is in general necessary. However, as indicated in Section

5.2.1, the calculation of the gravity gradients to be used in equation (5.15) presents difficulties.

Another aspect that has to be considered is the use of the spherical harmonic coefficients of available geopotential models to generate gravity anomalies. The subtraction from the gravity anomaly data of gravity anomalies calculated from geopotential expansions makes the residual field suitable for planar approximation (i.e., flat-Earth) methods. The geopotential models available today have a resolution of 55 km. Thus, by referencing the local data to them, a smaller area for integration is needed in the Poisson integral equation. The resulting upward continued field will be the sum of the field generated at elevation by the Poisson integration with the residual gravity anomaly data, and of the field generated by the geopotential model at the upward continuation elevation. Equation (5.11) can be used for the latter calculation with (a + h₀) instead of r.

5.2.3 Indirect Method of Upward Continuation

The indirect method computationally removes from the surface free-air gravity anomaly data the gravitational effects caused by shallow topographic masses. These effects have a high frequency character, representing the very short wavelength part of the gravity anomaly field. As suggested in Section 5.2.3, spherical harmonic expansions of the geopotential are used as a reference representing the long and part of the medium wavelength component of the gravity anomaly field.

The vertical attraction on the Earth's surface generated by the topographic masses lying between it and the geoid can be expressed as

$$\Delta g^{t1} = 2\pi G \rho h - \delta g_{tc} \tag{5.19}$$

where $2\pi G \rho h$ is the attraction of the Bouguer plate and δg_{tc} denotes the terrain correction.

Considering a reference topographic surface of heights h^S, the masses between the latter surface and the geoid generate a vertical attraction on the reference topography expressed as

$$\Delta g^{t2} = 2\pi G \rho h^S - \delta g_{tc}^S \tag{5.20}$$

where the terms have the same meaning as those in equation (5.19). For example, the reference topographic surface in equations (5.20) and (5.21) can be calculated from a spherical harmonic expansion of the topography of the same degree and order as the geopotential model.

Equations (5.19) and (5.20) are equivalent to equation (2.23) in Section 2.3.2; and the two terms on their right hand side are given respectively by the equations (2.21) and (2.22).

The topographic gravity anomaly resulting from the difference of the former and the latter vertical attractions is equal to

$$\Delta g^t = 2\pi G \rho (h - h^S) - (\delta g_{tc} - \delta g_{tc}^S) \qquad (5.21)$$

The residual gravity anomaly is obtained by subtracting the spherical harmonic generated anomaly Δg^S and by removing the topographic anomaly Δg^t, as

$$\Delta g^r = \Delta g_s - \Delta g^S - \Delta g^t \qquad (5.22)$$

or

$$\Delta g^r = \Delta g_s - \Delta g^S - 2\pi G \rho (h - h^S) + (\delta g_{tc} - \delta g_{tc}^S) \qquad (5.23)$$

The resulting gravity anomaly in equation (5.23) is called the residual refined Bouguer anomaly. The reduction of the gravity anomalies in this manner (i.e., residual terrain model reduction) and their use in the upward continuation of gravity data in a mountainous area was suggested by Forsberg (1984a). Cruz and Laskovsky (1984) used this approach for upward continuation of surface free-air gravity anomalies.

The residual refined Bouguer gravity anomalies are very smooth and are assumed to be on the reference topographic surface. Before they are input in the Poisson integral for upward continuation, they must be terrain corrected on the reference topographic surface (i.e, add δg_{tc}^S). The upward continued residual gravity anomaly field at the upward continuation h_0 is calculated with the equation

$$(\Delta g^r + \delta g_{tc}^S)_{h_0} = \frac{h_0}{2\pi} \iint_A \frac{(\Delta g^r + \delta g_{tc}^S)}{l_0^3} dxdy \qquad (5.24)$$

The total upward continued gravity anomaly field is the sum of the following terms: Poisson integration values of the residual refined Bouguer gravity anomalies calculated with equation (5.24); spherical harmonic anomalies Δg^S calculated with equation (5.11); and integration of the gravitational effects of the removed topographic masses with equation (2.29), where the elevation of the computation point (i.e., z_1) is equal to the upward computation distance.

This study deals with the application of the Poisson integration for the upward continuation of surface gravity anomalies. Least-squares collocation is another approach that can be used to upward continue surface gravity anomalies. An advantage of the latter method is that there is no requirement for the gravity anomaly data to be located on a level surface. However, the method requires large matrix inversion. Sünkel (1981a), Rapp (1978) and Cruz (1985) have investigated the use of least-squares collocation in the upward continuation of surface gravity anomalies.

5.3 Upward Continuation Error Propagation

The dominant source of error in the upward continuation procedure are the errors in the original random point surface gravity anomaly data and the errors resulting from the prediction procedure. These two errors should be considered as limiting factors in the quality of the upward continued field. The scale of the original error variances will be reflected into the scale of the upward continued variances. The correlation between the mean surface gravity anomaly blocks used in the upward continuation calculations is directly related to the spacing of the initial point data. Because the correlated errors do not attenuate quickly, large correlation lengths of the errors in the gravity anomaly field at the reference level will have an adverse effect in the upward continuation procedure.

Systematic errors present in the surface gravity anomaly data propagate in the upward continuation calculation with the Poisson integral (Moritz, 1962) as

$$\varepsilon_{h_0}(x,y) = \frac{h_0}{2\pi} \iint_A \varepsilon(x',y') \frac{dx'\,dy'}{l_0^3}$$

(5.25)

Moritz (1962) gives as a statistical estimate of the upward continuation procedure, the mean square error, formulated as

$$m_{\Delta g h_0}^2 = \frac{h_0^2}{4\pi^2} \iint_{xy} \iint_{x'y'} \sigma(x,y,x',y') \frac{dx\,dy}{l_0^3} \frac{dx'\,dy'}{l_0^3}$$

(5.26)

where $\sigma(x, y, x', y') = M(\varepsilon', \varepsilon)$ is the error covariance function that statistically characterizes the errors $\varepsilon(x, y)$ in Δg and M is a suitable averaging operator (Heiskanen and Moritz, 1967; Moritz, 1980).

The error covariance function of the gravity anomalies can be modelled by a Gaussian function [see equation (3.22)], which is dependent only on the distance between data points, as

$$\sigma(x,y,x',y') = C_0 e^{-A^2 s^2} = C(s)$$

(5.27)

with the constant $A = \sqrt{\ln 2} \, / \, X_{1/2}$, where $X_{1/2}$ is the correlation length. With the premise that the ratio $X_{1/2}/h_0$ is small, Moritz (1962) gives for equation (5.27) a simple form to calculate the mean square error present in the upward continued gravity anomaly field, as

$$m_{\Delta g h_0}^2 = \frac{1}{8h_0^2} \frac{C_0}{A^2}$$

(5.28)

The above equation can be used as a measure of precision when the flat-Earth (i.e., planar) approximation is used. For spherical-Earth approximation, Cruz and Laskovsky (1984) have shown that the error propagation through the upward continuation operation is at the same level with the former.

If correlations between the adjoining mean blocks are not taken into account, the mean square error of prediction in the upward continued field due to the quality of the original data (i.e., error variances $m_{\Delta g}^2$) can be calculated according to Rapp (1966) as

$$m_{\Delta g_{h_0}}^2 = \frac{h_0^2}{(2\pi)^2} \iint_A m_{\Delta g}^2 (\frac{dxdy}{l_0^3})^2 \qquad (5.29)$$

This should be considered as a relative measure of precision, i.e. only the relative degree of attenuation of the errors is relevant.

Moritz (1962), Sünkel (1981a) and Cruz and Laskovsky (1984) have investigated also the effect of the representation error, which is the result of the substitution in the calculations of a continuous function by a step function in terms of Δg (i.e., mean blocks). The effect is insignificant by comparison with the errors coming from the surface data.

There is a systematic error component that comes from the extent of the area of integration used in the computation of the upward continuation field with the equation (5.8) of the Poisson integral. Heiskanen and Moritz (1967) have investigated the average value effect of the distant regions in the upward continuation calculations. For an average value of the gravity anomalies $\overline{\Delta g}$ in areas beyond a distance s_0, the effect $\bar{\epsilon}$ is

$$\bar{\epsilon} = \frac{h_0}{s_0} \overline{\Delta g} \qquad (5.30)$$

From this equation, it results that the integration area A must be approximately proportional to h_0 in order to obtain with the Poisson integral [see equation (5.8)] the same error $\bar{\epsilon}$ for different upward continuation elevations.

5.4 Upward Continuation of Surface Free-air Gravity Anomalies in the Kananaskis Area

Investigation Area and Data

The investigation area in Kananaskis was described in Chapters 2, 3 and 4. The 1' x 1' (i.e., 1.9 km x 1.8 km) grid of surface free-air gravity anomalies, terrain corrected, bounded by latitudes 50°15' and 51°30' and by longitudes 244°15' and 245°30' (i.e., Kananaskis extended area), constitute the primary data used in the upward continuation operation. Grids of the same resolution of gravity anomalies at the reference surface and at

higher altitudes were generated from the spherical harmonic coefficients of the geopotential model OSU91A to degree and order 360 (Rapp et al., 1991). For the indirect method, digital elevation models of the topography and of the mean topography over the Kananaskis area were also part of the data. The digital elevation model of mean topographic heights was generated by averaging elevations in rectangular blocks of 30' x 30' for each point of the grid.

Using the data mentioned above, upward continued gravity anomaly fields will be computed at 3 km and at 4 km, respectively, above the geoid over the area between latitudes 50°30' and 51°15' and between longitudes 244°30' and 245°15' (i.e., Kananaskis core area).

Direct Method of Upward Continuation

The gridded surface free-air gravity anomalies (terrain corrected) are reduced to geopotential model gravity anomalies. With the residual gravity anomaly data, mean values are calculated for each 1' x 1' block of the grid. These data are assumed at the geoid level. This assumption can introduce significant distortions in the upward continued gravity field in an area with rugged topography. As it was discussed in Section 5.2, there is an uncertainty in the upward continuation distance due to the uncertainty in the vertical location of the reference surface for the gravity anomaly data. To investigate the sensitivity of the upward continuation process in the data, computations were carried out with the residual gravity anomalies in the Poisson integral given in planar approximation [i.e., equation (5.18)] with upward continuation distances of 1 km, 2 km, 3 km and 4 km, respectively. Though the upward continuation is mainly a local calculation (i.e., a radius around the computation point 10 times the upward continuation distance is in general sufficient), all the data were used in the integration calculation for each point. The gravity anomaly field at altitude is obtained by adding to the residual upward continued field, the contribution coming from the geopotential model evaluated [i.e., equation (5.11)] at altitude.

The statistics of the results for the Kananaskis core area are given in Table 5.1. The root mean square variation, in mGal, of the gravity anomaly field, decreases for each 1 km increase in altitude by 6.2, 4.6, 2.1 and 1.9, respectively. These numbers indicate that the gravity anomaly field attenuates by 8.2%, 6.6%, 3.2% and 2.9%, respectively. The largest changes occur at low altitudes.

Table 5.1 Statistics of sensitivity of free-air gravity anomalies with change in upward continuation distance (Unit: mGal)

Contin. Dist.	Minimum	Maximum	Mean	Std. Dev.	RMS
0 km	-28.8	175.1	67.0	39.8	78.0
1 km	-8.4	139.3	64.5	31.6	71.8
2 km	-1.7	108.5	62.5	24.8	67.2
3 km	1.3	96.7	61.2	22.1	65.1
4 km	3.1	89.0	59.9	20.4	63.2

Figure 5.1 and Figure 5.2 portray the upward continued gravity anomaly fields for the upward continuation distances of 3 km and 4 km, respectively.

Calculations with the Poisson integral were carried out also with the assumption that the residual gravity anomalies refer to a surface with the elevation corresponding to the average elevation over the area (i.e., 1.84 km for the Kananaskis extended area). In this case, the residual gravity anomalies are upward continued from the elevation of the reference surface to 3 km and 4 km altitudes from the geoid, respectively. The statistics of the computation results are given in Table 5.2 and the contour plans are shown in Figure 5.3 and Figure 5.4, respectively.

Table 5.2 Statistics of upward continuation by direct method of free-air gravity anomalies (data considered at a mean elevation of 1.84 km) (Unit: mGal)

Contin. Dist.	Minimum	Maximum	Mean	Std. Dev.
3 km	-3.0	117.4	63.8	26.6
4 km	-0.8	105.9	62.6	24.2

To assess the direct method, these results will be compared subsequently with the results produced by the other methods investigated in this study.
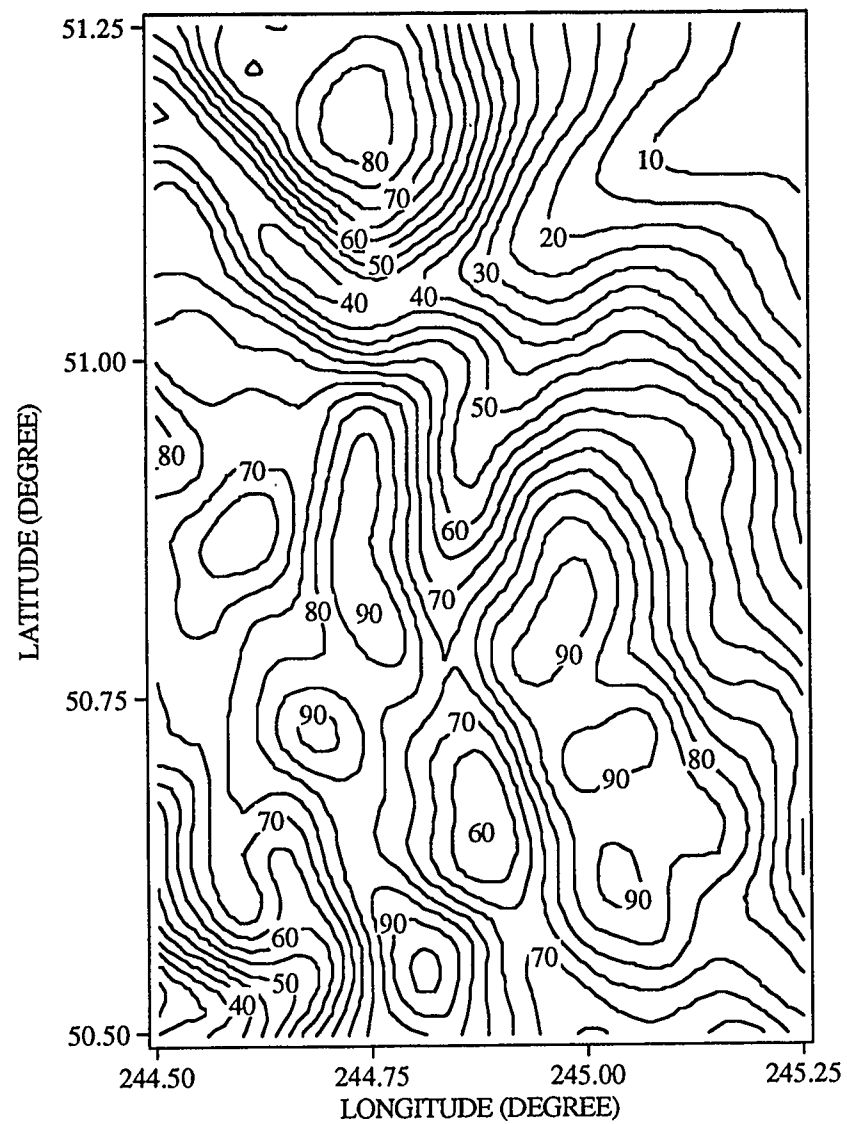
Figure 5.1 Upward continued free-air gravity anomalies (reduction to geoid is neglected) by the direct method (Contour interval: 5 mGal; upward continuation level: 3 km)

Figure 5.2 Upward continued free-air gravity anomalies (reduction to geoid is neglected) by the direct method (Contour interval: 5 mGal; upward continuation level: 4 km)
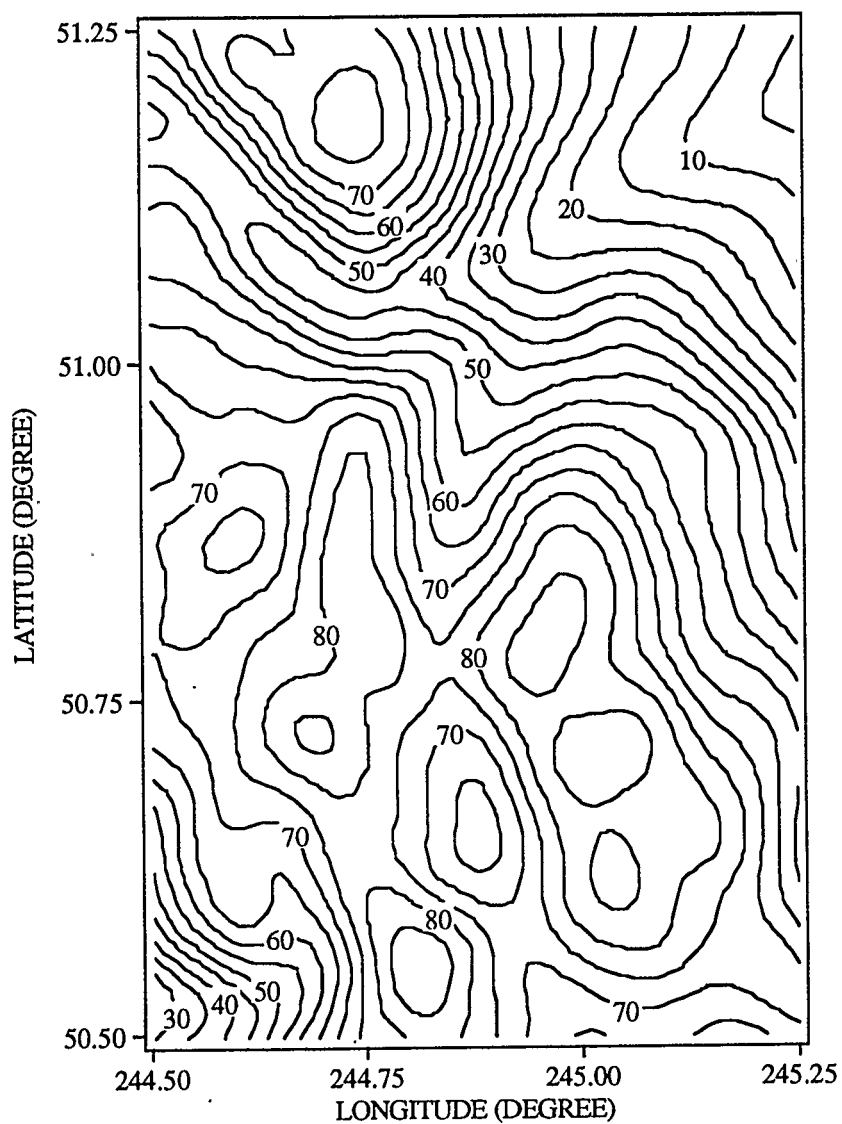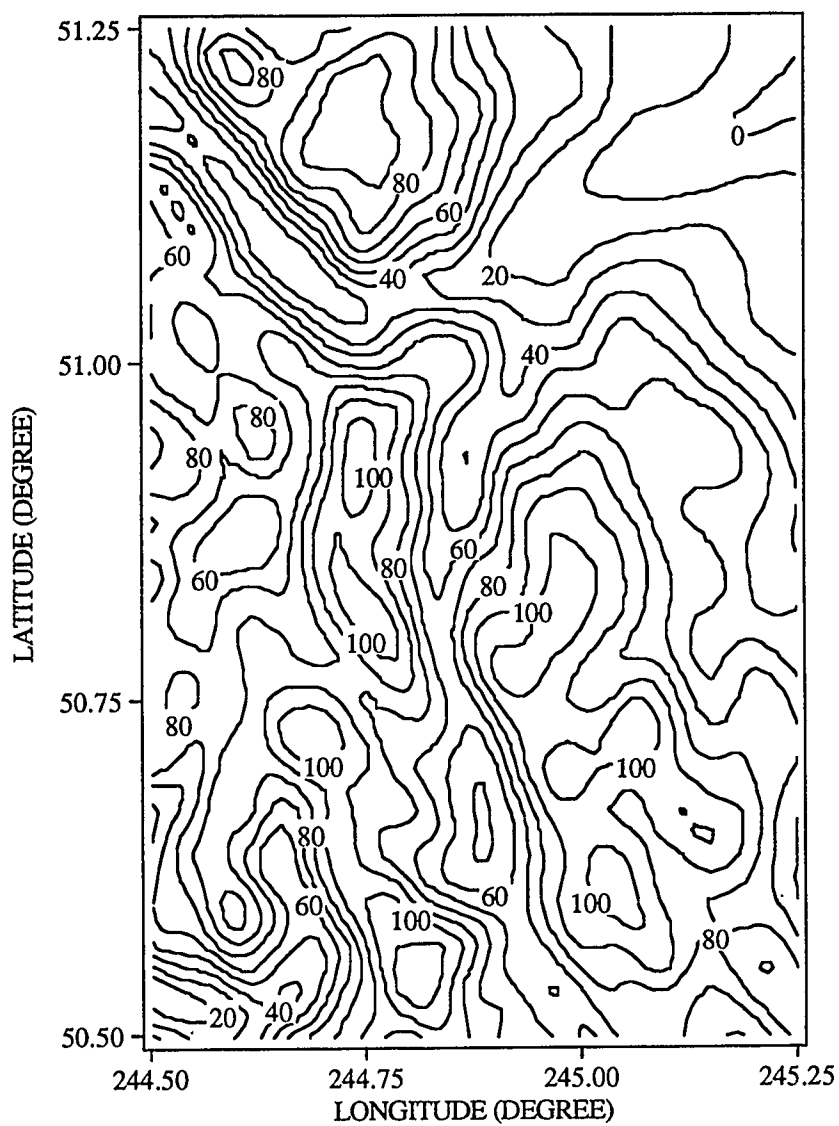
Figure 5.3 Upward continued free-air gravity anomalies (data considered at a mean
elevation of 1.84 km) by the direct method

(Contour interval: 10 mGal; upward continuation level: 3 km)

Figure 5.4 Upward continued free-air gravity anomalies (data considered at a mean
elevation of 1.84 km) by the direct method

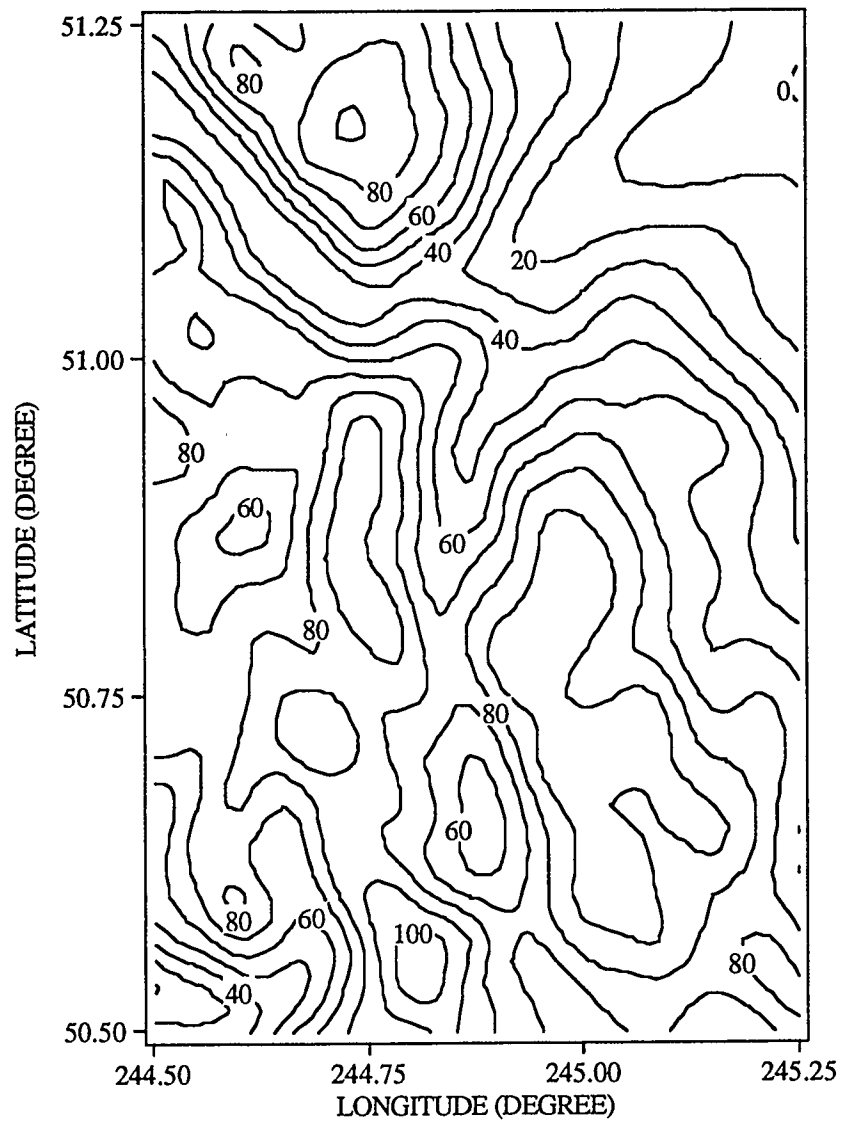(Contour interval: 10 mGal; upward continuation level: 4 km)

Indirect Method of Upward Continuation

In the indirect method, the residual gravity anomaly data result from the reduction of the surface gravity anomalies to the geopotential model and by subtracting the gravitational effects caused by topographic masses lying between the surface of the Earth and a smooth surface, representing mean elevations over the area. The latter reduction is realized by subtracting the result obtained from equation (5.21). The first term on the right hand side is obtained by subtracting the two 1' x 1' elevation grids (i.e., digital elevation model of the topographic surface and digital elevation model of the average elevations) and multiplying with the Bouguer gradient (i.e., 0.1119). The terrain corrections necessary to calculate the second term on the right hand side of equation (5.21) were obtained by prism integration using equation (2.29) with the computer program given by Forsberg (1984a). The resulting residual gravity anomaly field (i.e., residual refined Bouguer gravity anomalies) is very smooth and assumed to refer to the average elevation surface. Its statistics (i.e., minimum, maximum, mean and standard deviation), in mGal, are -35.9, 33.4, 4.1 and 11.2, respectively. Following the procedure given in Section 5.2.3, upward continued gravity anomaly fields were computed. The statistics of the results are given in Table 5.3 and the contour plans are shown in Figures 5.5 and Figure 5.6, respectively.

Table 5.3 Statistics of upward continuation by the indirect method of free-air gravity anomalies (Unit: mGal)

Contin. Dist.	Minimum	Maximum	Mean	Std. Dev.
3 km	-5.0	115.4	61.7	26.3
4 km	-2.8	104.1	60.5	24.0

A cursory examination of the data presented in Tables 5.2 and 5.3 shows that the values in the latter table are slightly lower.

For a better view of the variation of the gravity anomaly field in the upward continuation process two profiles were chosen for investigation, one at latitude 50°53', between longitudes 244°38' and 245°08' (i.e., 35.1 km); the other at longitude 244°53', between latitudes 50°40' and 51°05' (i.e., 46.3 km). These profiles are located in the area where there is a high density of point gravity anomaly data, and thus the gravity anomaly model is considered more reliable. Also, the variations in topography and the gravity anomaly field

are large. For each profile, the statistics considered regard elevations, surface free-air gravity anomalies, and upward continued gravity anomalies at 3 km and 4 km altitude. The statistics are given in Table 5.4 and Table 5.5 for the latitude and the longitude profiles, respectively; and the plots for each profile are given in Figure 5.7 and Figure 5.8, respectively.
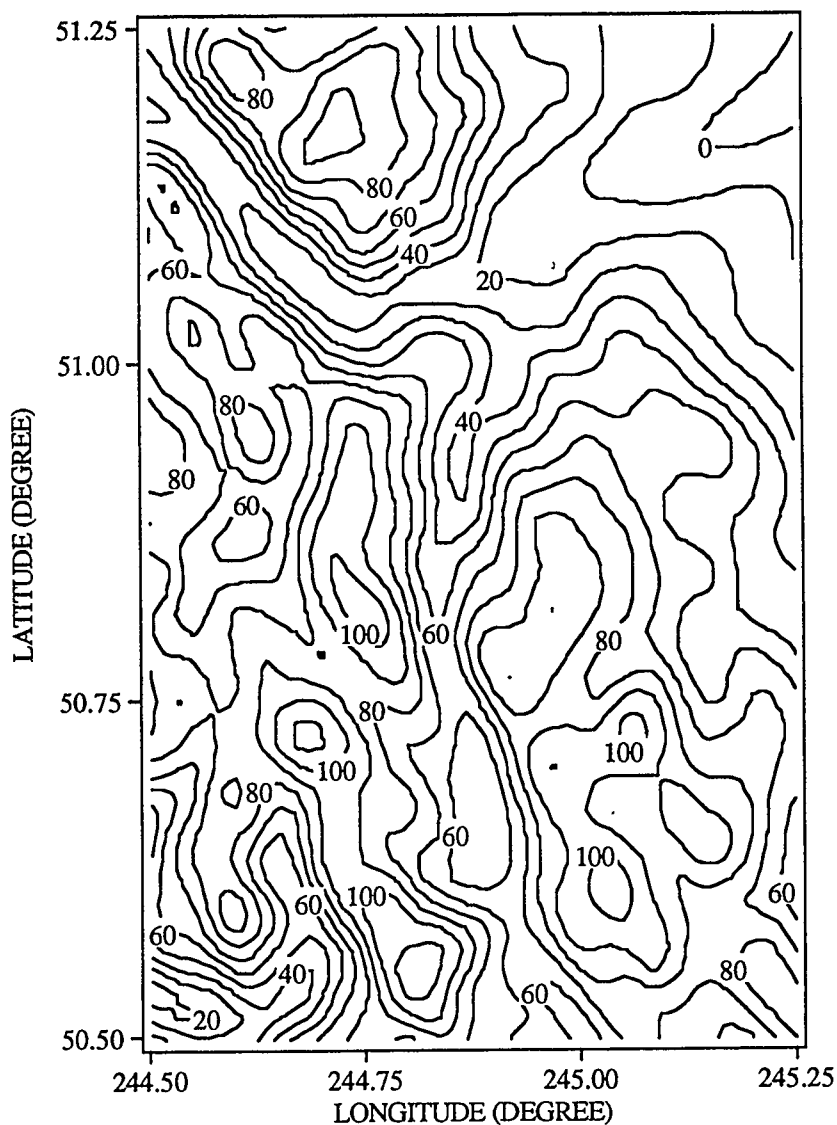

Figure 5.5 Upward continued free-air gravity anomalies by the indirect method
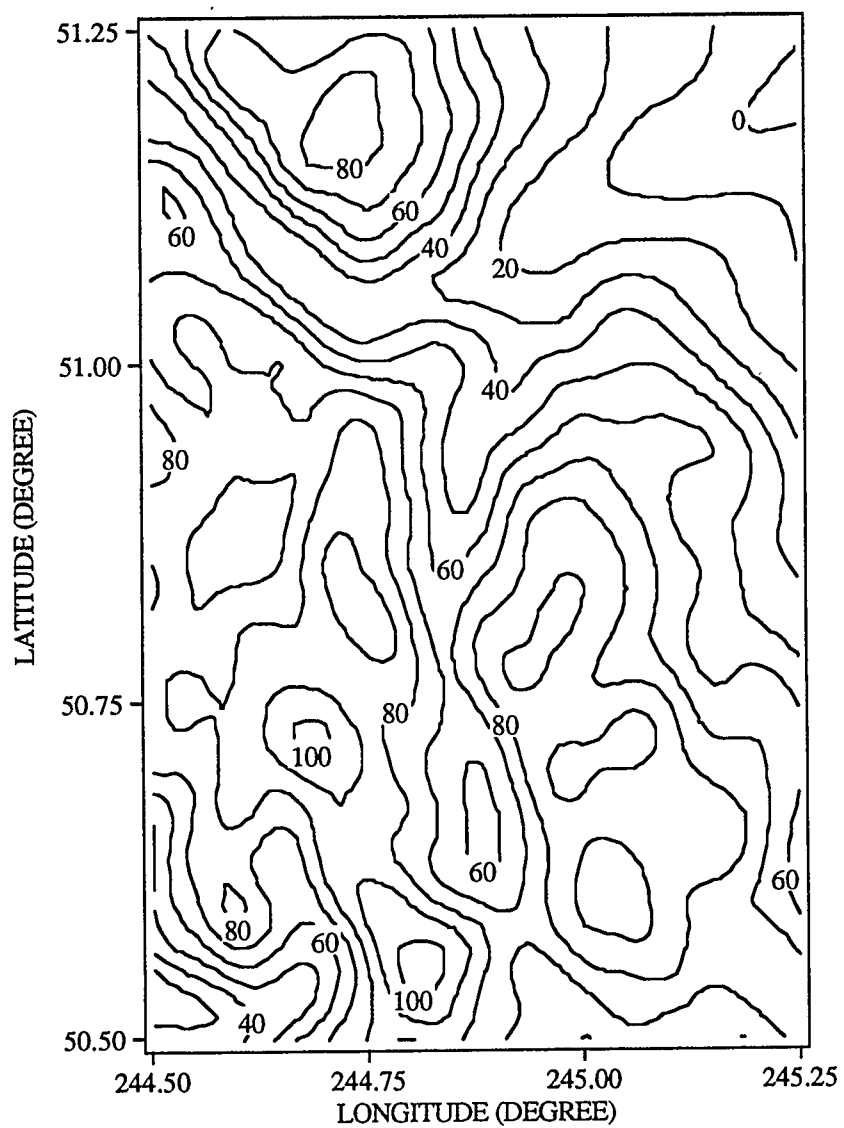(Contour interval: 10 mGal; upward continuation level: 3 km)

Figure 5.6 Upward continued free-air gravity anomalies by the indirect method
(Contour interval: 10 mGal; upward continuation level: 4 km)

Table 5.4 Statistics of profiles at latitude 50°53' between longitudes 244°38' and 245°08' of elevations, surface and upward continued by the indirect method of free-air gravity anomalies (Units: elevation, m; gravity anomaly, mGal)

Profile	Minimum	Maximum	Mean	Std. Dev.
Elevation	1614.0	2489.5	2056.56	271.9
Surface Anom.	27.9	125.1	79.0	31.4
Anom. at 3 km	43.2	96.6	73.9	16.3
Anom. at 4 km	51.1	89.7	72.2	12.0

Table 5.5 Statistics of profiles at longitude 244°53' between latitudes 50°40' and 51°05' of elevations, surface and upward continued by the indirect method of free-air gravity anomalies (Units: elevation, m; gravity anomaly, mGal)

Profile	Minimum	Maximum	Mean	Std. Dev.
Elevation	1299.0	2424.1	1790.7	330.9
Surface Anom.	-3.2	117.9	48.8	37.0
Anom. at 3 km	19.7	90.7	53.6	19.5
Anom. at 4 km	23.8	84.2	55.4	17.5

113

Figure 5.7 Profiles at latitude 50°53' of (a) elevation, (b) surface free-air gravity anomalies, upward continued anomalies by the indirect method at elevations of (c) 3 km and (d) 4 km

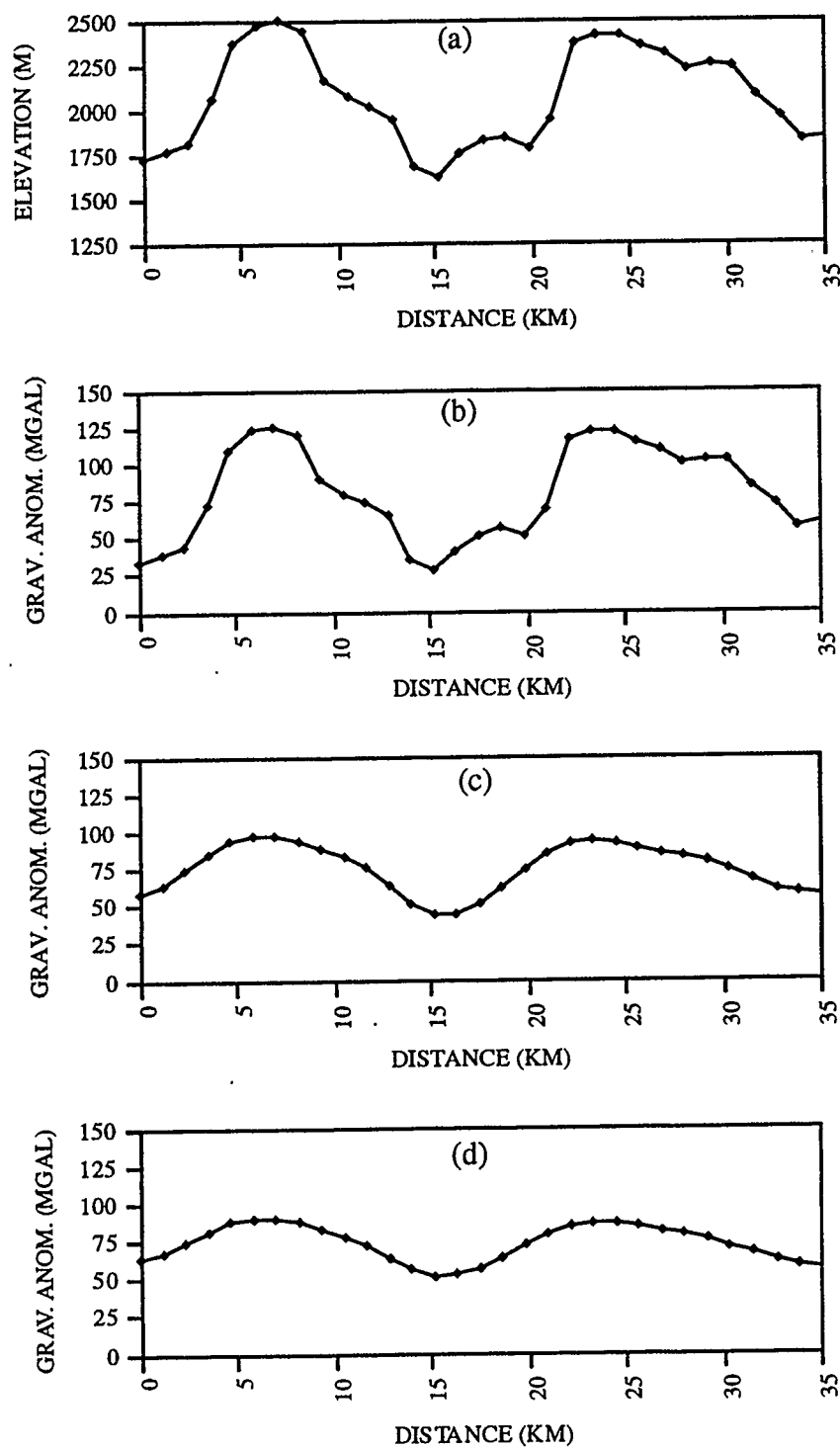**Figure 5.8** Profiles at longitude 244°53' of (a) elevation, (b) surface free-air gravity anomalies, upward continued anomalies by the indirect method at elevations of (c) 3 km and (d) 4 km
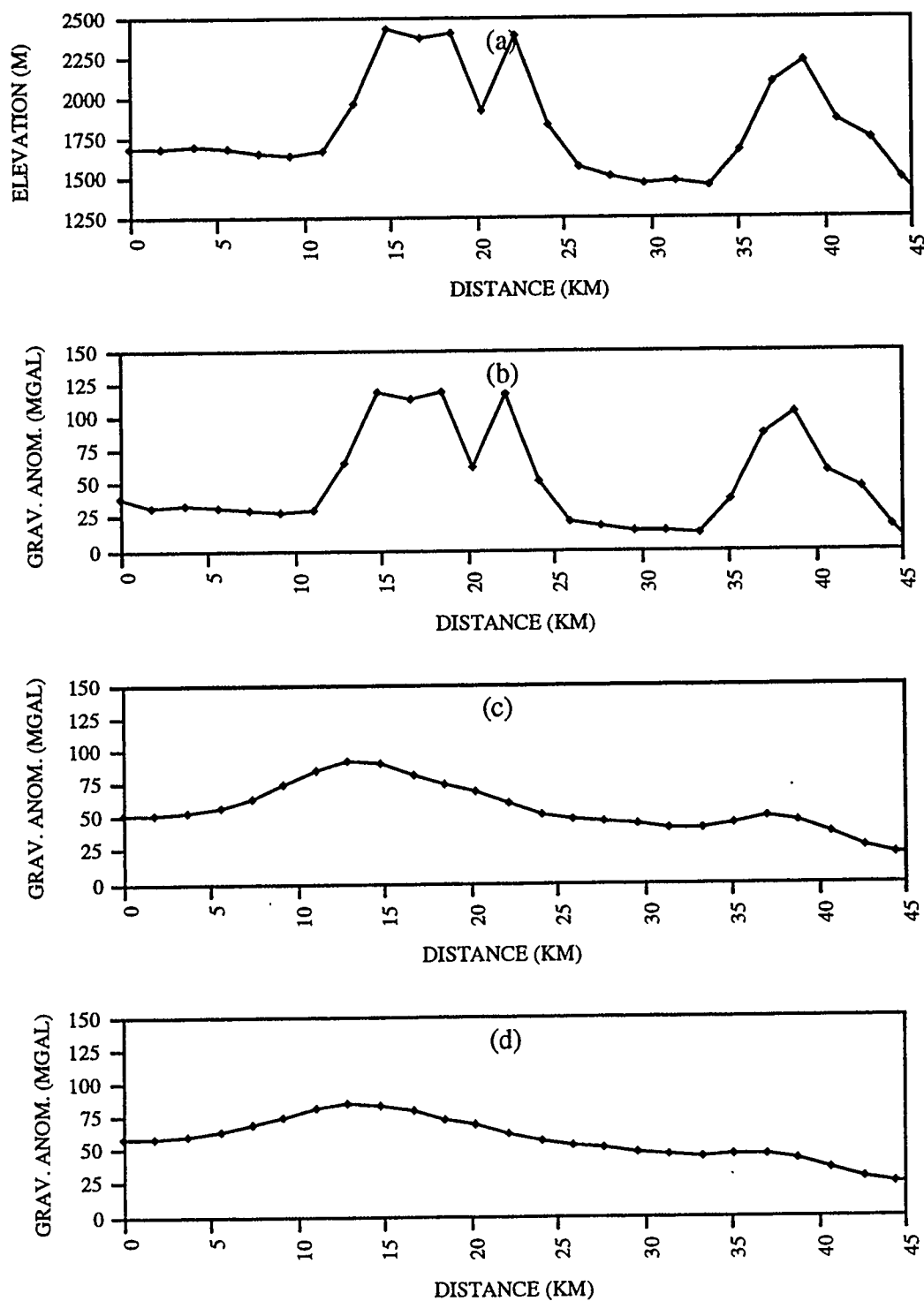
Data Error Propagation

In order to obtain information regarding the relative magnitude of the propagated standard deviations at altitude, calculations with equation (5.26) were carried out. However, no correlations were considered in the upward continuation process [see equation (5.29)]. The data used were the standard deviations estimated in Section 3.4.1.

The arbitrary scaling of the standard deviations on the reference surface will cause a corresponding scaling of the upward continued standard deviations. Only the degree of tapering of the data has a more realistic meaning. The statistics of the results are given in Table 5.6 and the contour plans are shown in Figure 5.9. Considering the values given in Tables 3.10 and/or 3.11, the root mean square variation in the data reduces by 85% from the reference surface to 3 km altitude. From 3 km altitude to 4 km altitude, the root mean square variation in the data reduces by 45%.
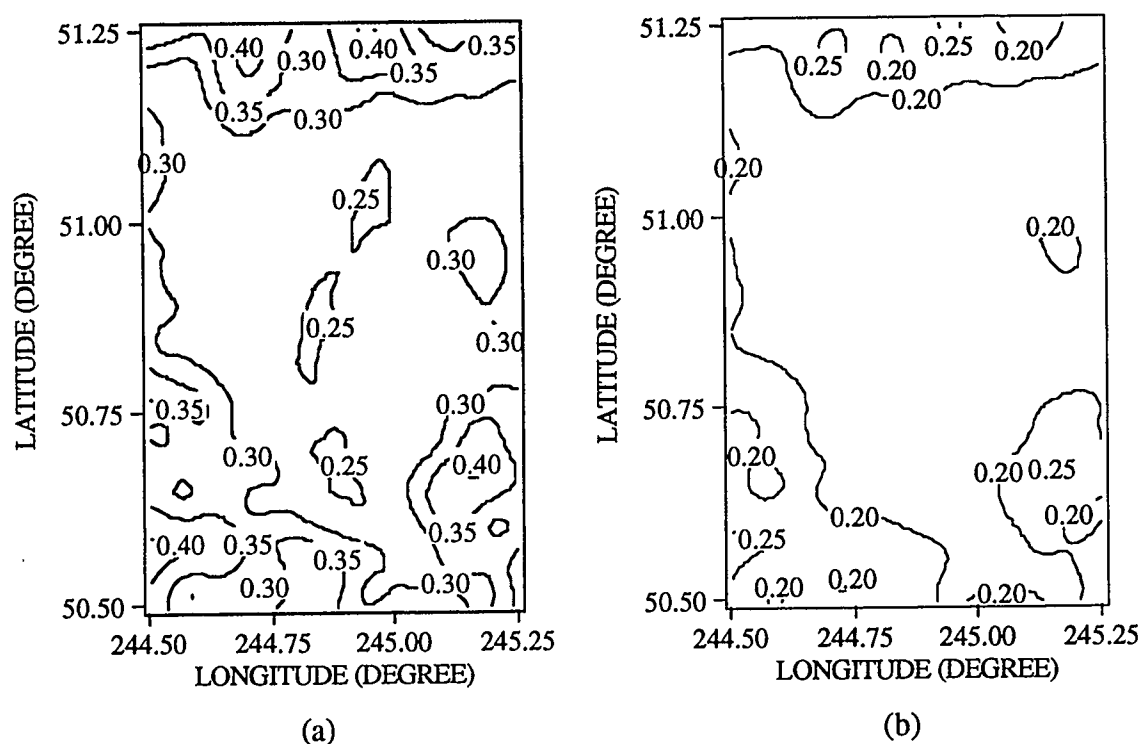

(a)   (b)

Figure 5.9 Upward continued standard deviations of surface free-air gravity anomalies
[Contour interval: 0.05 mGal; upward continuation levels: (a) 3 km, (b) 4 km]

Table 5.6 Statistics of upward continuation of standard deviations of surface free-air gravity anomalies (Unit: mGal)

Contin. Dist.	Minimum	Maximum	Mean	Std. Dev.
3 km	0.25	0.41	0.30	0.04
4 km	0.16	0.26	0.19	0.03

In Section 3.4.3, free-air gravity anomaly errors were computed on a 1' x 1' grid for the Kananaskis extended area. The errors in the data appear to be weakly correlated and the upward continuation shows that these errors attenuate considerably with the altitude. Table 5.7 and Figure 5.10 present the statistics of the results and the contour plans, respectively.
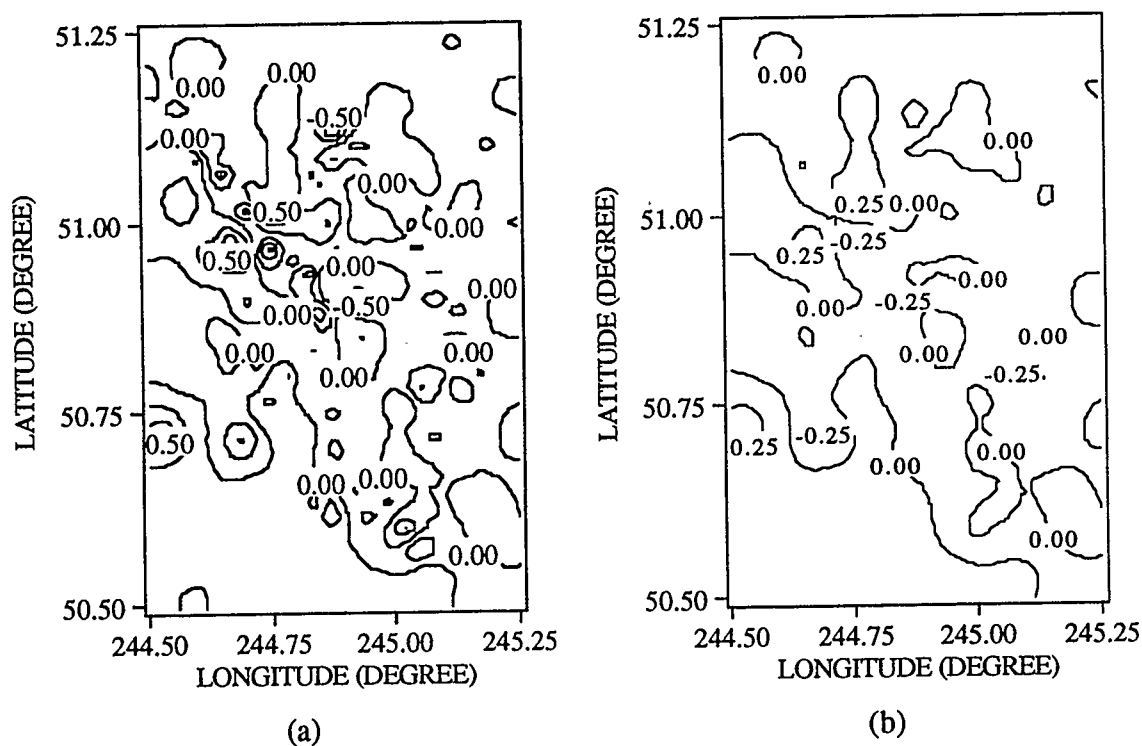

(a)   (b)

Figure 5.10 Upward continued errors of surface free-air gravity anomalies
[Contour interval: 0.25 mGal; upward continuation levels: (a) 3 km, (b) 4 km]

Table 5.7 Statistics of upward continuation errors of surface free-air gravity anomalies

(Unit: mGal)

Contin. Dist.	Minimum	Maximum	Mean	Std. Dev.
3 km	-0.8	0.8	0.0	0.2
4 km	-0.3	0.4	0.0	0.1

Comparison of Results and Other Studies

A comparison between the results given from the direct method of upward continuation and from point mass modelling (see Section 4.4) under the same assumption (i.e., the gravity anomaly values are considered to refer to the geoid), indicate similar results. The root mean square variation, in mGal, in the estimated gravity anomaly fields at 3 km and 4 km above the geoid are for the point mass model 65.4 and 63.5, respectively, and for the direct method, 65.1 and 63.3, respectively.

Table 5.8 Statistics of the discrepancies between the direct upward continuation method and point mass modelling on a 1' x 1' grid in the Kananaskis core area

(Unit: mGal)

Contin. Dist.	Minimum	Maximum	Mean	Std. Dev.	RMS
3 km	-3.0	3.6	-0.3	0.7	0.8
4 km	-1.5	1.9	-0.1	0.4	0.4

A clearer indication of the differences in results between the methods is given by examining common profiles. The profiles indicated on page 109 (see also Tables 5.4 and 5.5, and Figures 5.7 and 5.8) were used. The statistics of the results are given in Table 5.9 and Table 5.10 for the latitude and longitude profile, respectively. Figure 5.11 and Figure 5.12 show the respective plots. From the examination of this material it is concluded that the two methods perform in the same manner.

Table 5.9 Statistics of the discrepancies between the direct upward continuation method and point mass modelling on a profile at latitude 50°53' (Unit: mGal)

Contin. Dist.	Minimum	Maximum	Mean	Std. Dev.	RMS
3 km	-1.0	0.2	-0.3	0.3	0.4
4 km	-0.7	0.3	-0.1	0.3	0.3

Table 5.10 Statistics of the discrepancies between the direct upward continuation method and point mass modelling on a profile at longitude 244°53' (Unit: mGal)

Contin. Dist.	Minimum	Maximum	Mean	Std. Dev.	RMS
3 km	-2.5	1.3	-0.1	0.8	0.8
4 km	-1.4	0.6	0.0	0.4	0.4

Figure 5.11 Profiles at latitude 50°53' of differences between the direct upward continuation method and point mass modelling at (a) 3 km and (b) 4 km (Unit: mGal)

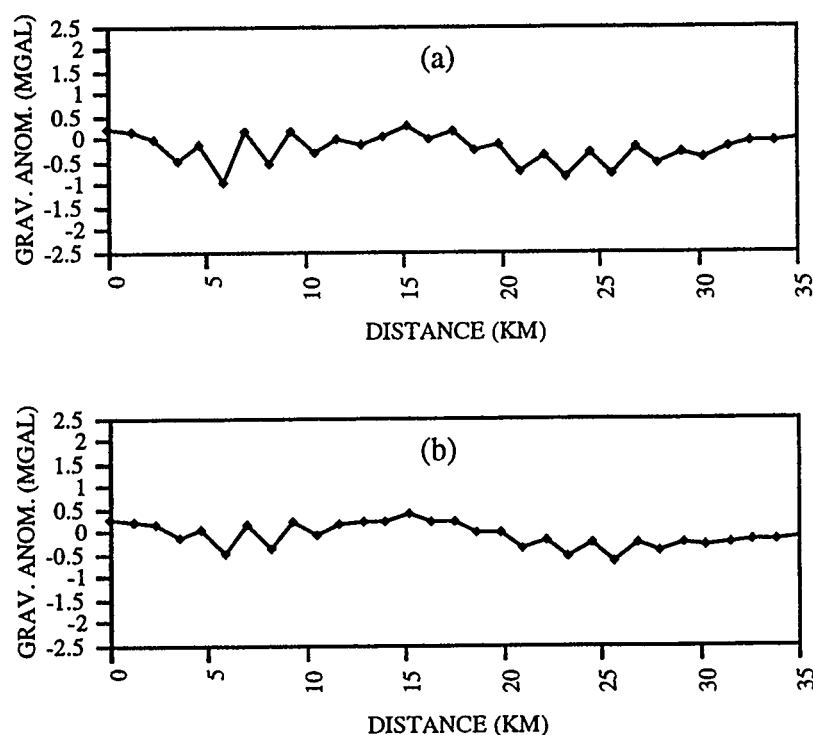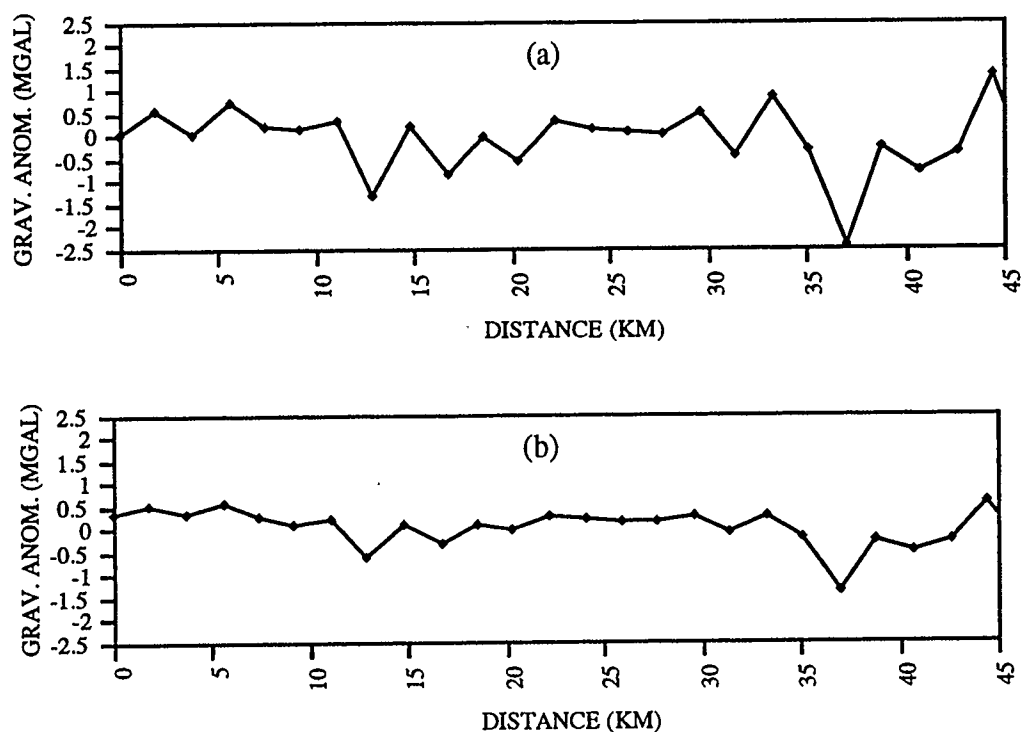**Figure 5.12** Profiles at longitude 244°53' of differences between the direct upward continuation method and point mass modelling at (a) 3 km and (b) 4 km (Unit: mGal)

The differences between the indirect and direct methods for upward continuation seem more pronounced. For the data from Table 5.2 and Table 5.3, the root mean square variation, in mGal, for the upward continued gravity anomaly fields at 3 km and 4 km above the geoid are for the direct method 69.1 and 67.1, respectively, and for the indirect method 67.1 and 65.1, respectively. The results of the upward continued profiles obtained from the direct and indirect methods, show significant discrepancies. The statistics are given in Table 5.11 for the latitude profile and in Table 5.12 for the longitude profile. The direct method results present a negative bias at the level of -3.5 mGal, and the root mean square difference is at the level of 4.4 mGal. Figures 5.13 and 5.14 show the respective profile plots.

Table 5.11 Statistics of discrepancies between the indirect and direct upward continuation methods on a profile at latitude 50°53' (Unit: mGal)

Contin. Dist.	Minimum	Maximum	Mean	Std. Dev.	RMS
3 km	-6.6	4.4	-3.4	2.7	4.3
4 km	-6.2	3.2	-3.4	2.3	4.1

Table 5.12 Statistics of discrepancies between the indirect and direct upward continuation methods on a profile at longitude 244°53' (Unit: mGal)

Contin. Dist.	Minimum	Maximum	Mean	Std. Dev.	RMS
3 km	-9.5	2.6	-3.6	2.9	4.6
4 km	-7.7	1.8	-3.7	2.3	4.4

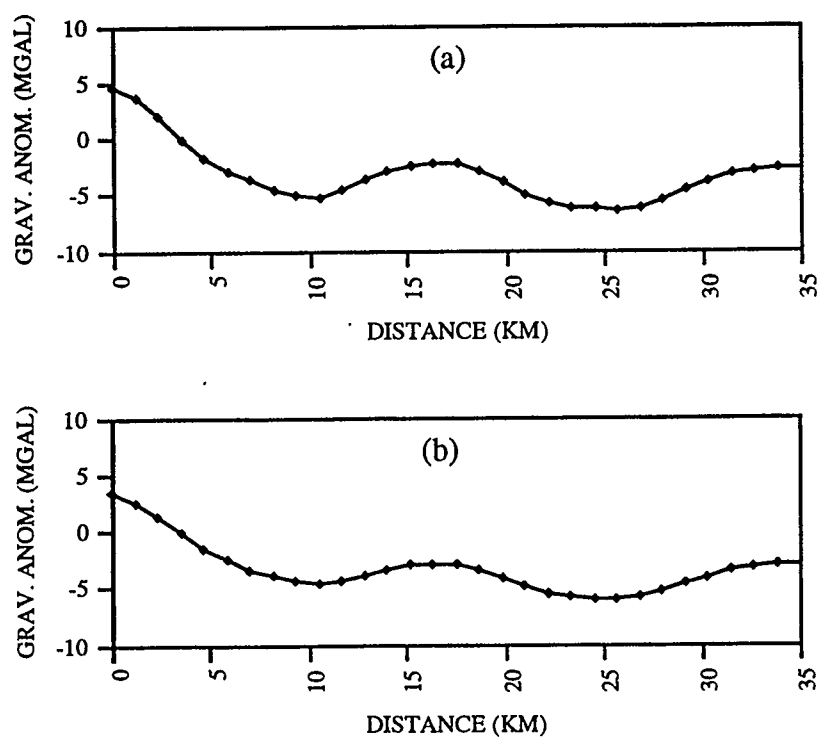**Figure 5.13** Profiles at latitude 50°53' of differences between the indirect and direct upward continuation methods at (a) 3 km and (b) 4 km (Unit: mGal)
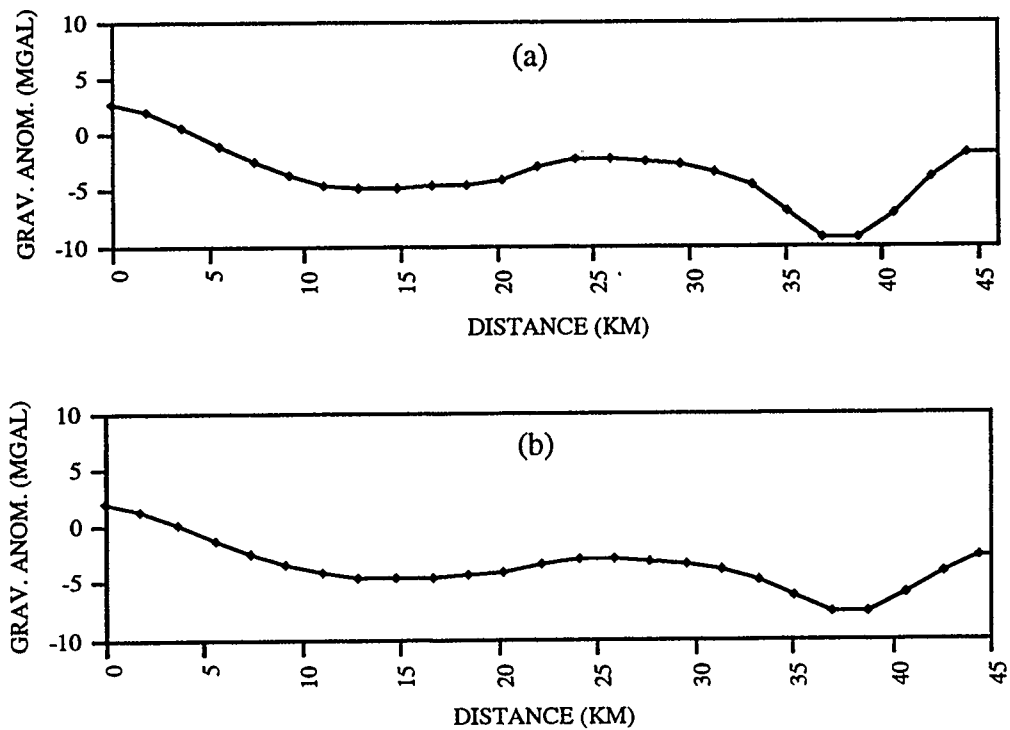
Figure 5.14 Profiles at longitude 244°53' of differences between the indirect and direct upward continuation methods at (a) 3 km and (b) 4 km (Unit: mGal)

Comparison of the discrepancy profiles with the respective elevation profiles show a negative correlation. This indicates that the reduction of the anomaly data plays a role in the upward continuation results. Because the indirect method of upward continuation has taken into account the large variations in the gravity field in the computation process, it is considered to give better results than the direct method.

CHAPTER 6

SUMMARY, CONCLUSIONS AND RECOMMENDATIONS

The objective of the research to produce a gravity model for a mountainous area with large variations in the gravity field, by combining terrestrial gravity data with elevation data, has been accomplished. The area investigated is in the Canadian Rocky Mountains, situated between latitudes 50°15' and 51°30' and between longitudes 244°15' and 245°30'. The gravity model developed covers an area bounded by latitudes 50°30' and 51°15' and longitudes 244°30' and 245°15'; part of the Kananaskis area lies within these limits. The gravity model will be used to test the performance of an airborne system for detailed the mapping of the gravity field of the Earth.

The different aspects treated in order to construct the gravity field model comprise: collection of gravity data and of topographic data from existing sources and by measurement ; unified treatment (i.e., processing) of all the available data to produce point terrain corrected free-air, refined Bouguer and isostatic gravity anomalies; prediction of regular patterns (i.e., grids) of gravity anomalies from the random point data; spatial (i.e., at elevation above the reference surface) computation of gravity anomalies. From the geodetic point of view, the gravity model is three-dimensional. The reason is that the topographic information is integral part in the terrestrial gravity modelling process and because the model was constructed also at altitudes above the Earth.

The first stage in the investigation dealt with the gravimetric and topographic data collection. Because the gravimetric data originated from different sources, an attempt was made to eliminate apparent inconsistencies in the data and to apply standard reductions in the derivation of free-air, refined Bouguer and isostatic gravity anomalies. The (surface) free-air gravity anomalies were calculated by subtracting the normal gravity formulated with the parameters of GRS80. The dependence of the normal vertical gradient on latitude and

the inclusion of its second-order term, together with the atmospheric correction was considered in the free-air reduction. To account for irregularities of the topography from the Bouguer plate, the gravity anomalies were terrain corrected. The terrain corrections were calculated by prism integration with different resolutions (i.e., 0.1 km, 1 km, 5 km, respectively) for the digital elevation model, according to the distance from the computation point. The computations were carried out up to and including the Heyford zone O.

Bouguer gravity anomalies were determined from the free-air gravity anomalies by eliminating the attraction of the Bouguer plate, calculated with standard density of 2.67 g/cm^3. The resulting anomalies are the refined Bouguer gravity anomalies. Their field is smoother than that of the free-air gravity anomalies and thus are more suitable for prediction at other locations.

Isostatic gravity anomalies were calculated in order to investigate their possible use for prediction of gravity anomalies. The isostatic reduction was carried out according to the Airy-Heiskanen model; with density contrast (i.e., difference) of 0.6 g/cm^3 and normal thickness of the Earth's crust of 30 km. The computation of the attraction of the topography and of its isostatic compensation were computed by prismoidal integration, in the same manner as for the terrain corrections.

The free-air gravity anomalies show a strong correlation with the topographic elevations (i.e., correlation coefficient is 0.99) and they vary over a wide range. The estimated Bouguer gradient for the entire area is 0.1107 which is only 1% less than the standard value of 0.1119. The Bouguer gravity anomalies are smoother but because of the mountainous area, show a negative bias and attain large values. They are not correlated with the local elevations (i.e., correlation coefficient is -0.07). The isostaic gravity anomalies vary in the same range as the Bouguer anomalies, but are small with a mean of zero. They show correlation with the elevations (i.e., correlation coefficient is 0.20).

All the gravimetric data available in the area (i.e., 371 gravity points) were put into a data base which contains for each random point the following: identification number; geographic latitude and longitude; elevation; gravity (with the exception of the points from the North America Gravity data base); free-air, Bouguer and isostatic gravity anomalies; standard deviations for the spatial coordinates and for the free-air and Bouguer gravity anomalies. The mean standard deviations for the latter two anomalies are 1.0 mGal and 0.7 mGal,

respectively. Inconsistencies found in the data were corrected on the basis of the available information.

The random gravity points are distributed reasonably well over the topography elevation range within the area. Their horizontal layout is, however, uneven, from data spacing of under 1 km within parts of the core area to 9 km in the extended area. The next stage in the investigation addressed the problem of creating from the existing random gravity points a more homogenous data set of gravity anomalies on a grid of 1' x 1' (i.e., 1.9 km x 1.2 km). Two methods of prediction are used for this purpose, namely least squares collocation and weighted means.

The least-squares collocation solution formulation is based on the covariance function of signals (i.e., in this case gravity anomalies). After a pre-selection of the point gravity anomaly data to reflect more objectively the overall data distribution in the area, local empirical covariance functions were estimated for each type of anomaly available (i.e., free-air, Bouguer and isostatic). The trend in the data was removed by the subtracting the mean and polynomial surfaces of first and second degree, respectively. For the free-air gravity anomalies, their correlation with elevations was eliminated first. The essential parameters (i.e., variance of gravity anomalies, correlation length and variance of horizontal gradients) of the empirical covariance functions are for practical purposes the same when a second degree surface polynomial is used for trend elimination in the data. Also, for this latter, case the resulting variance is smaller and the estimated standard deviations for the signals are scaled better.

Several analytical functions were used to model the empirical covariance functions. The predicted gravity anomalies appeared not very sensitive to the choice of the analytical model. However, the estimated standard deviations were influenced more significantly. Arbitrarily, the second-order Markov model was used in the least squares solution. First, a grid of Bouguer gravity anomalies were predicted together with their standard deviations. The grid of free-air gravity anomalies was calculated by combining the former anomalies with the digital elevation model and using the constant 0.1119 for the Bouguer gradient. The standard deviation of the gridded free-air gravity anomalies was calculated by error propagation from the estimated standard deviations of Bouguer gravity anomaly and of elevation grids. These estimations should be viewed more in a relative sense and external comparisons are necessary for a better assessment. However, they can give an indication of

the areas were the model is stronger. It appears that in the area bounded by latitudes 50°40' and 51°05' and by longitudes 244°38' and 245°08', the standard deviations of the predicted free-air gravity anomalies is at a level of 1 mGal to 1.5 mGal. It would have been expected for the model to be stronger in this area, because the largest concentration of irregularly distributed gravity points are located here.

The method of weighted means based on the inverse distance raised to a power was also investigated for the prediction of gravity anomalies. It was concluded that, for powers of prediction equal or greater than two, there were no significant differences between the predicted values.

Several tests were carried out to compare the performance of the two methods of prediction used in this investigation; these involved the use of different data patterns. When all the available points are used to predict gridded gravity anomalies, the original data in the Kananaskis core area are recovered from the grid at the level of 1.2 mGal and 1.3 mGal, when using least-squares collocation and weighted means, respectively. Other statistics, namely the root mean square discrepancy and the power of prediction, indicated a slightly better performance of the least-squares collocation method. However, for practical purposes, with the available data in this investigation, the two methods produce the same results.

Statistics for the predicted grids of free-air, Bouguer and isostatic gravity anomalies were calculated. The empirical covariance functions were estimated and their essential parameters determined. The latter parameters indicate a smoother field which is expected to result in the prediction process. The same conclusions regarding the trend reduction were reached as before. For the gridded free-air gravity anomalies, a reduction was carried out by subtracting values calculated from spherical harmonic coefficients of the geopotential model OSU91A. This produced smaller values for each essential parameter of the empirical covariance functions. A further reduction of these gravity anomalies by a residual terrain model, removes (or reduces) the influences coming from the short wavelength of the topography. The variances are reduced again and the correlation length increases, giving a better prediction property to the covariance function.

Furthermore, the anisotropy characteristics and the resolution of the gravity anomaly field were investigated. Two-dimensional covariance functions calculated for all the predicted

gravity anomaly grids indicate that they contain a degree of anisotropy. The anomaly degree variances calculated from the covariance functions were modeled by parametric logarithmic expressions. They indicate that 1 mGal resolution of the gravity anomaly field in the Kananaskis area is possible with a 2.5 km to 3 km point gravity anomaly data spacing and by taking into account the topographic effects associated with the rugged topography. Even with the current existing spacing of 4 km in the Kananaskis core area, the resolution of the field is realized at better than 1.5 mGal.

The last main task of this investigation is to model the terrestrial surface gravity anomalies at various elevations. The gravity anomaly model at elevation is required for testing the airborne gravity based system. Two approaches were considered, namely spatial modelling of gravity anomalies by point masses and upward continuation of the surface gravity anomalies with the Poisson integration.

The terrain corrected surface free-air gravity anomalies were reduced first by gravity anomalies calculated from spherical harmonic coefficients of the geopotential model OSU91A. The latter anomalies represent the long and part of the medium wavelength of the gravity anomaly field, coming from outside the local area. The resulting residual anomaly field is modelled by point masses located on two layers. The depth for each layer is determined from the power spectral density corresponding to the residual gravity anomalies covariance function, when plotted logarithmically. The residual medium wavelength part and the short wavelength part of the gravity anomaly field are modelled by the point masses on the deep layer and on the shallow layer, respectively. With this two-layer point mass model, the gravity anomaly field is calculated spatially at elevations of 3 km and of 4 km above the geoid, respectively. The contribution coming from outside of the area, calculated now at elevation from the geopotential model, are added to the gravity anomalies modelled by the point masses. An attenuation in the field of approximately 3% is estimated from the root mean square variation of the gravity anomaly models at 3 km and 4 km, respectively. This attenuation becomes less pronounced with the increase in elevation.

It should be mentioned that, in these computations, the surface free-air gravity anomalies were considered equal with anomalies at the geoid level. In areas with high and steep mountains this could introduce significant errors in the calculations. Certain aspects regarding the influence of the assumptions made in the manner in which the data is treated

are addressed in the upward continuation of free-air gravity anomalies using the Poisson integral.

The upward continuation computation with the Poisson integral was used here in planar approximation. Three approaches of treating the gravity anomaly data were investigated: terrain corrected surface free-air gravity anomalies reduced to a geopotential model and considered to refer to the geoid; terrain corrected surface free-air gravity anomalies reduced to a geopotential model and considered to refer to a surface corresponding to the mean elevation over the area; terrain corrected surface free-air gravity anomalies reduced to a geopotential model and to a residual terrain model. The former two cases constitute a direct method of calculation and the latter an indirect method of calculation (i.e., the influence of the topographic variations are considered separately in the computation process). The upward continued gravity anomaly field calculated by the indirect method is the result of the following: upward continuation with the Poisson integral of the residual gravity anomalies; gravitational effects at elevation of the removed residual terrain model; and geopotential model contribution at altitude.

The comparison of free-air gravity anomalies calculated at altitude by the direct upward continuation method and by point mass modelling show that the two methods perform in a similar manner. The root mean square difference for the gravity anomaly field at 3 km altitude is approximately 0.8 mGal. The use of the indirect method produced results very different from the direct method with a root mean square difference of approximately 4.5 mGal. The differences resulting from the latter comparison appear to be negatively correlated with the topography. The use of different assumptions in the data reduction show that results can vary significantly for each case. For high accuracy requirements, the topographic effects must be considered, especially in mountainous areas. These differences are more pronounced at lower elevations and appear to diminish with an increase in elevation. The testing of the airborne gravity system will be attempted at altitudes as low as possible over the Kananaskis area (i.e., approximately 3 km to 3.5 km). Thus, good gravity anomaly models at these elevations are of importance.

The analysis of estimated standard deviations for gravity anomalies in Kananaskis indicate that in the area bounded by latitudes 50°40' and 51°05' and by longitudes 244°38' and 245°08', the gravity anomaly model is stronger. Thus it is recommended that within this area the gravity based airborne system should be tested. The precision and the error contour

plots for the gravity anomalies give indication where new gravity measurements should be taken and/or where the point height information should be improved. From this investigation it can be concluded that few new gravity measurements are needed in the area. Attention should be devoted to improve the height information associated with the random point data. If additional gravity measurements will be carried out, they must be made in conjunction with good elevation determinations. Also, the available digital elevation models have to be improved (i.e., corrected). Their use is essential for modelling the effects of the rugged topography in the Kananaskis area in modelling the gravity field. Additional computational investigations to validate the current results are desirable. For example, the use of analytical downward continuation of the surface free-air gravity anomalies to a reference surface for the upward continuation should be investigated. The use of least-squares collocation can also be considered as a possible method of upward continuation.

As a final conclusion, though the three-dimensional gravity model for the Kananaskis area can still be improved, the information available so far can assist the gravity based airborne system at this stage in its development.

REFERENCES

Abd-Elmotaal, H., Statistical Behavior of the Free-Air, Bouguer and Isostatic Anomalies in Austria. Bulletin Géodèsique, 66, pp. 325-335, 1992.

Barnett, C. T., Theoretical Modeling of the Magnetic and Gravitational Fields of an Arbitrary Shaped Three-Dimensional Body. Geophysics, Vol. 41, No. 6, pp. 1353-1364, 1976.

Bhattacharyya, B. K., Some General Properties of Potential Fields in Space and Frequency Domain: A Review. Geoexploration, Vol. 5, pp. 127-143, 1967.

Bhaskara Rao, D., M. J. Prakash and N. Ramesh Babu, 3D and 21/2D Modeling of Gravity Anomalies With Variable Density Contrast. Geophysical Prospecting, 38, pp. 411-422, 1990.

Blais, J. A. and R. Ferland, Optimization in Gravimetric Terrain Corrections. Canadian Journal of Earth Sciences, Vol. 21, No. 5, pp. 505-515, 1984.

Brigham, E. O., The Fast Fourier Transform and Its Applications. Prentice Hall, Inc., New Jersey, February, 1974.

Briggs, I. C., Machine Contouring Using Minimum Curvature. Geophysics, Vol. 39, No. 1, pp. 39-48, 1974.

Brozena, J. M., GPS and Airborne Gravimetry: Recent Progress and Future Plans. Bulletin Géodèsique, No. 65, pp. 116-121, 1991.

Brozena, J. M. and M. F. Peters, An Airborne Gravity Study of Eastern North Carolina. Geophysics, Vol. 53, No. 2, pp. 245-253, 1988.

Brozena, J. M., G. L. Mader and M. F. Peters, Interferometric Global Positioning System: Three-Dimensional Positioning Source for Airborne Gravimetry. Journal of Geophysical Research, Vol. 94, No. B9, pp. 12,153-12,162., 1989.

Buck, R.J. and J. G. Tanner, Storage and Retrieval of Gravity Data. Bulletin Géodèsique, No. 103, pp. 63-84, 1972.

Cartwright, D. E. and A. C. Edden, Corrected Tables of Tidal Harmonics. Geophys. J. R. Astr. Soc., 33, pp. 253-264, 1973.

Cartwright, D. E. and R. J. Tayler, New Computations of the Tide-Generating Potential. Geophys. J. R. Astr. Soc., 23, pp. 45-74, 1971.

Colombo, O. L., The Role of GPS/INS in Mapping the Earth's Gravity Field in the 1990's. In: K. P. Schwarz and G. Lachapelle (eds.), Kinematic Systems in Geodesy, Surveying, and Remote Sensing, IAG Symposium No. 107, pp. 463- 476, Banff, Alberta, September, 1990.

Cordell, L. and R. G. Henderson, Iterative Three-Dimensional Solution of Gravity Anomaly Data Using a Digital Computer. Geophysics, Vol. 33, No. 4, pp. 596-601, 1968.

Cruz, J. Y., Disturbance Vector in Space From Surface Gravity Anomalies Using Complementary Models. Report No. 366, Dept. of Geodetic Science and Surveying, The Ohio State University, Columbus, Ohio, August, 1985.

Cruz, J. Y. and P. Laskowski, Upward Continuation of Surface Gravity Anomalies. Report No. 360, Dept. of Geodetic Science and Surveying, The Ohio State University, Columbus, Ohio, December, 1984.

Dobrin, M. B. and C. H. Savit, Introduction to Geophysical Prospecting, 4th ed. McGraw-Hill, Inc., New York, 1988.

Drewes, H., Zur Ausgleichung von Gravimeternetzen. Zeitschrift fur Vermessungswesen, Nr. 10, pp. 485-496, 1978.

Forsberg, R., A Study of Terrain Reductions, Density Anomalies and Geophysical Inversion Methods in Gravity Field Modeling. Report No. 355, Dept. of Geodetic Science and Surveying, The Ohio State University, Columbus, Ohio, April, 1984a.

Forsberg, R., Local Covariance Functions and Density Distributions. Report No. 356, Dept. of Geodetic Science and Surveying, The Ohio State University, Columbus, Ohio, June, 1984b.

Forsberg, R., Gravity Field Terrain Effect Computation by FFT. Bulletin Géodèsique, Vol. 59, pp. 342-360, 1985.

Forsberg, R., Inertial Geodesy in a Rough Gravity Field. UCSE Report No. 30009, Div. of Surveying Engineering, The University of Calgary, Calgary, Alberta, April, 1986.

Forsberg, R. and C. C. Tscherning, Deflection and Gravity Anomaly Prediction for Inertial Positioning Using Collocation. In: K.P. Schwarz (ed.), Proceedings of the ISS Symposium, pp. 89-105, Banff, Canada, June, 1981a.

Forsberg, R. and C. C. Tscherning, The Use of Height Data in Gravity Field Approximation by Collocation. Journal of Geophysical Research, Vol. 86, No. B9, pp. 7843-7854, 1981b.

Goad, C. C., C. C. Tscherning and M. M. Chin, Gravity Empirical Covariance Values for the Continental United States. Journal of Geophysical Research, Vol. 89, No. B9, pp. 7962-7968, 1984.

Götze, H. J. and B. Lahmeyer, Application of Three-Dimensional Iterative Modeling in Gravity and Magnetics. Geophysics, Vol. 53, No. 8, pp. 1096-1108, 1988.

Hammer, S., Terrain Corrections for Gravimeter Stations. Geophysics, Vol. 10, pp. 184-194, 1939.

Hammer, S., Airborne Gravimetry Is Here. Geophysics Vol. 48, pp. 213-223, 1983.

Heiskanen, W. A. and F. A. Vening Meinesz, The Earth and Its Gravity Field. McGraw-Hill Book Company, Inc., New York, 1958.

Heiskanen, W. A. and H. Moritz, Physical Geodesy. W. H. Freeman and Company, San Francisco, California, 1967.

Hirvonen, R. A. and H. Moritz, Practical Computation of Gravity at High Altitudes. Report No. 27, Institute of Geodesy, Photogrammetry and Cartography, The Ohio State University, May, 1963.

International Association of Geodesy (I. A. G.), Geodetic Reference System 1967. Bulletin Géodèsique, Publ. Spec. No. 3, 1971.

Jekeli, C., An Investigation of Two Models for the Degree Variances of Global Covariance Functions. Report No. 275, Dept. of Geodetic Science and Surveying, The Ohio State University, Columbus, Ohio, 1978.

Kassim, F. A., An Evaluation of Three Techniques for the Prediction of Gravity Anomalies in Canada. Technical Report No. 73, Dept. of Surveying Engineering, University of New Brunswick, Fredericton, N. B., September, 1980.

Kearsley, A. H. W., Sideris, M. G., Krynski, J., Forsberg, R. and Schwarz, K. P., White Sands Revisited - A Comparison of Techniques to Predict Deflections of the Vertical. Report No. 30007 of the Division of Surveying Engineering, The University of Calgary, Calgary, Alberta, 1985.

Knickmeyer, E. T., Vector Gravimetry by a Combination of Inertial and GPS Satellite Measurements. UCSE Report No. 20035, Dept. of Surveying Engineering, The University of Calgary, September, 1990.

Krieg, L. A., Mathematical Modeling of the Behavior of the Lacoste and Romberg "G" Gravity Meter for Use in Gravity Network Adjustments and Data Analyses. Report No. 321, Dept. of Geodetic Science and Surveying,.The Ohio State University, Columbus, Ohio, November, 1981.

Lachapelle, G. and K. P. Schwarz, Empirical Determination of the Gravity Anomaly Covariance Function in Mountainous Areas. The Canadian Surveyor, Vol. 34, No. 3, pp. 251-264, 1980.

Lachapelle, G., K. P. Schwarz, and A. Mainville, Empirical Investigations on the Anisotropy of the Free Air Gravity Anomaly Covariance Function. Bolletino di Geodesia e Scienze Affini, No. 1, 1983.

LaCoste, L. J. B., J. Ford, R. Bowles, and K. Archer, Gravity Measurements in an Airplane Using State-of-the-Art Navigation and Altimetry. Geophysics, Vol. 47, pp. 832-838, 1983.

LaFehr, T. R., Standardization in Gravity Reduction. Geophysics, Vol. 56, No. 8, pp. 1170-1178, 1991.

Li, Y. C. , Optimal Spectral Geoid Determination. UCGE Reports Number 20050, Department of Geomatics Engineering, Calgary, Alberta, June 1993.

Li, Y. C. and M. G. Sideris, Improved Gravimetric Terrain Corrections. Paper accepted by Geophysical Journal International, 1994.

Merry, C. L., Gravity Anomaly Prediction Using Local Collocation. In: K. P. Schwarz (ed.), Techniques to Predict Gravity Anomalies and Deflections of the Vertical in Mountainous Areas, pp. 52-63, Publication 30004, Div. of Surveying Engineering, The University of Calgary, Calgary, Alberta, April 1983.

McConnell, K., The Organization and Management of Canada's National Gravity Data Base. Bulletin Géodèsique, Vol. 56, pp. 134-148, 1982.

Milne, D., Gravity Densification in the Kananaskis Area. ENSU 500 Survey Project, Division of Surveying Engineering, The University of Calgary, May, 1986.

Morelli, C., Modern Standards for Gravity Surveys. Geophysics, Vol. 41, No. 5, p. 1051, 1976.

Morelli, C., C. Gantar, T. Honkasalo, R. K., McConnell, J. C. Tanner, B. Szabo, U. Uotila, C. T. Whalen, The International Standardization Net 1971 (ISGN71). I.U.G.G-I.A.G. Publ. Spec. No. 4, Paris, 1974.

Morrison, F. F. and B. C. Douglas, A Comparison of Gravity Prediction Methods on Actual and Simulated Data. Geophysics, Vol. 49, No. 10, pp. 1774-1780, 1984.

Moritz, H., Studies on the Accuracy of the Computation of Gravity in High Elevations. Report No. 21, Institute of Geodesy, Photogrammetry and Cartography, No. 9, The Ohio State University, April, 1962.

Moritz, H., Linear Solutions of the Geodetic Boundary-Value Problem. Report No. 79, Dept. of Geodetic Science and Surveying, The Ohio State University, December, 1966.

Moritz, H., On the Use of the Terrain Correction in Solving Molodensky's Problem. Report No. 108, Dept. of Geodetic Science and Surveying, The Ohio State University, May, 1968.

Moritz, H., Advanced Least-Squares Methods. Report No. 175, Dept. of Geodetic Science and Surveying, The Ohio State University, Columbus, Ohio, 1972.

Moritz, H., Covariance Functions in Least-Squares Collocation. Report No. 240, Dept. of Geodetic Science and Surveying, The Ohio State University, Columbus, Ohio, 1976.

Moritz, H., On the Computation of a Global Covariance Model. Report No. 255, Dept. of Geodetic Science and Surveying, The Ohio State University, Columbus, Ohio, June, 1977.

Moritz, H., Least Squares Collocation. Reviews of Geophysics and Space Physics, Vol. 16, No. 3, pp. 421-430, 1978.

Moritz, H., Advanced Physical Geodesy. H. Wichmann Verlag, Karlsruhe, 1980.

Moritz, H., Geodetic Reference System 1980. In: C. C. Tscherning (ed.), The Geodesist's Handbook, Bulletin Géodèsique, Vol. 58, pp. 338-398, 1984.

Nettleton, L. L., Gravity and Magnetics in Oil Prospecting. McGraw-Hill Book Company, New York, 1976.

Nilsen, T. H., Washington Gravity Base Station Network. State of Washington, Dept. of Natural Resources, Division of Geology and Earth Resources, Information Circular 59, 1976.

Parasnis, D. S., Principles of Applied Geophysics, 3rd ed. Chapman and Hall, London, England, 1979.

Peng, M., Topographic Effects on Gravity and Gradiometry by the 3D FFT and FHT Methods. UCGE Reports, Department of Geomatics Engineering, Calgary, Alberta, 1994.

Peng, M., Y. C. Li and M. G. Sideris, First Results on the Computation of Terrain Corrections by the 3-D FFT Method. Paper accepted for publication in Bulletin Geodesique, 1994.

Rapp, R. H., The Prediction of Point and Mean Gravity Anomalies through the Use of a Digital Computer. Report No. 43, Institute of Geodesy, Photogrammetry and Cartography, The Ohio State University, June, 1964.

Rapp, R. H., A Fortran Program for the Upward Continuation of Gravity Anomalies. Report No. 62, Dept. of Geodetic Science, The Ohio State University, February, 1966.

Rapp, R. H., Results of the Application of Least Squares Collocation to Selected Geodetic Problems in Approximation Methods in Geodesy. In: H. Moritz and H. Sünkel (eds.), Herbert Wichman Verlag, Karlsruhe, pp. 117-156, 1978.

Rapp, R. H., A Fortran Program for the Computation of Gravimetric Quantities from High Degree Spherical Harmonic Expansions. Report No. 334, Department of Geodetic Science and Surveying, The Ohio State University, Columbus, Ohio, September, 1982.

Rapp, R. H., M. Wang and N. Pavlis, The Ohio State 1991 Geopotential and Sea Surface Topography Harmonic Coefficient Models. Report No. 410, Department of Geodetic Science and Surveying, The Ohio State University, Columbus, Ohio, 1991.

Schwarz, K. P., Data Types and Their Spectral Properties. In: K. P. Schwarz (ed.), Proceedings of the Beijing International Summer School on Local Gravity Field Approximation, Division of Surveying Engineering, The University of Calgary, Calgary, Publication 60003, pp. 1-66, January, 1985.

Schwarz, K. P. and G. Lachapelle, Local Characteristics of the Gravity Anomaly Covariance Function. Bulletin Geodesique, 54, pp. 21-36, 1980.

Schwarz, K. P., M. G. Sideris and R. Forsberg, The Use of FFT Techniques in Physical Geodesy. Geophysical Journal International, Vol. 100, pp. 485-514, 1990.

Schwarz, K. P., O. Colombo, G. Hein, E. T. Knickmeyer, Requirements for Airborne Vector Gravimetry. In: O. L. Colombo (ed.), IAG Symposia, Symposium No. 110, From Space to Greenland: Charting Gravity With Space and Airborne Instruments, pp. 273-283, 1991.

Schwarz, K. P., M. Wei and J. Krynski, Report on Gravimetric and Gradiometric Aiding of Inertial Navigation Systems, Dept. of Surveying Engineering, The University of Calgary, Calgary, Alberta, April, 1992.

Sideris, M. G., Computation of Gravimetric Terrain Corrections Using Fast Fourier Transform Techniques. UCSE Rep. No. 20007, Division of Surveying Engineering, The University of Calgary, Calgary, Alberta, March, 1984.

Sideris, M. G., Rigorous Gravimetric Terrain Modelling Using Molodensky's Operator. Manuscripta Geodaetica, 15, pp. 15-97, 1990.

Sideris, M. G. and Y. Li, Gravity Field Convolutions Without Windowing and Edge Effects. Bulletin Geodesique, Vol. 67, No. 2, 1993.

Sjöberg, L., Test of a Kalman Model and a Deterministic Model for Prediction of Gravity Anomalies. Report of the Royal Institute of Technology, Division of Geodesy, Stockholm, 1975.

Smith, W. H. F. and P. Wessel, Gridding with Continuous Curvature Splines in Tension. Geophysics, Vol. 55, No. 3, pp. 293-305, 1990.

Sünkel, H., Approximation of Covariance Function by Non-Positive Definite Functions. Report No. 271, Dept. of Geodetic Science and Surveying, The Ohio State University, Columbus, Ohio, 1978.

Sünkel, H., A Covariance Approximation Procedure. Report No. 286, Dept. of Geodetic Science and Surveying, The Ohio State University, Columbus, Ohio, March, 1979.

Sünkel, H., Feasibility Studies for the Prediction of the Gravity Disturbance Vector in High Altitudes. Report No. 311, Dept. of Geodetic Science and Surveying, The Ohio State University, Columbus, Ohio, March, 1981a.

Sünkel, H., The Estimation of Free-Air Anomalies. Report No. 315, Dept. of Geodetic Science and Surveying, The Ohio State University, Columbus, Ohio, September, 1981b.

Sünkel, H., Point Mass Models and the Anomalous Gravitational Field. Report No. 328, Dept. of Geodetic Science and Surveying, The Ohio State University, Columbus, Ohio, December, 1981c.

Sünkel, H., The Generation of a Mass Point Model From Surface Gravity Data. Report No. 353, Dept. of Geodetic Science and Surveying, The Ohio State University, Columbus, Ohio, December, 1983.

Sünkel, H., On the Reduction of Gravity Data for the Prediction of the Gravity Disturbance Vector at Altitudes. Report No. 359, Dept. of Geodetic Science and Surveying, The Ohio State University, Columbus, Ohio, July, 1984.

Sünkel, H. and Kraiger, G., The Prediction of Free-Air Anomalies. Manuscripta Geodaetica, Vol. 8, pp. 229-248, 1983.

Telford, W. M., L. P. Geldart and R. E. Sheriff, Applied Geophysics, 2nd ed. Cambridge University Press, New York, 1990.

Talwani, M. and M. Ewing, Rapid Computation of Gravitational Attraction of Three-Dimensional Bodies of Arbitrary Shape. Geophysics, Vol. 25, pp. 203-225, 1960.

Torge, W., Observation Strategy and -Technique in Gravimetry. In: B. S. Harsson (ed.), Optimization of Geodetic Operations, pp. 126-210, Norges Geografiske Oppmäling, Publ. 3, 1984.

Torge, W., Gravimetry. Walter de Gruyter, Berlin, 1989.

Tscherning, C. C., Application of Collocation for the Planning of Gravity Surveys. Bulletin Géodèsique, No. 116, pp. 183-198, 1975.

Tscherning, C. C. (ed.), Proceedings of the International Symposium Management of Geodetic Data, Geodætisk Institut, Meddelelse No. 55, Kœbenhaven, Danmark, August, 1981.

Tscherning, C. C., Local Approximation of the Gravity Potential by Least Squares Collocation. In: K. P. Schwarz (ed.), Proceedings of the Beijing International Summer School on Local Gravity Field Approximation, Div. of Surveying Engineering, The University of Calgary, Calgary, Publication 60003, pp. 277-357, January, 1985.

Tscherning, C. C. and R. Forsberg, Prediction Test Using Least Squares Collocation and Residual Terrain Reduction. In: K. P. Schwarz (ed.), Techniques to Predict Gravity Anomalies and Deflections of the Vertical in Mountainous Areas, pp. 84-91, Publication 30004, Div. of Surveying Engineering, The University of Calgary, Calgary, Alberta, April, 1983.

Tscherning, C. C. and R. H. Rapp, Closed Covariance Expressions for Gravity Anomalies, Geoid Undulations, and Deflections of the Vertical Implied by Anomaly Degree Variance Models. Report No. 208, Dept. of Geodetic Science and Surveying, The Ohio State University, Columbus, Ohio, 1974.

Tscherning, C. C., R. H. Rapp and C. C. Goad, A Comparison of Methods for Computing Gravimetric Quantities from High Degree Spherical Harmonic Expansions. Manuscripta Geodaetica, Vol. 8, pp. 249-272, 1983.

Uotila, U. A., Analysis of Correlation Between Free-Air Anomalies and Elevations. Report No. 94, Dept. of Geodetic Science and Surveying, The Ohio State University, Columbus, Ohio, 1967.

Uotila, U. A., World Gravity Standards. In: Applications of Geodesy to Geodynamics, pp. 237-238, Report No. 280, Dept. of Geodetic Science and Surveying, The Ohio State University, Columbus, Ohio, October, 1978.

Vassiliou, A., Numerical Techniques for Processing Airborne Data. UCSE Report No. 20017, Division of Surveying Engineering, The University of Calgary, Calgary, Alberta, May, 1986.

Vassiliou, A. A. and K. P. Schwarz, Study of the High-Frequency Spectrum of the Anomalous Gravity Potential. Journal of Geophysical Research, Vol. 92, No. B1, pp. 609-617, 1987.

Vermeer, M., A Frequency Domain Approach to Optimal Geophysical Data Gridding. Manuscripta Geodaetica, Vol. 17, pp. 141-154, 1992.

Wang, Y. M., Downward Continuation of the Free-Air Gravity Anomalies to the Ellipsoid Using the Gradient Solution, Poisson's Integral and Terrain Correction-Numerical Comparison and the Computations. Report No. 393, Dept. of Geodetic Science and Surveying, The Ohio State University, Columbus, Ohio, June, 1988.

Woollard, G. P., The Gravity Meter as a Geodetic Instrument. Geophysics, Vol. 15, No. 1, pp. 1-29, January, 1950.